



Scientific Report 2012-2013

Scientific Report

2012-2013

Table of contents

| | |
|--------------------------|----------------|
| foreword | <i>pag. 1</i> |
| organization | <i>pag. 2</i> |
| people | <i>pag. 3</i> |
| highlights | <i>pag. 7</i> |
| publications | <i>pag. 65</i> |
| projects & grants | <i>pag. 75</i> |
| CnrNano life | <i>pag. 81</i> |
| outreach & communication | <i>pag. 88</i> |

During 2012 and 2013, the research activities of the Institute of Nanoscience achieved an increasing impact in the national and international contest. This is demonstrated by the high number of papers published on high impact journals; also, in 2012 Nano was the Cnr institute that published the largest number of papers in the Nature Group Journals.

Furthermore, in the last two years the Institute of Nanoscience was very successful in obtaining funding via projects. I would like to mention the success obtained by the Nano researchers in highly competitive projects such as European ERC (starting and advanced) and Italian FIRB "Futuro in Ricerca" projects which have allowed young researchers to start new frontier research activities in autonomy. Another strategic element of the project activity of Nano is the participation in the Graphene Flagship, an initiative recently supported by the EU for the next ten years, devoted to the development of graphene for new technologies, which are expected to produce a revolution in several industrial sectors. The Institute of Nanoscience is one of the two Cnr institutes which are leading a strategic activity within the Flagship program.

The large number of young researchers and students is still an important and very positive aspect of this Institute. At the beginning of 2014 the Institute had 73 permanent and 29 fixed-term staff members and about 60 researchers with doctoral and post-doctoral fellowships. Associated researchers from University (63 of which have permanent positions) also actively contribute to the research and project activities of the Institute.

This is the second Activity Report of this Institute. In the following pages the main achievements and events of 2012 and 2013 are presented. Further and updated information about our activities can be found at our website, <http://www.nano.cnr.it>.

I would like to thank Roberta De Donatis, Stefan Heun, Paola Luches, Luisa Neri, Daniele Sanvitto, and Maddalena Scandola for their precious help in the making of this Report.



A handwritten signature in blue ink that reads "Lucia Sorba".

Lucia Sorba
Director of Institute of Nanoscience

Organization

Director of the Institute Lucia Sorba

Directors of the Centers

| | |
|-----------|----------------|
| Pisa NEST | Lucia Sorba |
| Lecce NNL | Giuseppe Gigli |
| Modena S3 | Elisa Molinari |

Administrative Secretary Maria Grazia Angelini

Communication Maddalena Scandola

Executive Board

CnrNano Researchers Andrea Camposeo, Milena De Giorgi, Paola Luches, Marco Polini,
Gian Michele Ratto

Administrative and Technical Staff Ciro Urso

Affiliated researchers Andrea Alessandrini, Massimo De Vittorio, Stefano Frabboni,
Giuseppe Grosso



People

CnrNano Researchers

Gianluca Accorsi NNL
 Alessandra Aloisi NNL
 Valentina Arima NNL
 Dario Ballarini NNL
 Valerio Bellini S3
 Stefania Benedetti S3
 Andrea Bertoni S3
 Ranieri Bizzarri NEST
 Laura Blasi NNL
 Giorgia Brancolini S3
 Franco Calabi NNL
 Arrigo Calzolari S3
 Andrea Camposeo NNL
 Andrea Candini S3
 Agostina Lia Capodilupo NNL
 Luigi Carbone NNL
 Riccardo Castagna NEST
 Fabrizio Castellano NEST
 Alessandra Catellani S3
 Marco Cecchini NEST
 Giovanni Checcucci NEST
 Stefano Corni S3
 Valdis Corradini S3
 Barbara Cortese NNL
 Massimo Cuscunà NNL
 Milena De Giorgi NNL
 Pompilio Del Carro NNL
 Loretta Laureana Del Mercato NNL
 Fabio Della Sala NNL
 Alessandro Della Torre NNL
 Alessandro di Bona S3
 Rosa Di Felice S3
 Eduardo Fabiano NNL
 Paolo Facci S3
 Riccardo Farchioni NEST
 Andrea Ferretti S3
 Antonio Gaballo NNL
 Gian Carlo Gazzadi S3
 Francesco Ghetti NEST
 Alberto Ghirri S3
 Francesco Giazotto NEST
 Vincenzo Grillo S3
 Roberto Grisorio NNL
 Stefan Heun NEST
 Stefano Leporatti NNL
 Paola Luches S3
 Vincenzo Maiorano NNL
 Carmela Martinelli NNL
 Riccardo Nifosì NEST

Concetta Nobile NNL
 Guido Paolicelli S3
 Daniela Parisi NEST
 Adriana Grazia Passaseo NNL
 Teresa Pellegrino NNL
 Luana Persano NNL
 Marco Pieruccini S3
 Stefano Pittalis S3
 Marco Polini NEST
 Deborah Prezzi S3
 Alessandra Quarta NNL
 Gian Michele Ratto NEST
 Maria Clelia Righi S3
 Aurora Rizzo NNL
 Stefano Roddaro NEST
 Massimo Rontani S3
 Carlo Andrea Rozzi S3
 Daniele Sanvitto NNL
 Antonella Sgarbossa NEST
 Lucia Sorba NEST
 Fabio Taddei NEST
 Vittorianna Tasco NNL
 Maria Teresa Todaro NNL
 Andrea Tomadin NEST
 Valentina Tozzini NEST
 Alessandro Tredicucci NEST
 Paolo Emilio Trevisanutto NNL
 Filippo Troiani S3
 Daniele Varsano S3
 Stefano Veronesi NEST
 Alessandro Vezzani S3
 Ilenia Viola NNL
 Miriam Serena Vitiello NEST

CnrNano Post-docs

Carles Oriol Altimiras Martin NEST
 Mario Amado Montero NEST
 Sara Antonini NEST
 Valentina Arcadio NNL
 Daniel Balleza Mejia S3
 Luca Bellucci S3
 Maria Rosa Belviso NNL
 Andrea Benassi S3
 Federica Bianco NEST
 Monica Bianco NNL
 Igor Bodrenko NNL
 Maria Camarasa Gómez NEST
 Vito Dario Camiola NEST
 Martino Alfredo Cappellutti NEST
 Fabrizio Caprioli NNL

Claudia Carlucci NNL
 Carles Oriol Altimiras Martin NEST
 Mario Amado Montero NEST
 Sara Antonini NEST
 Valentina Arcadio NNL
 Daniel Balleza Mejia S3
 Luca Bellucci S3
 Maria Rosa Belviso NNL
 Andrea Benassi S3
 Federica Bianco NEST
 Monica Bianco NNL
 Igor Bodrenko NNL
 Maria Camarasa Gómez NEST
 Vito Dario Camiola NEST
 Martino Alfredo Cappellutti NEST
 Fabrizio Caprioli NNL
 Claudia Carlucci NNL
 Matteo Carrega NEST
 Oliver Carrillo S3
 Ciro Cecconi S3
 Maria Serena Chiriaco NNL
 Caterina Cocchi S3
 Pino D'Amico S3
 Alain Delgado Gran S3
 Francesca Di Benedetto NNL
 Riccardo Di Corato NNL
 Flavia Viola Di Girolamo NEST
 Mariagrazia Di Luca NEST
 Stefano Donati NNL
 Marco Esposito NNL
 Filippo Fabbri NNL
 Omid Faizy Namarvar S3
 Raffaele Faoro NEST
 Ashwanth C. Francis NEST
 Tahereh Ghane S3
 Salvatore Girardo NNL
 Valentino Libero Pio Guerra NNL
 Nemany A. Nemany Hanafy NNL
 Elena Husanu NEST
 Donata Iandolo NNL
 Carola La Tegola NNL
 Francesca Lezzi NNL
 Rita Manco NNL
 Federica Mangione NNL
 Maria José Martínez Pérez NEST
 Luca Masini NEST
 Rosanna Mastria NNL
 Maria Moffa NNL
 Giovanni Morello NNL
 Jonna Marika Paajaste NEST
 Ilaria Elena Palamà NNL

Riccardo Parra NEST
 Claudia Maria Pereira Cardoso S3
 Iolanda Pio NNL
 Silvio Pipolo S3
 Giovanni Potente NNL
 Elisabetta Primiceri NNL
 Alberto Ronzani NEST
 Miguel Royo Valls S3
 José Francisco Saenz Cogollo S3
 Mian Akif Safeen NEST
 Immanuel V. Samidass S3
 Riccardo Scarfiello NNL
 Angela Scrascia NNL
 Daniela Simeone NNL
 Davide Spirito NEST
 Barbara Storti NEST
 Wenming Sun S3
 Elisabetta Tarentini NNL
 Aleksandrs Terentjevs NNL
 Francesco Todisco NNL
 Dimitrios Toroz S3
 Vanira Trifiletti NNL
 Manoj Tripathi S3
 Fabio Trovato NEST
 Sandro Usseglio Nanot NNL
 Emanuela Ventrella NNL
 Viviana Vergaro NNL
 Valeria Videtta NNL
 Orazio Vittorio NEST
 Shudong Wang S3
 Laura Zanetti Polzi S3
 Alessandra Zizzari NNL

Affiliated Researchers

Marco Affronte S3
 Andrea Alessandrini S3
 Giuseppe Amoretti S3
 Athanasia Athanasiou NNL
 Fabio Beltram NEST
 Carlo Maria Bertoni S3
 Roberto Biagi S3
 Diego Bisero S3
 Olmes Bisi S3
 Martino Bolognesi S3
 Annalisa Bonfiglio S3
 Paolo Bordone S3
 Carlo Augusto Bortolotti S3
 Rossella Brunetti S3
 Marilia Junqueira Caldas S3
 Franco Carillo NEST

Giovanni Carlotti S3
 Carlo Cavazzoni S3
 Luca Chirolli NEST
 Giuseppe Ciccarella NNL
 Francesco Ciccarello NEST
 Roberto Cingolani NNL
 Renato Colle NEST
 Maurizio Enrico Corti S3
 Pantaleo Davide Cozzoli NNL
 Sergio D'Addato S3
 Maria Luisa De Giorgi NNL
 Valentina De Renzi S3
 Francesca De Rienzo S3
 Massimo De Vittorio NNL
 Elena Degoli S3
 Umberto del Pennino S3
 Nicolas Didier NEST
 Alberto Di Lieto NEST
 Daniele Ercolani NEST
 Rosario Fazio NEST
 Mauro Ferrario S3
 Stefano Frabboni S3
 Anna Maria Garbesi S3
 Giuseppe Gigli NNL
 Vittorio Giovannetti NEST
 Guido Goldoni S3
 Giuseppe Grosso NEST
 Carlo Jacoboni S3
 Biswajit Karmakar NEST
 Silvia Landi NEST
 Alessandro Lascialfari S3
 Stefano Luin NEST
 Rita Magri S3
 Franca Manghi S3
 Ivan Marri S3
 Giuseppe Maruccio NNL
 Elisabetta Marulli NNL
 Marco Mazzeo NNL
 Claudia Menozzi S3
 Elisa Molinari S3
 Umberto Muscatello S3
 David Neilson NEST
 Stefano Ossicini S3
 Gioacchino Massimo Palma NEST
 Vittorio Pellegrini NEST
 Pasqualantonio Pingue NEST
 Dario Pisignano NNL
 Andrea Pucci NEST
 Stefano Pugnetti NEST
 Angelo Rettori S3
 Rosaria Rinaldi NNL

Davide Rossini NEST
 Alice Ruini S3
 Andrea Sacchetti S3
 Bruno Samori S3
 Paolo Santini S3
 Concita Sibilia NNL
 Marco Sola S3
 Alessandra Toncelli NEST
 Mauro Tonelli NEST
 Sergio Valeri S3
 Tiziano Verri NNL
 Cristiano Viappiani NEST
 Michele Virgilio NEST
 Giampaolo Zuccheri S3

Affiliated Post-Docs

Amit Kumar Agarwal NEST
 Pietro Artoni NEST
 Antonella Battisti NEST
 Eleonora Bellini NNL
 Enrico Benassi S3
 Mariano Biasiucci NNL
 Alessandro Cannavale NNL
 Alberto Carlini NEST
 Piero Cosseddu S3
 Riccardo Degl'Innocenti NEST
 Antonella De Pasquale NEST
 Lorenzo Dominici NNL
 Elena Favilla NEST
 Salvatore Gambino NNL
 Andrea Gamucci NEST
 Carlo Giansante NNL
 Andrea Iagallo NEST
 Emanuela Jacchetti NEST
 Giacomo Levita S3
 Ang Li NEST
 Andrea Listorti NNL
 Laura Marchetti NEST
 Andrea Mari NEST
 Fabrizio Mariano NNL
 Leonardo Mazza NEST
 Viktor Mukherjee NEST
 Michele Nobile NEST
 Mariela Rodriguez Otazo S3
 Francesco Rossella NEST
 Miguel Royo Valls S3
 Ilaria Tonazzini NEST
 Davide Venturelli NEST
 Leonardo Viti NEST
 Vladimir Voccoli NEST

People

Valerio Voliani NEST
Antonella Zacheo NNL
Simone Zanotto NEST

Affiliated PhD students

Christian Alvino S3
Gaelle Françoise Arnaud S3
Simone Barbarino NEST
Laura Basiricò S3
Luca Bergamini S3
Matteo Bertocchi S3
Marzio De Corato S3
Gian Luca De Gregorio NNL
Alessandro Farace NEST
Francesco Ferrara NNL
Marco Gibertini NEST
Umesh Prasad Gomes NEST
Karina A. Guerrero Becerra S3
Martiros Khurshudyan S3
Mirgender Kumar NEST
Karsten Leding Jensen S3
Annamaria Lisotti S3
Anna Loiudice NNL
Erfan Mafakheribashmagh S3
Francesco Malara NNL
Letizia Mariotti NEST
Simone Marocchi S3
Francesco Mazza NEST
Sandro Meucci NEST
Anna Grazia Monteduro NNL
Domenico Montemurro NEST
Massimo Morandini NEST
Mariangela Mortato NNL
Naqvi Mohsin Mubarak S3
Federico Pagliuca S3
Nicola Paradiso NEST
Paola Pareo NNL
Francesca Pederzoli NEST
Dimitri F. M. Pellegrino NEST
Paolo Petrangolini S3
Alessandro Pitanti NEST
Liberato Pizza NEST
Alessandro Principi NEST
Marco Reguzzoni S3
Lorenzo Romeo NEST
Marta Rosa S3
Mattia Sacchi S3
Andrea Secchi S3
Ilaria Siloi S3
Blanca Silva Fernandez NNL

Punam Sonar S3
Maria Chiara Spadaro S3
Sebastian Sulis Sato NEST
Marco Travagliati NEST
Ilaria Valenti S3
Stefano Valentini NEST
Anna Vianelli S3
Azzurra Volpi NEST

Administrative Staff

Maria Grazia Angelini S3
Elisa Bolognesi S3
Tommaso De Carlo NNL
Luca Del Prete NEST
Lucia Francini NEST
Sandro Guerrazzi NEST
Carmela Iannotta S3
Patrizia Pucci NEST
Maria Giovanna Santoro NNL
Anna Grazia Stefani S3
Ciro Urso NNL
Alessandro Zammillo NNL

Technical Staff

Antonio Graziano Antico NNL
Benedetta Antonazzo NNL
Paolo Barbieri NNL
Ivana Bianco NNL
Davide Calanca S3
Adriana Campa NNL
Sonia Carallo NNL
Giorgio Casalini S3
Paolo Cazzato NNL
Eliana D'Amone NNL
Stefania D'Amone NNL
Gianvito De Iaco NNL
Gianmichele Epifani NNL
Vittorio Federico Fiorelli NNL
Antonio Domenico Gigante NNL
Diego Mangiullo NNL
Mariangela Margarito NNL
Luisa Neri S3
Riccardo Pallini NEST
Elisabetta Perrone NNL
Silvia Rizzo NNL
Maddalena Scandola S3
Gabriella Zammillo NNL

Support Staff @ Genova

Matilde Bolla
Barbara Cagnana
Enrico Camauli
Marco Campani
Paola Corezzola
Monica Dalla Libera
Roberta De Donatis
Fabio Distefano
Francesca Fortunati
Maria Carla Garbarino
Giuseppe Genovese
Danilo Imperatore
Tatiana Marescalchi
Marco Punginelli
Liliana Sciaccaluga
Simone Spinozzi



Highlights Nanotechnology

3D polymer particles by two-photon continuous flow lithography

The control of the shape and composition of polymer particles is a fundamental issue to tailor functional properties, such as self-assembly and diffusion capability. This is particularly crucial for micro-objects with three-dimensional (3D) shape, because of the low production throughput of most of available synthesis methods. Here we introduce a new approach for the production of 3D particles, which combines microfluidics and two-photon lithography. Micro-objects with 3D shapes, low surface roughness and sub-micrometer features are reproduced in continuous runs, greatly increasing the throughput of conventional lithographic methods.

The two-photon continuous flow lithography (TP-CFL) is schematized in Fig. 1 a. A near-infrared, fs-laser is focused in a fluidic micro-channel, where a continuous flow of a pre-polymer solution is established by means of external pumps. The pre-polymer is cured in a small volume (< 400 nm) close to the laser focus, by two-photon absorption. The shape of the so-produced particles is given by the superposition of flow and laser spot motion. For instance, helical particles can be produced by a circular movement of the laser beam in a plane perpendicular to the flow direction (Fig. 1 b-f). In this way we obtained micro-objects with various shapes, such as spherical, bow-tie and helical particles, and polymer fibers (Fig. 1 g-i), varying the laser position and focusing conditions.

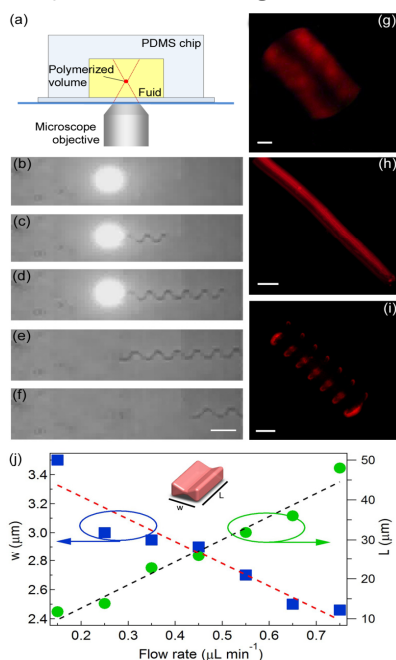


Figure 1.

(a) Schematics of the device geometry and TP-CFL set-up. (b-f) Sequence of frames imaging the synthesis of helical particles. Scale bar: $20 \mu\text{m}$. Time interval between consecutive frames = 600 ms. The bright spot in (b)-(d) corresponds to the laser beam, whereas the pre-polymer flows from left to right. (g-i) Confocal fluorescence microscopy images of bow-tie, fiber and helical particles, respectively. Scale bars: $10 \mu\text{m}$. (j) Bow-tie particle width (w , squares, left vertical scale) and length (L , circles, right scale) vs. solution flow rate. Dashed lines are guide for the eyes.

Contact Person

Andrea Camposeo (andrea.camposeo@nano.cnr.it)

Collaborators

S. C. Laza, M. Polo, A. A. R. Neves, R. Cingolani, D. Pisignano.

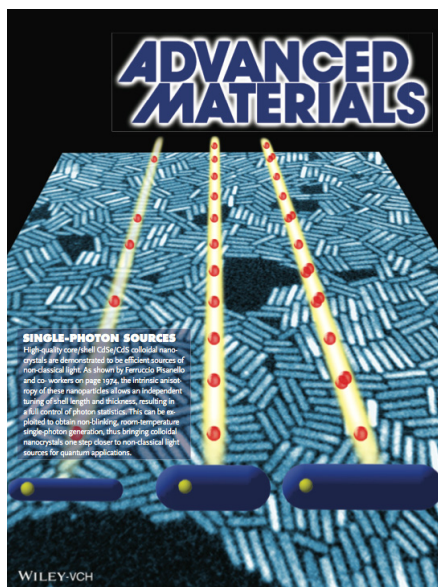
Related publication

Two-photon continuous flow lithography. S. C. Laza, M. Polo, A. A. R. Neves, R. Cingolani, A. Camposeo, and D. Pisignano, *Adv. Mater.* **24**, 1304-1308 (2012).

Single Photon Sources for Quantum Cryptography

CdSe/CdS dot-in-rod (DR) nanocrystals, i.e., semiconductor nanoparticles consisting of a CdSe spherical core surrounded by a rod-shaped CdS shell, recently emerged as efficient sources of non-classical light for quantum cryptography applications. Shell size and shape of DRs dramatically affect their quantum emission properties and single photon emission effectiveness, and they can be exploited to engineer next generation single photon sources for quantum cryptography.

In the field of quantum cryptography based on single photon sources, one of the main goals is the realization of room temperature, non-blinking and high versatile quantum emitters. Several materials have been proposed in past years to achieve this goal, such as color center in diamond nanocrystals, epitaxially grown quantum dots or single molecules. An appealing and cutting edge technology is nowadays represented by colloidal core/shell nanocrystals (NCs), i.e., wet-chemically synthesized semiconductor nanoparticles composed of a crystalline core around which a spherical shell is usually grown. Because of their ultra small size, NCs experience ultra-strong confinement regime and enhance mutual charge-carriers interactions. This increases the efficiency of phenomena that are usually neglected in bulk semiconductors. One of them is non-radiative Auger recombination process, producing pronounced photoluminescence fluctuations due to random ionization of the nanoparticle. Recently, the attention of the scientific community has been focused on the realization of non-blinking nanoparticles, but this usually leads to a drastic reduction of their single photon emission performances, a necessary condition for truly quantum communications.



We experimentally show that NCs size, shape and composition engineering allows one to tune the optical properties of these nanoparticles, thus creating a suitable infrastructure for the optimization of next generation quantum light emitters. Our approach is based on a particular type of colloidal nano-heterostructures, composed of a spherical CdSe core surrounded by a rod like CdS shell. We have already demonstrated that this dot-in-a-rod (DR) configuration can emit single photons with well-defined quantum states following a dipole like radiation pattern. We recently found that the asymmetry of electrons wavefunction can be exploited to obtain both non-blinking behavior and single photon emission, opening the way efficient room temperature quantum light generation.

Figure 1.

Cover of Advanced Material (Wiley) representing the influence of shell length and thickness on single photon and blinking properties of CdSe/CdS dot-in-rods (DRs)

Contact Person

Massimo De Vittorio (massimo.devittorio@unisalento.it)

Collaborators

F. Pisanello, G. Leménager, L. Martiradonna, L. Carbone, S. Vezzoli, P. Desfonds, P. D. Cozzoli, J.-P. Hermier, E. Giacobino, R. Cingolani, A. Bramati

Related publication

Non-blinking single photon generation with anisotropic colloidal nanocrystals: towards room-temperature efficient colloidal quantum sources. F. Pisanello et al., Adv. Mater. **25**, 1974–80 (2013).

Exploring functionalities of Molecular Nanomagnets at the single molecule level

Molecular Nanomagnets (MNM) exhibit fascinating functionalities and they can be used in disparate fields like, for instance, for qubit encoding in quantum information processing or as molecular coolers. Open question is whether these functionalities are still effective when molecules are dispersed on a substrate. In this context, we have developed new procedures for the deposition of MNM on substrates in controlled conditions and for the detection of their functionalities. Thanks to the high element-specificity, chemical selectivity and sub-monolayer sensitivity of the X-ray Magnetic Circular Dichroism we checked to what extent properties of the MNM are retained at the single molecule level. Here we report two paradigmatic examples of this research line.

i) Magnetic anisotropy of Cr₇Ni spin clusters on surfaces.

In two consecutive articles, we addressed the problem of controlling the orientation and determining the magnetic anisotropy in isolated molecular spin clusters. We have investigated the case of molecular Cr₇Ni rings –suitable for qubit encoding- sublimated in ultra-high vacuum conditions and assembled in an ordered fashion on Au(111) surface by using XMCD and theoretical calculations. Fixing the experimental conditions at a temperature $T = 8\text{ K}$ and a magnetic field of 5 T, the angular-dependence of the dichroic signal reveals an easy-axis anisotropy for the Ni magnetization along the direction perpendicular to the ring while the magnetization of the whole Cr₇Ni molecule is preferentially aligned within the ring plane. These features are well reproduced by spin Hamiltonian simulations, which reflect the character of the $S = 3/2$ first excited multiplet, dominating at $T = 8\text{ K}$ and 5 T. Density functional theory (DFT) calculations show that local spin orbit interactions determine an easy axis anisotropy at the Ni site while the Cr magnetic moment turns out to be more isotropic. This is the first direct observation of the interplay between the single ion and the overall magnetic anisotropy in complex (polynuclear) molecular systems

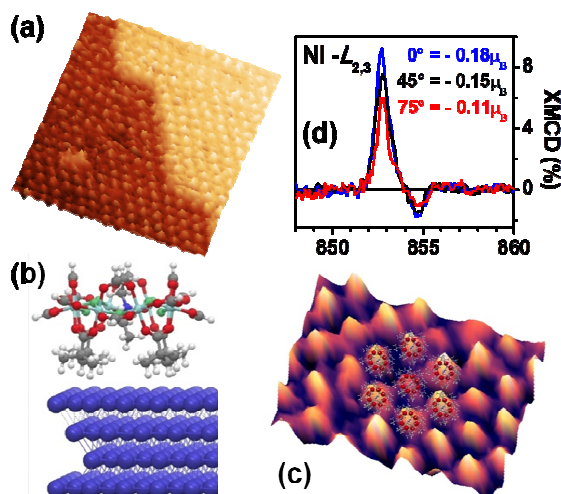


Figure 1.

(a) STM image of a self-assembled monolayer (ML) of Cr₇Ni-bu deposited by sublimation on gold surface. (b) Cr₇Ni-bu molecule on Au(111) after electronic and structural minimization performed by DFT. (c) High-resolution STM image with, superimposed the DFT-predicted structure. Since the interaction among Cr₇Ni-bu molecules is isotropic, to minimize the energy of the system, they assemble themselves with a hexagonal packing. (d) The XMCD spectra at the Ni L_{2,3} edges measured for 1ML on gold for different angles θ of the applied magnetic field, clearly shows an angular dependence which is a direct prove of the magnetic anisotropy of the Cr₇Ni-bu ring. The indicated values are the total magnetic moments at the Ni site.

Contact Persons

Valdis Corradini (valdis.corradini@unimore.it)
Alberto Ghirri (alberto.ghirri@nano.cnr.it)

Collaborators

R. Biagi, V. De Renzi, U. del Pennino, A. Candini, V. Bellini, S. Carretta, P. Santini, J. C. Cezar, E. Otero, G. Timco, R. E. P. Winpenny, R. J. Blagg, E. J. L. McInnes, M. Affronte

ii) Molecular refrigerators

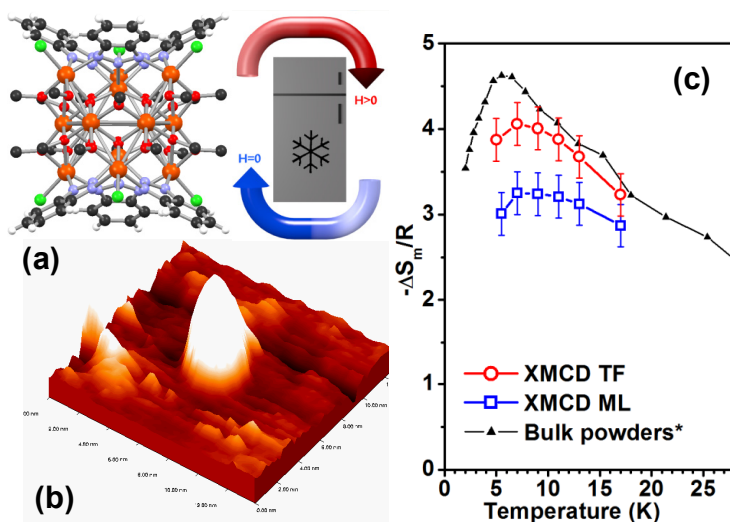
In this work we have investigated the molecular cooler $\text{Fe}_{14}(\text{bta})_6$ to demonstrate that a large magnetocaloric effect is a property held at the single molecule level. To this end, a sub-ML distributions of isolated molecular $\text{Fe}_{14}(\text{bta})_6$ nanomagnets was deposited intact on the Au(111) surface and investigated by XPS, STM, XAS and XMCD spectroscopy. The entropy variation as a function of the applied magnetic field was extracted from the magnetization curves. This allowed, for the first time, to directly observe large entropy variation at the level of single molecule and to establish that cooperative effects, like long range order -which is dominant in conventional magnetic refrigerants-, play only a minor role in this case and giant magnetic cooling power is available at molecular level.

Figure 2.

(a) Molecular structure of the $\text{Fe}_{14}(\text{bta})_6$ nanomagnet which can be considered like a small refrigerator.

(b) STM image of a sub-ML of $\text{Fe}_{14}(\text{bta})_6$ deposited on gold surface by liquid-phase.

(c) Entropy variation respect to temperature derived from the isothermal magnetization curves, vs applied magnetic field, for the Thick-Film and the sub-ML compared with bulk microcrystalline powders.



Related publications

Magnetic anisotropy of Cr₇Ni spin clusters on surfaces. V. Corradini, A. Ghirri, E. Garlatti, R. Biagi, V. De Renzi, U. del Pennino, V. Bellini, S. Carretta, P. Santini, G. Timco, R. E. P. Winpenny, and M. Affronte, *Adv. Funct. Mater.* **22**, 3706-3713 (2012).

Magnetic cooling at single molecule level: a spectroscopic investigation on isolated molecules on surface. V. Corradini, A. Ghirri, A. Candini, R. Biagi, U. del Pennino, G. Dotti, E. Otero, F. Choueikani, R. J. Blagg, E. J. L. McInnes, and M. Affronte, *Adv. Mater.* **25**, 2816-2820 (2013).

The Josephson heat interferometer

The Josephson effect has profound implications going well beyond electrical transport. In 1965, Maki and Griffin predicted that the interplay between Cooper pairs and quasiparticles in tunneling events would provide heat currents with quantum coherence. This phenomenon manifests as a phase-dependent component of the heat current flowing through a thermally biased Josephson junction but its existence was never confirmed experimentally. We describe here the first observation of heat interference and heat diffraction in Josephson-based superconducting microcircuits. Our findings confirm the veracity of the abovementioned predictions and, combined with well-known methods for superconducting phase-biasing, provide a completely new way of mastering heat at the nanoscale.

We have demonstrated the existence of phase-dependent thermal transport through a Josephson heat interferometer. This device is very similar to the well-known electric Superconducting Quantum Interference Device (SQUID). It consists of two superconducting electrodes weakly connected through two Josephson junctions forming a ring threaded by a magnetic field (see Fig. 1a). Unlike conventional SQUIDS, the Josephson heat interferometer must be temperature biased. For this purpose one of the two SQUID branches is heated up to approximately 500 mK while keeping the other one at the minimum temperature, i.e., 240 mK. By varying the magnetic field threading the loop it is possible to modify the macroscopic phase difference between the two condensates, inducing heat interference. The latter is practically reflected into a Φ_0 -periodic variation of the temperature of the hot branch as seen in Fig. 1a, Φ_0 being the flux quantum. Our experiments reveal unequivocally that the phase dependent fraction of the heat current is transmitted from the cold to the hot source, and that heat, which is usually associated with disorder, behaves coherently. Behind these striking consequences lies precisely the Josephson effect, as the phase of the Cooper pair condensate is encoded in the wave functions of the un-paired quasiparticles that transport thermal energy as well as electrical charge.

Even more challenging, we set out to demonstrate the existence of coherent heat diffraction through a single-slit. The latter is realized by means of an extended Josephson junction, as J. S. Rowell did 50 years ago to measure the diffraction pattern of the electric Josephson current. Our device, shown in Fig. 1b, consists of two thermally biased tunnel-coupled superconducting electrodes to which an in-plane magnetic field is applied. Heat diffraction leads to a characteristic Fraunhofer-like temperature modulation that we observe experimentally. These findings provide the complementary demonstration of the “thermal” Josephson effect in weakly-coupled superconductors.

In the same way that the quantum properties of electric charge are being exploited in practical devices, these fascinating properties might lead to completely novel applications. In this regard the realization of *coherent heat circuits* consisting of, for instance, coherent heat transistors, diodes and splitters can be envisioned.

Contact Person Francesco Giazotto (francesco.giazotto@nano.cnr.it)

Collaborators C. Altimiras, A. Fornieri, M.J. Martínez-Pérez, P. Solinas.

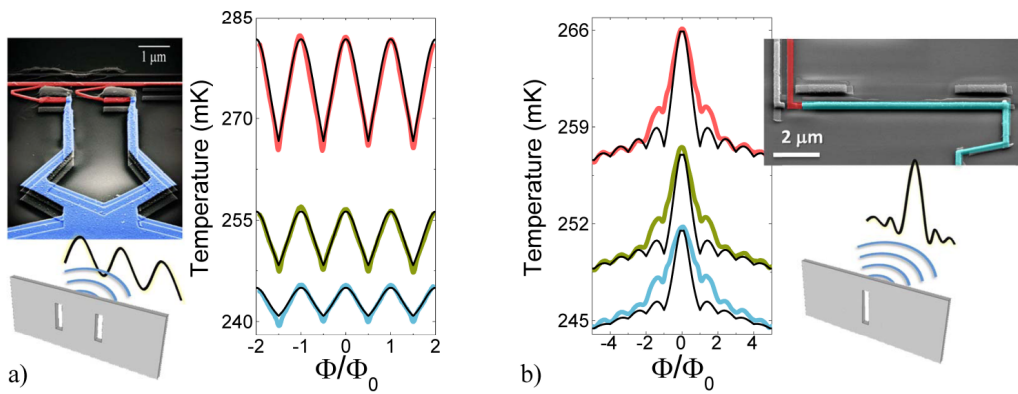


Figure 1.

a) Pseudo-color SEM micrograph of the heat interferometer and temperature modulation (red = hot, blue = cold) of the normal metal electrode coupled to the thermal SQUID. As predicted by the theory, temperature is Φ_0 -periodic in Φ , like the Josephson critical current. b) The temperature modulation resembles a Fraunhofer-like diffraction pattern when heat is transmitted through an extended Josephson junction (SEM image). Color lines are measured temperatures, while black lines are theoretical fits to the experimental data. Both these phenomena occur in full analogy with light interference (a) or diffraction (b) induced by a double- (a) or single- (b) slit, respectively.

Related publication

The Josephson heat interferometer. F. Giazotto and M. J. Martínez-Pérez, *Nature* **492**, 401 (2012).

Hybrid Organic and Inorganic Photovoltaics

In the quest of high efficiency energy sources, recent breakthroughs in the realization of solar cells that exploit wet-chemically prepared hybrid organic/inorganic compounds such as mixed halide perovskite and colloidal nanocrystals (NCs) as active functional elements have drawn the attention of the scientific community to such nanomaterials. In our work we explore the application of both iodide/chloride mixed-halide perovskite $\text{CH}_3\text{NH}_3\text{PbI}_{3-x}\text{Cl}_x$ and IR-absorbing PbS NCs in different device architectures towards high efficiency solution processable solar cells.

Among the early results of the pioneer reports on perovskite-based solar cells, probably the most intriguing discover concerned the application of a iodide/chloride mixed-halide perovskite $\text{CH}_3\text{NH}_3\text{PbI}_{3-x}\text{Cl}_x$ in a so called “meso-superstructured” Solid State Solar Cell, where the perovskite is concomitantly capable of both absorbing light and transporting charge within a mesoporous network. However, an investigation on the exact materials composition and structure is still missing. We have presented a detailed investigation on I/Cl mixed halide self-assembling perovskites.

We showed that Cl incorporation is allowed only at low concentrations (below 3– 4%) in I-based perovskites. The strong difference in the halogen ionic radii interferes with the formation of a continuous solid solution. However, even if the material band gap remains substantially unchanged, incorporation of Cl as a dopant dramatically improves the charge transport within the perovskite layer.

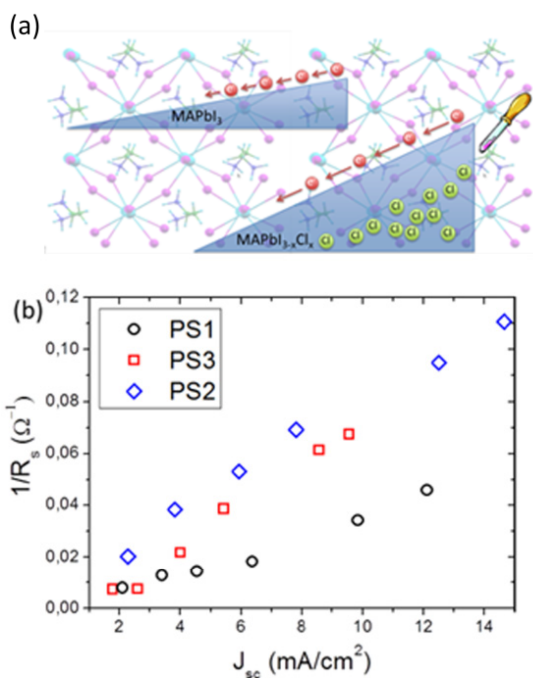


Figure 1.

(a) Cartoon representing the beneficial effect of Cl-doping on the perovskite transport properties. (b) The relationship between reciprocal series resistance and short circuit current density (J_{sc}) for the cells fabricated from $\text{CH}_3\text{NH}_3\text{PbI}_3$ (PS1), $\text{CH}_3\text{NH}_3\text{PbI}_{3-x}\text{Cl}_x$ (PS2) and one intermediate form (PS3). J_{sc} was obtained as a function of light intensity.

Contact Persons

Aurora Rizzo (aurora.rizzo@nano.cnr.it)
Silvia Colella (silvia.colella@nano.cnr.it)

Concerning NC based solar cells, the most efficient NC-based system for photovoltaic application consists of a low band gap PbS quantum dots (QDs) as light harvester coupled with transition-metal oxide TiO_2 as electron acceptor. Despite the tremendous improvement in performance PbS QDs/ TiO_2 solar cells remain far less appealing for potential implementation into flexible plastic technology and large-scale industrial manufacturing because the preparation of the relevant TiO_2 acceptor film usually requires harsh high-temperature processing. We report on the fabrication of high-efficiency all-inorganic solar cells by a novel approach that involves processing of colloidal PbS QDs and anisotropic TiO_2 NCs under room-temperature conditions. The use of preformed TiO_2 NRs avoids the application of a high-temperature annealing step to achieve the oxide in the required crystalline form. In addition, gentle post-deposition processing routes, which are based on mild acidic treatments of PbS QDs and UV-light irradiation of TiO_2 NRs, respectively, are exploited to remove the insulating capping surfactants from the NC surface at room-temperature. Through these procedures we have realized solar cell devices that achieve a power conversion efficiency of $\sim 3.6\%$ on glass and $\sim 1.8\%$ on PET substrates, which is the highest ever reported for entirely inorganic-NC-based solar cells on plastic support.

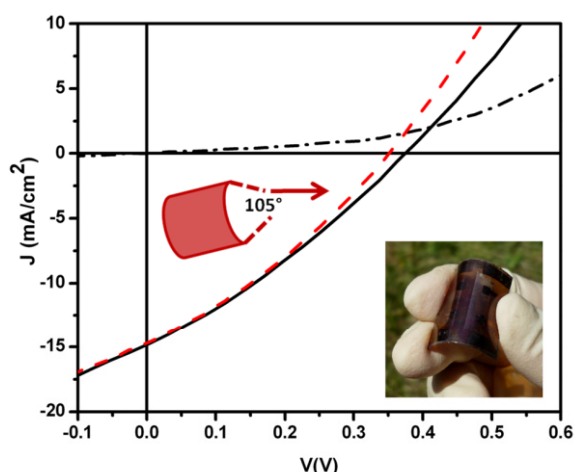


Figure 2.

TiO_2 -NR/PbS-QD NC photovoltaic devices on plastic substrate. Current density-voltage characteristics of the photovoltaic device under zero illumination (dot black curve) and standard illumination when flat (continuous black curve, 1.8% power conversion efficiency) and released to flat after bent to a curvature of 105° (red curve, 1.7% power conversion efficiency). Inset, photograph of the TiO_2 -NR/PbS-QD plastic solar cell.

Related publications

MAPbI_{3-x}Cl_x Mixed Halide Perovskite for Hybrid Solar Cells: The Role of Chloride as Dopant on the Transport and Structural Properties. S. Colella, E. Mosconi, P. Fedeli, A. Listorti, F. Gazza, F. Orlandi, P. Ferro, T. Besagni, A. Rizzo, G. Calestani, G. Gigli, F. De Angelis, and R. Mosca, *Chemistry of Materials* **25**, 4613 (2013).

Fabrication of flexible all-inorganic nanocrystal solar cells by room-temperature processing. A. Loidice, A. Rizzo, G. Grancini, M. Biasiucci, R. Belviso, M. Corricelli, M. L. Curri, M. Striccoli, A. Agostiano, P. D. Cozzoli, A. Petrozza, G. Lanzani, and G. Gigli, *Energy & Environmental Science* **6**, 1565 (2013).

Nanoscale Thermoelectrics

Thermoelectric physics has been attracting a revived interest in recent years. This is mostly due to the progress of nanoscience and nanotechnology and to the opportunities offered for the design of novel nanostructures able to outperform known bulk materials. Activities at CnrNano have led to the establishment of a new platform for the investigation of the thermoelectric properties of isolated nanostructures. A promising large thermovoltage in excess of 1mV was obtained over single InAs semiconductor nanowires and a novel method for the estimation of electron mobility based on the Seebeck effect was demonstrated.

The achievement of efficient solid-state thermoelectric converters requires a non-trivial control of interdependent material parameters and can be expressed in terms of the maximization of the figure of merit $ZT = \sigma S^2 T / \kappa$, where S is the Seebeck coefficient, σ and κ are the electrical and thermal conductivities, respectively, and T is the average operation temperature. Large ZT values proved elusive over the past decades despite the great design flexibility warranted by semiconductor heterostructured materials. While κ suppression in nanostructured materials has been successfully demonstrated, unclear and potentially wide optimization margins exist on the so-called “power factor” σS^2 . In particular, the role of band engineering remains still unclear and calls for a deeper investigation effort. An important aspect of research on nanoscale thermoelectrics consists in the development of reliable test platforms to benchmark the properties of these challenging materials.

Our research team at NANO-Pisa has recently demonstrated an innovative differential heater shown in Fig. 1, that allows to establish a very large thermal gradient up to 1 Kelvin degree over barely 100nm, while allowing to control the nanostructure electronic configuration by field effect. This set-up was used to precisely map the Seebeck coefficient of single nanowires as a function of the temperature and of the carrier density and to identify the best carrier density configuration for the maximization of their thermopower.

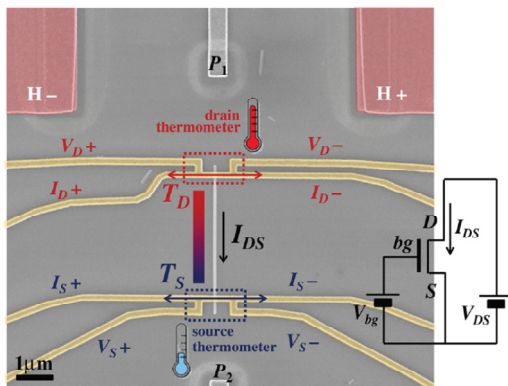


Figure 1.

Scanning electron micrograph of one of the studied devices: an InAs nanowire on a SiO_2/Si substrate is connected to two resistive Ti/Au thermometers (yellow). A strong thermal gradient is induced using a buried heater (contacts visible in pink). The setup allows the simultaneous determination of the IV characteristics of the nanowire and the induction and measurement of different temperatures T_1 and T_2 at the two contacts.

Contact Person

Stefano Roddaro (stefano.roddaro@nano.cnr.it)

Collaborators

D. Ercolani, F. Giazotto, V. Piazza, F. Rossella, L. Sorba, F. Beltram.

In particular, our experimental arrangement yielded a detailed mapping of $S(\sigma, T)$, $\sigma S^2(\sigma, T)$ and $S/T(\sigma, T)$, (see Fig. 2) that were compared with classic models for thermoelectric transport in degenerate semiconductors. The adopted approximations led to an alternative estimate of electron mobility $\mu_e \approx 11000 \text{ cm}^2/(\text{V s})$ in the InAs NW. This value is significantly larger than the one obtained by field-effect, $\mu_{e, \text{FE}} \approx 5000 \text{ cm}^2/(\text{V s})$, on the same wire. The discrepancy can be understood in terms of the influence of slow surface- and trap-charge dynamics on field-effect mobility measurements, an influence that was shown to be negligible on S vs σ dependence. The present results indicate that special care must be taken in the interpretation of transport results based on field effect in these nanostructures and cooling devices.

Work is in progress for the development of novel opto-electronic methods for the determination of the thermal conductivity of single wires and for the estimation of the ZT factor of our nanomaterials. Future perspectives include the investigation of thermoelectric effects in advanced quantum confined nanowires based on the InAs/InSb/InP III-V system, for the achievement of a more efficient energy conversion and of nanoscale heating.

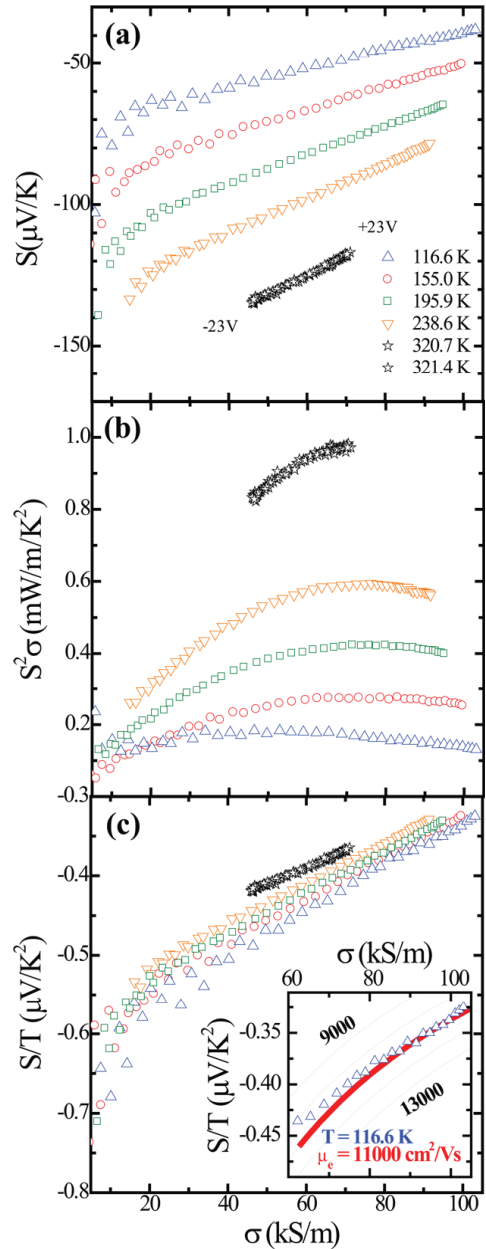


Figure 2.

Panel a: selected curves $S(\sigma)$ for one of the studied devices at temperatures $T = 116.6, 155.0, 195.9, 238.6, 320.7$, and 321.4 K . The corresponding power factor $S^2\sigma$ is shown in panel b. The dependence of S is slightly sublinear as visible in panel c, showing that S/T curves almost overlap between 120 K and 320 K. Inset: the dataset at $T = 116.6 \text{ K}$ is consistent with an electron mobility $\mu_e \approx 11000 \text{ cm}^2/(\text{V s})$ in the high carrier concentration limit.

Related publication

Giant Thermovoltage in Single InAs Nanowire Field-Effect Transistors. S. Roddaro, D. Ercolani, M. A. Safeen, S. Suomalainen, F. Rossella, F. Giazotto, L. Sorba, and F. Beltram, *Nano Lett* **13**, 3638 (2013).

Room-Temperature THz nanodetectors

Nanotransistors offer great prospect for the development of innovative THz detectors based on the non-linearity of transport characteristics. Semiconductor nanowires are appealing for their one-dimensional nature and intrinsically low capacitance of the devices, while graphene, with its record-high room-temperature mobility, has the potential to exploit plasma wave resonances in the transistor channel to achieve high-responsivity and tuneable detection. We have demonstrated a first generation of devices in both systems, with performances already strongly competitive in terms of noise, frequency range, as well as response speed.

Photodetection of far-infrared radiation is relevant for a variety of strategic imaging applications, ranging from medical diagnostics to process control and security. THz rays can in fact penetrate commonly used dielectric materials, otherwise opaque for visible and mid-infrared light, allowing detection of substance-specific spectroscopic features and a sub-millimeter diffraction-limited lateral resolution. In this perspective, the development of a breakthrough solid-state technology for fast, room-temperature (RT) THz detectors, eventually integrated in high-speed multi-pixel arrays, is highly desired.

Recently, electronic devices based on the gate-modulation of the conductance channel by the incoming radiation have been realized in high-electron-mobility transistors (HEMT), field effect transistors (FET), and Si-MOSFET architectures, showing fast response times and high detectivities, as well as the possibility of implementing multi-pixel focal-plane arrays. The operating mechanism of a FET detector is not trivial, but can be intuitively interpreted as deriving from the non-linear dependence of the FET channel current on the gate voltage near the pinch-off point.

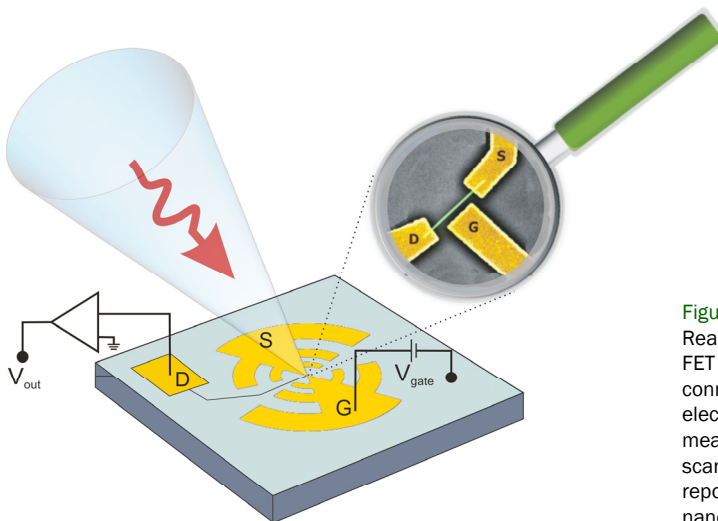


Figure 1.

Realization scheme of a nanostructured FET detector. Log periodic antennas are connected to source (S) and gate (G) electrodes, while output voltage is measured at the drain (D). In the inset, a scanning electron microscope picture is reported showing a FET based on an InAs nanowire channel.

Contact Person

Alessandro Tredicucci (alessandro.tredicucci@nano.cnr.it)

Collaborators

M. S. Vitiello, F. Beltram, S. De Bonis, D. Ercolani, V. Pellegrini, M. Polini, A. Pitanti, L. Romeo, L. Sorba, D. Spirito, A. Tomadin, L. Vicarelli, L. Viti, D. Coquillat, W. Knap, F. Teppe, A. Lombardo, A. C. Ferrari.

As nanoscale FET channel, the choice of InAs nanowires (NW), with narrow bandgap and degenerate Fermi-level pinning, reveals particularly successful in preserving good detecting performances while scaling down the dimension of the device to increase the detected frequency up to the 1.5-3 THz range, accessible with quantum cascade laser (QCL) sources. Photoresponse experiments performed by using either a 0.3 THz electronic source or a set of THz QCLs operating between 1.5 THz and 2.8 THz demonstrate that the responsivity is highly dependent on parameters like NW diameter, NW doping concentration, antenna design, impedance matching, etc. Values up to 110 V/W have been reached with impressive noise equivalent powers ($NEP \sim 6 \times 10^{-11}$ W/(Hz)^{1/2} and a MHz modulation bandwidth.

On the other hand, graphene supports plasma waves that are weakly damped in high-quality samples. Graphene plasma-based FET detectors have therefore the potential to outperform other terahertz detection technologies. In first experiments, a simple top-gate antenna-coupled configuration has been employed for the excitation of overdamped plasma waves in the channel of single- and bi-layer graphene FETs. At 300 GHz, responsivities of the order of V/W have been observed at room temperature, and the signal displays a characteristic change of polarity at the Dirac point, in good agreement with theoretical models. First imaging applications of the detector have also been developed.

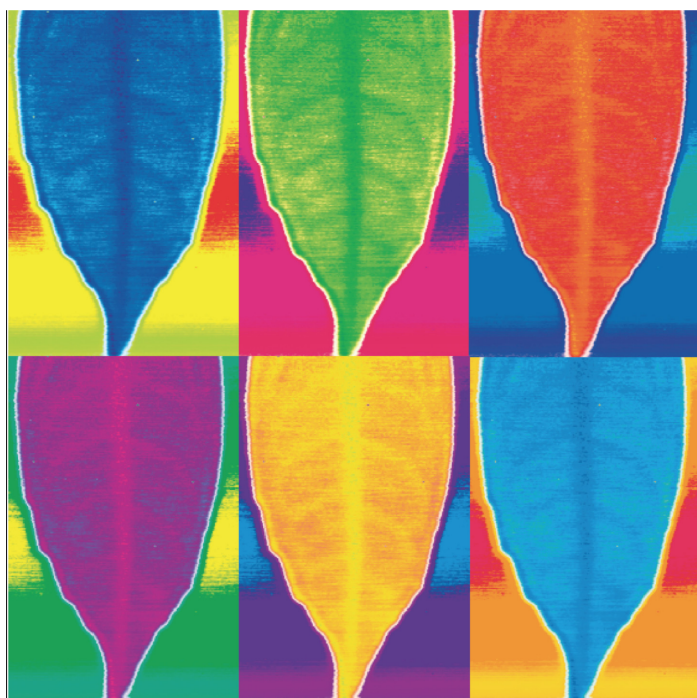


Figure 2.

THz "radiography" of a fresh leaf acquired at 300 GHz with a graphene FET sensor. Veins are clearly visible because of the higher water content.

Related publications

Graphene field-effect transistors as room-temperature terahertz detectors. L. Vicarelli, M. S. Vitiello, D. Coquillat, A. Lombardo, A. C. Ferrari, W. Knap, M. Polini, V. Pellegrini, and A. Tredicucci, *Nature Mater.* **11**, 865 (2012).

Semiconductor nanowires for highly sensitive, room-temperature detection of terahertz quantum cascade laser emission. M. S. Vitiello, L. Viti, L. Romeo, D. Ercolani, G. Scalari, J. Faist, F. Beltram, L. Sorba, and A. Tredicucci, *Appl. Phys. Lett.* **100**, 241101 (2012).

Terahertz Quantum Cascade Lasers

Quantum Cascade Lasers (QCLs) can be considered the primary achievement of electronic band structure engineering, showing how artificial materials can be created by quantum design with tailor-made properties otherwise non-existing in nature. This makes QCLs powerful testing grounds for the fundamental physical parameters determined by their quantum nature, like the intrinsic linewidth (LW) of the laser emission. The potential of Terahertz QCLs as quantum limited linewidth sources for metrological-oriented applications is here demonstrated together with their versatility as active media to realize high power quasi-crystal resonators and to address biomedical or spectroscopic application is a low-loss guided configuration.

We recently reported experimental evidence of LW values approaching the quantum limit in THz QCLs. By performing noise measurements with unprecedented sensitivity levels we demonstrated that properly designed semiconductor-heterostructure lasers can unveil the mechanisms underlying the laser intrinsic phase-noise, revealing the link between the device properties and its quantum-limited LW. Stemming from their high spectral purity, THz QCLs are proving to be the key technology for a number of versatile techniques like cold molecules physics and high-precision trace-gas sensing. Properly combined with Frequency-Comb-Synthesizers providing a direct and broadband phase and frequency reference, THz QCLs enable metrological-grade spectroscopy with unprecedented sensitivity levels.

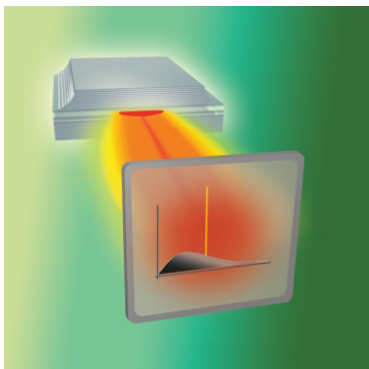


Figure 1.
Schematic sketch of the ultra-narrow emission linewidth of a THz QCL.

Tailoring the shape, the symmetry, and the frequency of the optical resonator eigenmodes while simultaneously allowing stable single mode operation is one of the main routes toward a practical implementation of the THz QCL technology in a large variety of application fields. Distributed feedback (DFB) action is one of the common routes toward this objective. Although DFB patterns are normally periodic in order to match the shape of guided plane waves, a fine control over vertical emission is also possible either via second-order Bragg reflections or by introducing optimally shaped defects in the periodic pattern. In this context, quasi-periodic lattices offer an elegant solution showing rich structures of Bragg peaks in their reciprocal space: we achieve vertical emission from THz QCLs based on a two-dimensional quasi-periodic Penrose photonic lattice with ≈ 60 mW peak power and peculiar conical beam profiles.

Contact Person Miriam Serena Vitiello (miriam.vitiello@sns.it)

Collaborators F. Castellano, M. Nobile, A. Ronzani, A. Tredicucci, S. Bartalini, A. Consolino, P. De Natale, V. Spagnolo, G. Scamarcio, H. E. Beere, D. A Ritchie, E. Linfield, G. Davis, L. Lee, O. Mitrofanov.

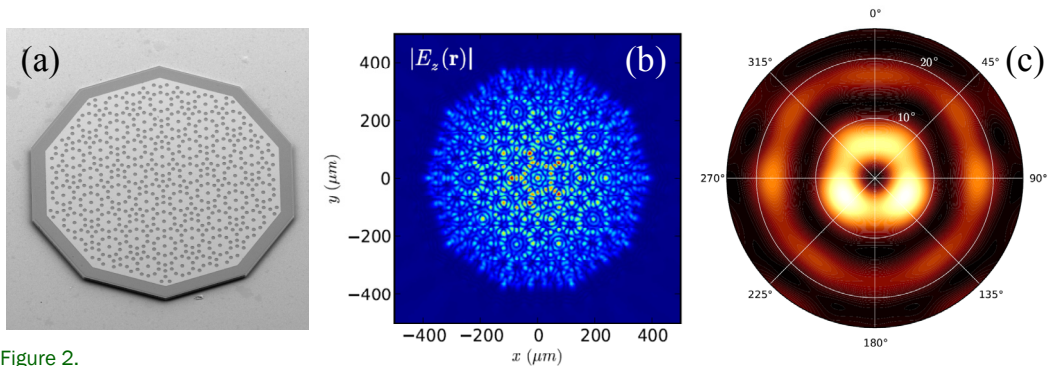


Figure 2.

(a) Scanning electron microscope (SEM) image of a double-metal vertical emitting THz QCL having a quasi period DFB Penrose pattern. (b) TM high quality factor eigenmode of the resonator simulated with the finite elements method on an equivalent 2D dielectric system confined by absorbing boundaries. (c) Measured far-field distribution.

Low-loss waveguides with good mode selectivity in the far-infrared are quite difficult to realize due to the high Ohmic losses in metals and the relatively high absorption coefficient of most dielectric materials in this spectral range. Recently we demonstrated a promising new experimental approach to efficiently couple THz QCL with THz hollow waveguides having a sequence of different metallic or dielectric inner coatings. Under proper polarization/coupling conditions, the TE_{01} and the TE_{11} waveguide modes can be easily converted to a hybrid one, allowing the propagation of THz QCL beams with transmission losses as low as 1.5 dB/m, bending losses <1.1 dB and reasonably high coupling efficiencies (87%), promising for either quartz enhanced photoacoustic sensing or endoscopic applications.

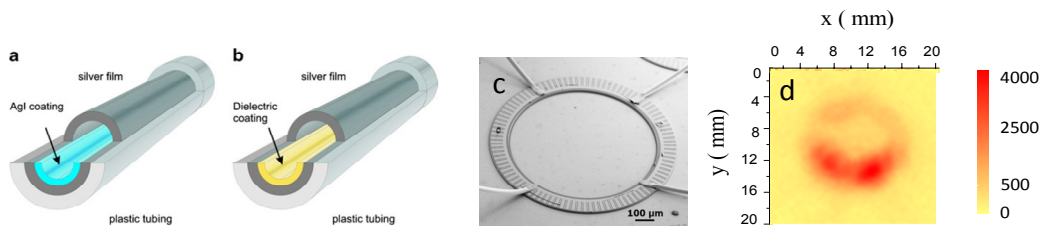


Figure 3.

(a) Schematic structure of a hollow Ag/AgI-coated polycarbonate waveguide and (b) the same with a dielectric layer deposited on silver film. (c) SEM image of a double-metal micro-ring THz QCL. (d) Far-field spatial intensity distribution of a 140 mm long waveguide with a 1.0 mm bore diameter having an ultrathin AgI coating of 1 μm and excited by an azimuthally polarized microring distributed QCL operating at 3.2 THz.

Related publication

Quantum-limited frequency fluctuations in a Terahertz laser. M. S. Vitiello, L. Consolino, S. Bartalini, A. Taschin, A. Tredicucci, M. Inguscio, and P. De Natale, *Nature Photon.* **6**, 525-528 (2012).

Piezoelectric devices based on nanofibers

Piezoelectric materials polarize by means of spatially-separated electrical charges of opposite sign in response to an external stimulus that produces a mechanical deformation. By properly designing both materials and devices a desired voltage bias can be generated. We have introduced large area, flexible piezoelectric materials that consist of free-standing, three-dimensional architectures of piezo-polymer nanofibers. Pressure sensors with ultra-high sensitivity in the low pressure regime (0.1 Pa) and the feasibility for use in solid-state accelerometers measuring physical movements, pulsations and changes in orientation have been demonstrated.

The development of multifunctional, portable and flexible devices for applications, which involve the integration with the human body or which optimize human-like manipulation schemes in robotics, is particularly relevant in the emerging field of self-powered electronics. In this framework, piezoelectric polymers, in forms that enable bending and stretching, are attractive for pressure/force sensors and mechanical energy harvesters. These materials exploit deformations induced by small pressures, mechanical vibration, stretching/compression and bending. Compared to inorganic materials, piezo-polymers combine structural robustness with ease and flexibility of processing and large sensitive areas. In the last few years, electrospinning, a promising nanofabrication method coupling electrical phenomena and fluids, has been demonstrated to be valuable for producing nanofibers with enhanced piezo-response. Indeed, elongational forces and electric fields naturally cause local electrical poling and, by consequence, enhanced properties. In this way we have realized free-standing films of highly aligned piezoelectric fibers (Fig. 1a and 1b) where the formation of inter-fibers mesoscopic joints promotes high mechanical robustness (Fig. 1c). Infrared spectroscopy and X-ray studies indicate that the piezoelectric properties of the array are enhanced with respect to films and fibers deposited in a random configuration. This result can be attributed to the combined effect of the high electric field and of strong stretching forces imparted during the array fabrication. The resulting superior characteristics make such array of fibers promising as building blocks for flexible, large area and lightweight devices. Ultra-high sensitivity for measuring pressure (0.1 Pa), accelerometers, vibrometers and orientational sensors have been achieved (Fig. 1d).

The research leading to these results has received funding from the European Research Council under the European Union's Seventh Framework Programme (FP7 ERC Starting Grant "NANO-JETS").

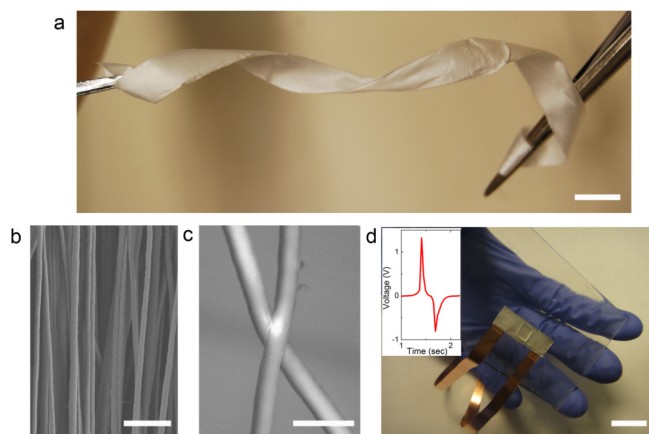


Figure 1.

a) Prototypal free-standing mat of piezo-fibers. Scale bar, 1 cm. b) SEM micrograph of aligned electrospun fibers. Scale bar, 2.5 μm . c) Particular of mutual inter-fiber joint formed during the deposition process. Scale bar, 1 μm . d) Photographs of a flexible device mounted on an elastomeric substrate. Inset: Voltage generated from the device under dynamic bending tests at 1 Hz.

Contact Person Luana Persano (luana.persano@nano.cnr.it)

Collaborators C. Dagdeviren, Y. Su, S. Girardo, D. Pisignano, Y. Huang, J. A. Rogers.

Related publication *High performance piezoelectric devices based on aligned arrays of nanofibers of poly(vinylidene fluoride-co-trifluoroethylene).* L. Persano, C. Dagdeviren, Y. Su, Y. Zhang, S. Girardo, D. Pisignano, Y. Huang, and J. A. Rogers, Nat. Commun. **4**, 1633 (2013).



Highlights Nanoscience

A polariton transistor, towards all-optical logics

Strongly coupled light-matter quasi-particles, polaritons, bring together the antagonist properties of photons and excitons (electron-hole pairs). Recently, these exotic semiconductor quasi-particles have shown to undergo the transition to a condensed state of matter called Bose-Einstein condensate (BEC). This feature empowers them with unique properties which are not limited to the investigation of fundamental questions regarding novel quantum phenomena of Bose-Einstein condensed fluids in a semiconductor chip and at room temperature, but indeed extend further into the semiconductor implementation of BEC to bring quantum physics in tomorrow's technology. In this work we have been able to demonstrate a fully working AND and OR gates by making use of a polariton transistor. Such a device shows a record activation power of a few atto Joules per square microns while using switching times of less than a few pico seconds.

In the past years, an incredibly rich phenomenology of quantum effects spanning from the demonstration of superfluid flow and persistent currents to the observation of a complex and important dynamics of vortex formation and movement has been shown to appear in polariton condensates. More recently, thanks to the easy way of controlling and manipulating polariton states, as well as their fast dynamics, it has been demonstrated that polaritons can be used as the perfect test-bed for the study of quantum phenomena which are hard to observe in other mesoscopic systems.

In this context, the observation of these quantum phenomena like condensation and superfluidity may open the way to the realisation of integrated semiconductor devices working with virtually no dissipation and no activation threshold (threshold-less lasers). The use of polariton quantum fluids, with organic and inorganic semiconductors, as mediating particles in integrated logics, which are not making use of electronic components, is highly appealing given the important non-linearities which are intrinsically inherited by such particles. Moreover, the ability to condense in a coherent state may lead to further advantage in terms of dissipation, heating, and the capability to carry extra information in the phase of the quantum state. The results presented in this work show that using polariton states with finite velocities it is possible to realize an all-optical transistor based on the propagation of polariton fluids in the chip plane. Furthermore, as shown schematically in figure 1, we demonstrate that one transistor is able to trigger the on state of another (spatially separated) transistor.

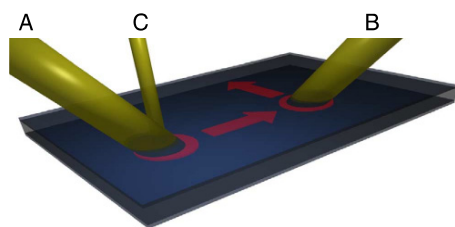


Figure 1.

Scheme of the working principle of a polariton transistor. A beam of light A is used as address for the first transistor. Another beam C, the control beam, can trigger the polariton state into resonance with A by exploiting the strong polariton interactions and letting a polariton flow, 20 times stronger, to travel towards the direction of another transistor B, which, in turn, will be triggered, demonstrating the cascability of the device.

Contact Person

Dario Ballarini (dario.ballarini@nano.cnr.it)

Collaborators

M. De Giorgi, E. Cancellieri, R. Houdré, E. Giacobino, R. Cingolani, A. Bramati, G. Gigli, D. Sanvitto.

This operation takes place all inside the microcavity, allowing for multiple interconnections to occur in the plane of the semiconductor chip. We can finally prove in figure 2, where two outputs are used as inputs into one transistor, the AND/OR logic operation as a three-terminal system. The natural extension of this research would be the exploit of the truly quantum nature of these fluids with the implementation of entanglement polariton pairs in quantum logic circuits.

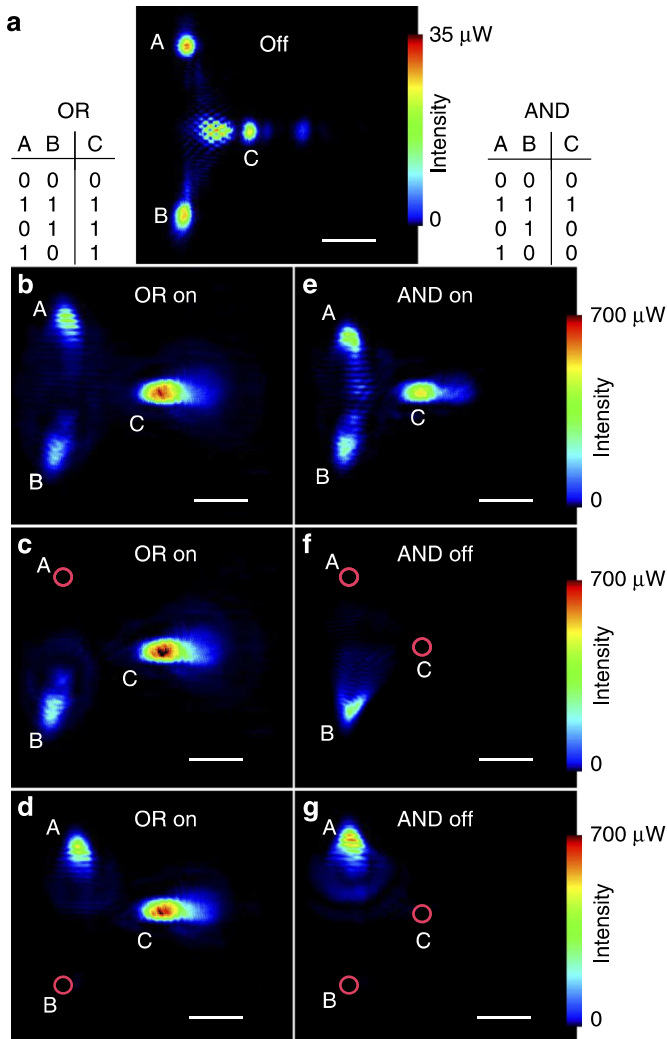


Figure 2.

Demonstration of an AND and OR gate using 3 polariton transistors; a) the off state; b), c), d) the logic OR operation; e), f), g) the logic AND operation.

Related publications *All-optical polariton transistor.* D. Ballarini, M. De Giorgi, E. Cancellieri, R. Houdré, E. Giacobino, R. Cingolani, A. Bramati, G. Gigli, and D. Sanvitto, *Nature Communication* **4**, 1778 (2013).

Control and Ultrafast Dynamics of a Two-Fluid Polariton Switch. M. De Giorgi, D. Ballarini, E. Cancellieri, F. M. Marchetti, M. H. Szymanska, C. Tejedor, R. Cingolani, E. Giacobino, A. Bramati, G. Gigli, and D. Sanvitto, *Physical Review Letters* **109**, 266407 (2012).

Oxide-driven self-assembly of ordered metal nanoparticles

Coincidence lattice formed between two mismatched thin films have been shown to act as template for the organization of nanoparticles. In this work we have shown that the periodicity generated on the surface of a crystalline MgO film grown on a Mo(001) support induces a long-range ordered ensemble of Fe nanoparticles for electronic, magnetic, and chemical applications. The structural and electronic properties of this super-lattice have been analyzed by means of scanning tunnelling microscopy and density functional theory. The variations in structure and electronic properties on the oxide surface modulate the adsorption landscape for metal atoms and give rise to the observed ordering phenomena.

Nanostructured surfaces of high uniformity form the basis for various applications in optics, heterogeneous catalysis and gas sensing. Whereas powerful lithographic techniques are available for patterning at the μm -scale, self-assembly is commonly exploited in the nm regime. For this purpose a suitable robust template is the regular network of misfit dislocations developed when thin films are grown on a substrate with slightly different lattice parameters. They introduce modulation of several surface electronic properties, such as workfunction, surface dipole, and available state-density for hybridization, producing binding sites that can be decorated with suitable nanoparticles.

We have explored the template effect induced by an MgO thin film grown on a Mo(001) support. The 5% lattice mismatch between the respective bulk systems leads to the development of a square-shaped coincidence lattice of 5.5 nm periodicity, strictly related to regular modulations of several MgO-Mo interface properties (Fig. 1a). This periodicity induces site-specific nucleation and spatial ordering of Fe nanoparticles with small size-distribution, as revealed by STM (Fig. 1b).

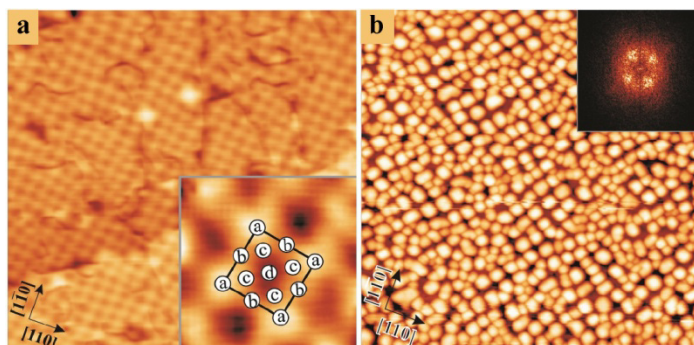


Figure 1.

STM topographic images of (a) 5 ML MgO/Mo(001) ($80 \times 80 \text{ nm}^2$) and (b) 3 ML Fe deposited onto ($100 \times 100 \text{ nm}^2$). Inset in (a) shows the superlattice cell and the relative sites (a site: Mg-on-Mo interfacial register; d site: O-on-Mo register). The spatial ordering of the Fe particles in (b) becomes evident in the fast-Fourier transform shown in the inset.

Contact Person

Stefania Benedetti (stefania.benedetti@nano.cnr.it)

Collaborators

S. Valeri, N. Nilius, H.-J. Freund, J. Goniakowski, C. Noguera.

The thermodynamic incentives for the observed organization are elucidated by DFT calculations (Fig. 2). Individual Fe atoms preferentially bind to regions of high workfunction that enable electron transfer from the ad-species into the support (Fig. 2a,c). Particle growth preferentially occurs in zones of contracted lattice parameter, where metal-metal and metal-oxide interactions can be optimized (Fig. 2b). Both constraints favor particle growth in the Mg-Mo domains of the lattice (site a). Owing to the high uniformity of the ensembles, distinct particle properties can thus be explored with non-local spectroscopic techniques. This opens the way to address fundamental questions in heterogeneous catalysis, magnetism, and nano-optics. As periodic modulations of surface properties are common for coincidence lattices, similar ordering phenomena are expected to occur for many other systems.

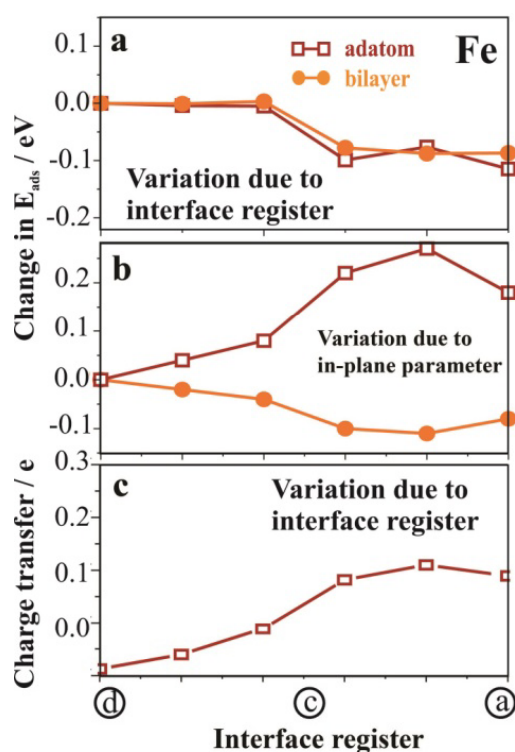


Figure 2.

Relative binding energies (per atom, as calculated by DFT) for Fe adatoms and bilayers adsorbed on a 3 ML thick MgO/Mo(001) film as a function of superlattice cell site (interface register) in Fig. 1a (a) due to charge transfer (calculated with a constant in-plane lattice parameter) and (b) related to in-plane parameter variation across the cell. (c) Charge transfer shown as a function of interface register.

Related publication

Steering the Growth of Metal Ad-particles via Interface Interactions Between a MgO Thin Film and a Mo Support. S. Benedetti, F. Stavale, S. Valeri, C. Noguera, H.-J. Freund, J. Goniakowski, and N. Nilius, Adv. Func. Mater. **23**, 75–80 (2013).

Metallic-like stoichiometric copper sulfide nanocrystals: phase- and shape-selective synthesis, near-infrared surface plasmon resonance properties, and their modeling

We have demonstrated a phase-selective colloidal route to anisotropic stoichiometric covellite CuS nanocrystals which can exhibit intense, size-tunable localized surface plasmon resonance (LSPR) in the near-infrared range despite their vacancy-undoped structure. On the basis of theoretical calculations performed by the Discrete Dipole Approximation method, the LSPR response of the nanocrystals and its geometry dependence have been interpreted as arising from the inherent metallic-like character of CuS, allowed by a significant density of lattice-constitutional valence-band free holes. Coherent excitation of symmetric radial breathing modes has been observed for the first time in transient absorption experiments at LSPR wavelengths.

Colloidal self-doped nanocrystals (NCs) of metal chalcogenides and oxides represent an emerging class of functional nanoscale entities with dual semiconductor–plasmonic nature, which integrate the distinctive optoelectronic properties of low-dimensional semiconductors and localized surface plasmon resonance (LSPR) response. The plasmonic behavior arises from collective oscillations of excess-free carriers associated with constitutional vacancies in the lattice, leading to intense extinction bands in the near-infrared (NIR) range.

The present work expands the available selection of plasmonic-active semiconductor NCs, demonstrating that a nonstoichiometric lattice may not represent a stringent material requirement for generating LSPRs. Here, we have focused on hexagonal covellite CuS, a stoichiometric member of the broad family of copper sulfides, which can intrinsically allow for a significant density of valence-band-delocalized holes without the need for intervening cation vacancies in the lattice. We have developed a colloidal approach for the phase-selective synthesis of monodisperse anisotropic CuS disk-shaped NCs that can be tailored over a broad range of adjustable sizes. The nanodisks exhibit a single, intense extinction band at NIR wavelengths, which entails the convoluted contributions of a minority out-of-plane and a dominant in-plane dipolar LSPR mode. The experimental spectra have been satisfactorily reproduced and interpreted on the basis of Discrete Dipole Approximation calculations performed within the framework of the Drude–Sommerfeld model. Combined experimental and theoretical analyses of the optical response of the nanodisks and its geometry dependence confirm the inherent metallic-like character of the stoichiometric hexagonal lattice of the NCs. The high density of free hole carriers supporting LSPR ($\sim 10^{22} \text{ cm}^{-3}$) and the NC monodispersity account for the unprecedented detection of coherent excitation of symmetric radial breathing modes in transient absorption experiments at LSPR wavelengths.

Contact Person Davide Cozzoli (davide.cozzoli@unisalento.it)

Collaborators Y. Xie, L. Carbone, C. Nobile, V. Grillo, S. D'Agostino, F. Della Sala, C. Giannini, D. Altamura, C. Oelsner, C. Krysch.

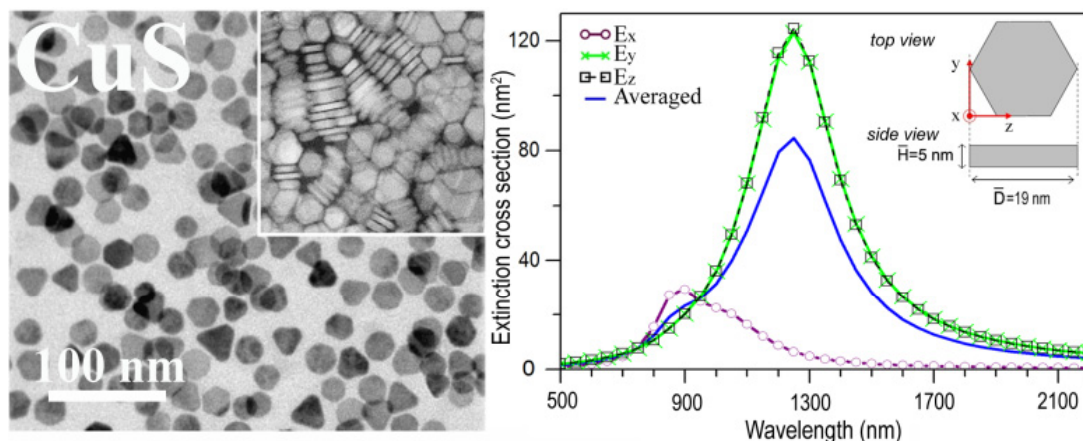


Figure 1.

Left panel: Bright-field and dark-field (inset) transmission electron microscopy images of colloidal CuS nanodisks. Right panel: Extinction scattering cross sections of CuS nanodisks (thickness=5 nm, diameter=19 nm) in solution phase, calculated for incident light polarized along the transverse (x) and longitudinal axis directions (y, z), and with orientational averaging.

Related publication

Metallic-like Stoichiometric Copper Sulfide Nanocrystals: Phase- and Shape-Selective Synthesis, Near-Infrared Surface Plasmon Resonance Properties, and Their Modeling. Y. Xie, L. Carbone, C. Nobile, V. Grillo, S. D'Agostino, F. Della Sala, C. Giannini, D. Altamura, C. Oelsner, C. Kryschi, and P. D. Cozzoli, *ACS Nano* **7**, 7352-7369 (2013).

Nonuniform scaling applied to surface energies of transition metals

The description of two dimensional charge distributions is of special interest for a variety of systems, from solid-solid interfaces, to sheet-shaped materials, topological insulators, and even simple systems as metal surfaces. The difficulty in describing a thin charge layer for conventional functionals of density functional theory is here overcome by a new generalized gradient approximation form that, by respecting scaling laws and exact constraints, properly describes both bulk properties and surface electronic behavior. Transition and noble metals are a practical, interesting example of first application of the new functional, which definitely improves surface energy prediction for these d-electrons correlated elements.

The quasi-two-dimensional (Q2D) electronic distributions constitute a challenge for density functional theory (DFT), due to the high non-locality inherent in the sharp charge-vacuum interface. Refined, high-level correlated methods can properly describe the dimensional 3D-2D crossover, at the price of high or unaffordable computational complexity and costs. In this work, it has been developed a generalized gradient approximation (GGA) exchange-correlation functional, called Q2D-GGA, built satisfying exact constraints and relations imposed by scaling laws. The Q2D-GGA has been tested on two model systems (see Fig. 1), and shown to perform quite well in the 2D regime, in agreement with benchmark data from high-correlated methods.

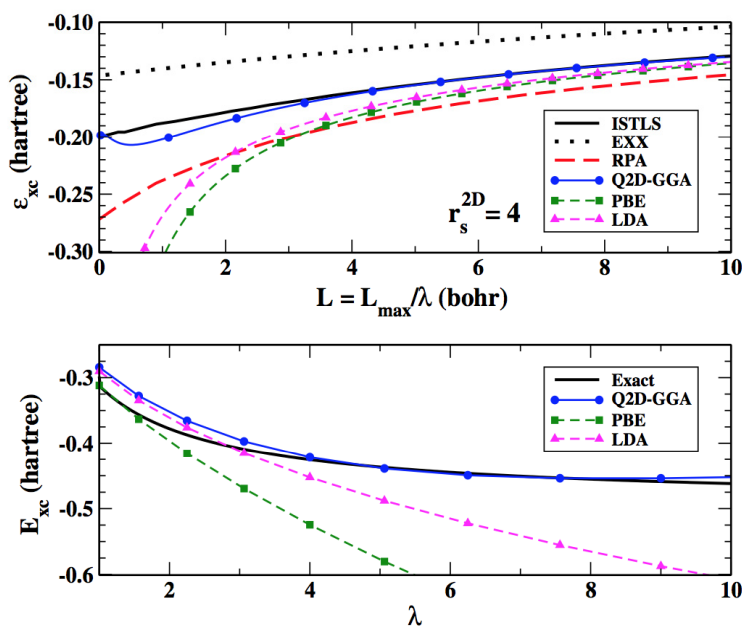


Figure 1. Exchange-correlation energy for (top) the infinite barrier model for the Q2D electron gas ($r_s^{2D} = 4$), as a function of the quantum-well thickness ($L_{\max} = 15.39$), and (bottom) for the non uniformly scaled hydrogen atom, as function of the scaling parameter λ . Results for the Q2D-GGA are compared with data from high-correlated methods and from other common functionals (LDA, PBE).

Contact Person Fabio Della Sala (fabio.dellasala@nano.cnr.it)

Collaborators L. Chiodo, L. A. Constantin, E. Fabiano.

The strength of the Q2D-GGA is well demonstrated when applied to a number of noble and transition metal (111) surfaces, from the quasi-free-electron Al to d-electrons Au and Pt. Q2D-GGA preserves the good quality description of the bulk structure, performing similarly to PBEsol that is specifically designed to improve bulk description.

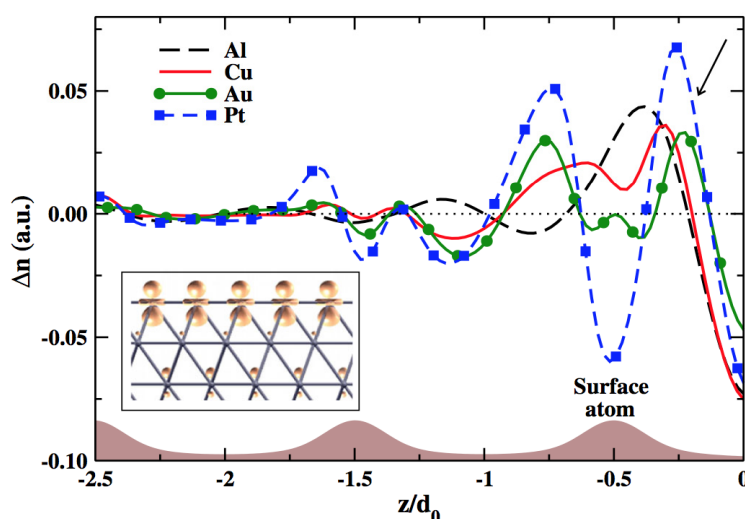


Figure 2.

Electron density difference between the surface and the ideal bulk phases, plotted versus the normalized distance, for selected metal surfaces. The distance between atomic layers has been normalized to align the atomic and surface positions of the various metals, independently on the lattice constant. We used surface plane-averaged densities, the center of the bond that is broken to form the surface is at $z=0$. Inset: Density isosurface of a Kohn-Sham orbital with d_{22} character at the surface.

The surface reduces symmetry along z , and orbitals with or without z component become splitted in energy. The electronic population rearrangement, to properly fill newly aligned electronic levels, induces a spatial redistribution with thin layers of charge, see for example curves for Au and Pt in the main panel. At Al and Cu surfaces the charge rearrangement is quite smooth. At the d-metals surfaces, instead, thanks to the spatial symmetry of d-electrons, the charge redistribution has the shape of thin charge layers localized just above and below the surface atomic layer.

At the same time, Q2D-GGA reproduces within a mean absolute error of 4% the surface energies of Ti, Rh, Pd, Pt, Au, being slightly less accurate in the cases of Al and Cu. The agreement with experiments is impressive in the cases of Au and Pd, much better than any other evaluated GGA, because the surface charge has exactly the thin layered shape the Q2D-GGA is aimed at describing.

The proposed Q2D functional can be therefore successfully applied, not only to model, test case systems, but also to real and interesting solid state systems and it has been proven able to describe bulk properties, without losing in accuracy, improving at the same time the surface description.

Q2D-GGA is implemented in Quantum Espresso (<http://www.quantum-espresso.org/>), Libxc (http://www.tddft.org/programs/octopus/wiki/index.php/Libxc_2.2.0) and freely available at <http://www.theory-nnl.it/software.php>.

Related publications *Nonuniform Scaling Applied to Surface Energies of Transition Metals.* L. Chiodo, L. A. Constantin, E. Fabiano, and F. Della Sala, Phys. Rev. Lett. **108**, 126402 (2012).

Selenium adsorption on Mo(110): A first-principles investigation. G. Roma and L. Chiodo, Phys. Rev. B **87**, 245420 (2013).

Minimal self-contained quantum dot refrigeration machine

We theoretically designed an electronic quantum refrigerator based on four quantum dots arranged in a square configuration, in contact with many thermal reservoirs. The system implements the minimal mechanism for acting as a self-contained quantum refrigerator, by operating without the requirement of external time-dependent work and demonstrating heat extraction from the coldest reservoir and the cooling of the nearby quantum-dot. We also discuss the operational nature of the definition of local temperatures in systems out of equilibrium and the importance of reference experimental regimes to define the regime of operation of small quantum thermal machines.

Minimal self-contained thermal machines are theoretical systems that perform a cycle based only on the steady-state heat transfer from thermal reservoirs at different temperatures, utilizing as few degrees of freedom as possible.

In this work we design an implementation of these machines operating by quantum mechanical tunneling, consisting of four quantum dots in a planar square array (named a “quadridot”) coupled to independent electron reservoirs as shown in Fig. 1-a. The couplings and the electrostatics interactions have been carefully chosen so that the quadridot could pump energy from the high temperature reservoir H and the low temperature reservoir C to the intermediate temperature reservoirs, thereby acting as a “quantum refrigerator” (Fig. 1-b).

To show this effect, we explicitly solve the open dynamics of the quadridot and study its asymptotic behavior.

In the Born-Markov-Secular limit we write a Lindblad equation for the reduced density matrix of the quadridot, which describes the effective dissipative and coherent interaction between the low-energy states of the system obtained after a Schrieffer-Wolff transformation.

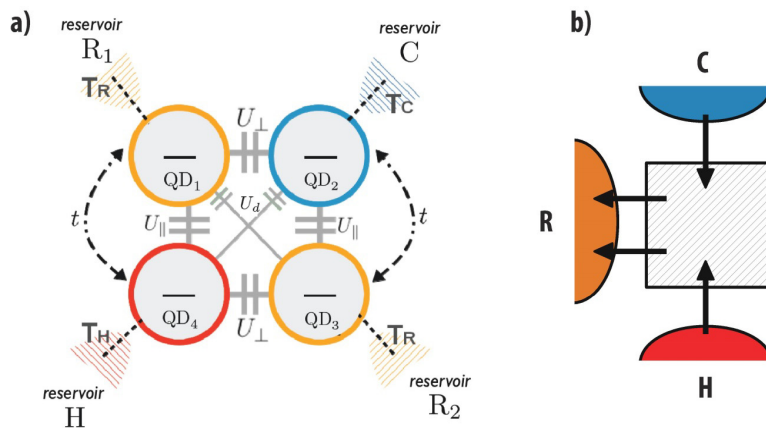


Figure 1.

a) The quadridot. The four quantum dots QD₁, QD₂, QD₃, and QD₄ are weakly coupled to the reservoirs R₁, C, R₂, and H, respectively, which are all grounded and maintained at temperatures $T_H > (T_{R1} = T_{R2} = T_R) > T_C$. Tunneling is allowed only between QD₁ and QD₄, and between QD₂ and QD₃.

b) Schematics of self-contained refrigerators: extracting heat from the C, H reservoirs and pumping it into R.

Contact Person Vittorio Giovannetti (v.giovannetti@sns.it)

Collaborators D. Venturelli, R. Fazio.

Numerically solving the steady state equation we observe that for each $T_C < T_R$, there exists a minimal threshold value for T_H above which the quadridot extracts heat from the cold reservoir C. This is shown in Fig. 2-a for $T_R=2$ and different values of U_d . The quadridot works as a refrigerator in the blue region. For given $T_H > T_R$, there is a minimal temperature (whose approximate value is analytically obtained) for the cold reservoir under which the effect cannot work. Interestingly, for $T_H/T_R \rightarrow \infty$ this value asymptotically converges toward a finite non-zero temperature which can be interpreted as the emergent absolute zero of the model.

This refrigeration effect is accompanied by a cooling of QD_2 , namely its effective local temperature $T_{(eff)C}$ decreases as T_H increases, for sufficiently high T_H .

However, being the quadridot a nanoscale system out-of-equilibrium, the definition of the local temperature must be operational. In Fig. 2-b we show an example of operation showing that depending on how the refrigeration effect is "switched on", we can achieve very different operational regimes. QD_2 might be either colder (in region I) or hotter (in region II) when the device extract heat from the C reservoir. Conversely, we might achieve a colder QD_2 also when the quadridot pumps heat into the colder bath (III).

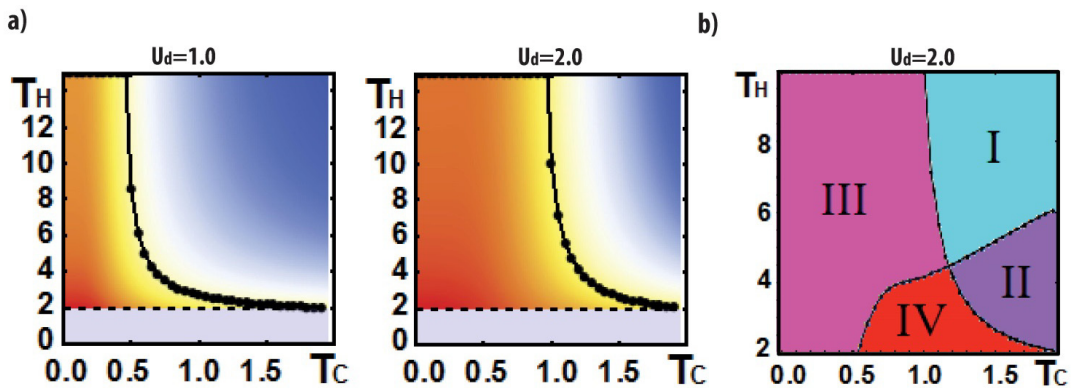


Figure 2.

a) Panels refer to different values of U_d . When T_H approaches the black curve, a change of sign in the heat flow occurs. For T_H above the threshold (blue region) the machine works as pictured in Fig. 1 b), extracting heat from the C, H reservoirs and pumping it into R. In the opposite regime (red region) heat cannot be extracted from C. Black dashed line above the grey region indicates $T_H = T_R = 2$. Blue/Red background color intensity is proportional to the actual heat pumped to/extracted from C. b) Comparison between heat extraction and single particle occupation for $U_d = 2$. In regions I/II the self-contained refrigerator is working (heat is extracted from C) while in regions III/IV the C bath receives heat. In regions I/III we have an effective decrease of the occupation number of QD_2 .

Related publication

Minimal Self-Contained Quantum Refrigeration Machine Based on Four Quantum Dots. D. Venturelli, R. Fazio, and V. Giovannetti, Phys. Rev. Lett. **110**, 256801 (2013).

Collective charge and spin excitations in radial semiconductor heterostructures

Radial heterostructures – free-standing semiconducting nanowires laterally overgrown by a multi-layer – represent an emerging new class of multi-functional nanomaterials. We investigated the peculiar properties of the collective excitations of the electron gas confined in co-axial layers in these systems. The impact of localization in quasi-1D and quasi-2D electronic channels and the discrete axial symmetry on collective spin and charge excitations and their Raman scattering cross-sections has been determined theoretically. The identification of electronic collective excitations in a set of light-scattering experiments allowed to demonstrate the first realization of a high-mobility electron system through modulation doping technique in these structures.

Free-standing semiconductor nanowires laterally overgrown by a multi-layer constitute an emerging new class of nanomaterials, which supplement traditional quasi-2D and quasi-1D systems. Indeed, these radial heterostructures can be engineered with high control to host an electronic system, e.g., in a co-axial quantum well (coQW, Fig. 1 left), with promising properties for future nanotechnologies. The critical issue of remote doping and ensuing formation of a high-mobility electron gas had not been solved until recently, though.

The formation of a high-mobility electron gas can be effectively exposed by detection of its collective excitations, namely plasmons, e.g., by inelastic light scattering (ILS) experiments. Due to electron-electron interaction and the prismatic symmetry, coQWs the electron gas is not uniformly distributed at the radial hetero-interface but rather forms tunnel-coupled quasi-1D and quasi-2D channels (Fig. 1 left), with peculiar, possibly degenerate intra- and inter-subband collective excitations (Fig. 1 right) between the two types of channels.

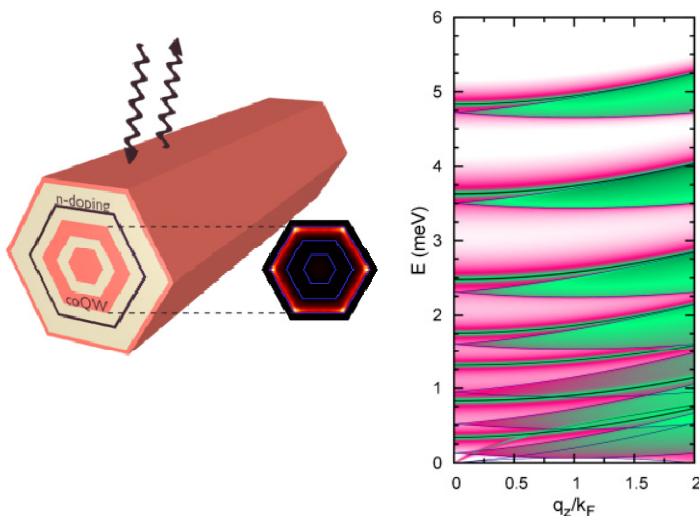


Figure 1. (left) Geometry of a remotely doped coQW with calculated electron gas density distribution. (right) Spectral strength of collective (plasmons) and single particle excitations in an electron gas in a coQW.

Contact Person Guido Goldoni (guido.goldoni@unimore.it)

Collaborators M. Royo Valls, A. Bertoni, I. Zardo, S. Funk, G. Abstreiter, J. Finley.

We have used a TDLDA approach to evaluate the density-density irreducible response function of the electron gas and to calculate the spectral properties of the electronic collective excitations in these systems, showing that the discrete axial symmetry influences collective spin and charge excitations dispersions and the Landau damping phenomenon in a peculiar way with respect to traditional structures. In addition, Raman scattering cross-section is strongly anisotropic in the azimuthal angle, and is able to selectively expose different excitations.

Calculations within the TDLDA approach proved to be of a predictive quality and could be directly compared with a set of light-scattering experiments (Fig. 2). This allowed to demonstrate the formation of the electron gas in a set of GaA/AlGaAs core-multi-shell nanowires containing a coQW which had been remotely doped. A high mobility of ~ 50000 (cm^2/Vs) could be inferred by comparison with simulations, thereby demonstrating the first successful realization of the modulation doping technique in this new class of nano-structures.

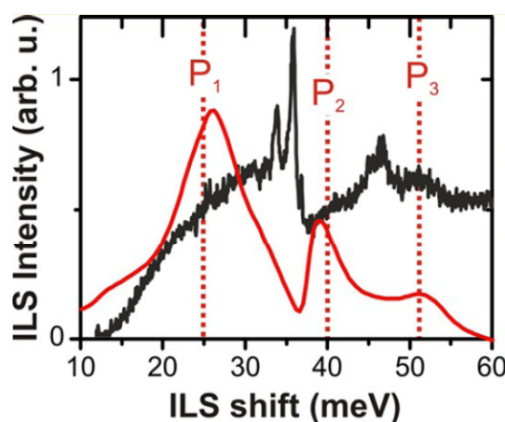


Figure 2.

Comparison between the measured (black) and predicted (red) ILS shift in a remotely doped coQW with $\sim 3 \times 10^{-7} \text{cm}^{-1}$ electrons.

Related publication

High mobility one- and two- dimensional electron systems in nanowire-based quantum heterostructures. S. Funk, M. Royo, I. Zardo, D. Rudolph, S. Morkötter, B. Mayer, J. Becker, A. Bechtold, S. Matich, M. Döblinger, M. Bichler, G. Koblmüller, J. J. Finley, A. Bertoni, G. Goldoni, and G. Abstreiter, *Nano Letters* **13**, 6189 (2013).

Playing with electron wavefunction: beam shaping, angular momentum and spin-polarization of an electron beam in an electron microscope

A recent breakthrough has been the introduction of electron beam with orbital angular momentum. Based on this, we proposed the design of a space-variant Wien filter that produces a spin-orbit interaction and permits to exploit such orbital momentum for the spin manipulation. When applied to an unpolarized beam, the proposed device, in combination with a suitable diffraction element, can act as a very effective spin-polarization filter. Such a device was for long considered unfeasible for fundamental reasons and would represent a large technical progress in microscopy. To prove its feasibility we also created a new fully quantum simulation approach to completely include spin effects.

A simple diffraction grating modulated by a dislocation produces, in the diffraction, beams with a well defined orbital angular momentum OAM. The recent introduction of such elements in electron optics has been a real revolution. The OAM is a degree of freedom so far neglected for electron beam. Soon after this invention, in collaboration with the optics group of Naples, and in particular E. Karimi, we found that OAM can be directly related to another hidden degree of freedom of electrons, namely, the spin.

In fact we found that a space variant Wien filter (where electric and magnetic fields are compensated) can be used to introduce a spin-orbit coupling. In particular, the magnetic field induces a spin half-turn and converts the corresponding spin variation into OAM of the beam itself by exploiting a geometrical phase arising in the spin manipulation.

The beam with different angular momentum would then diffract differently and therefore be spatially separated upon propagation. Therefore, when applied to an unpolarized input beam, the proposed device, in combination with a suitable diffraction element (i.e., a pinhole aperture), can act as a very effective spin-polarization filter.

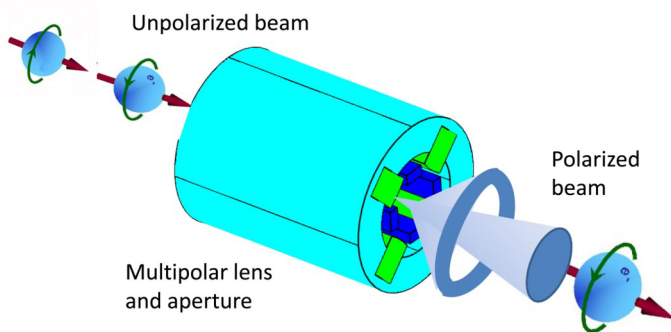


Figure 1.

Schematic of the polarizer: electrons in a mixed polarization state enter the multipolar lens of the wien filter and acquire or lose orbital angular momentum (OAM) by the interaction with the magnetic field and as a function of the initial spin state. The part of the beam with OAM equal to 0 and a well-defined spin propagates in the forward direction while other beams with different OAM form doughnut shaped beams that can be excluded using a pinhole.

Contact Person Vincenzo Grillo (vincenzo.grillo@nano.cnr.it)
Collaborators E. Karimi, L. Marrucci, E. Santamato, R. Boyd.

This idea seems to solve years of controversies that date back to Bohr who asserted a sort of interdiction principle for which the polarization of electron was not feasible with experiment that involved the concept of classical trajectories. In fact so far, the only way to obtain spin polarized electrons was to extract electrons from strained semiconductors where they lie in specific spin states.

We created a new simulation of the beam propagation in a given field distribution completely consistent with the non relativistic spin formalism and wave mechanics. Using this approach we were able to demonstrate the feasibility of the polarizer.

By a practical point of view the realization of the actual prototype is still in progress but surely the potentiality is in spin polarized microscopy, in particular a polarizer allows high brightness and a stronger flexibility in the use with respect to the present sources.

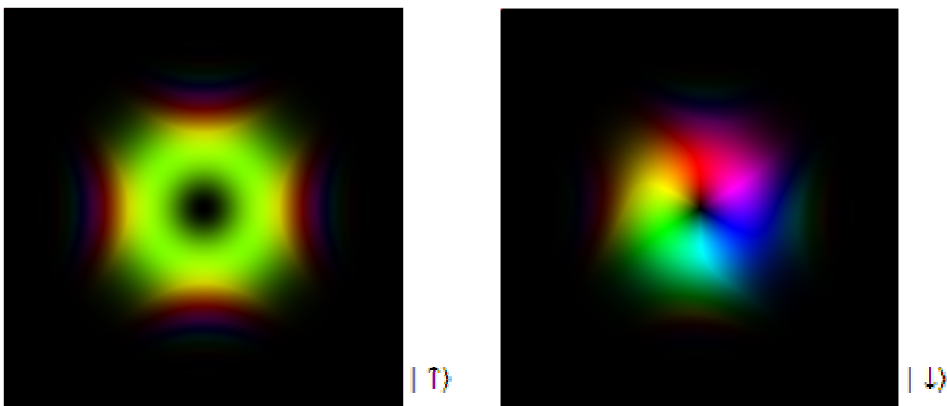


Figure 2.

Simulation of the exit wave at the exit of the quadrupolar Wien filter when spin \downarrow is introduced in the filter. The two spin states are separately plotted. The phase is encoded in the color while the brightness is proportional to the intensity. The phase of the beam that has undergone spin flip (left) is almost stationary and will produce in the far field a quasi-gaussian beam to be selected with a pinhole.

Related publications *Quantum simulation of a spin polarization device in an electron microscope.* V. Grillo, L. Marrucci, E. Karimi, R. Zanella, and E. Santamato, *New Journal of Physics* **15**, 093026 (2013).

Spin-to-Orbital Angular Momentum Conversion and Spin-Polarization Filtering in Electron Beam. E. Karimi, L. Marrucci, V. Grillo, and E. Santamato, *Phys. Rev. Lett.* **108**, 044801 (2012).

Teaching silicon new tricks

Silicon is cheap, easy to handle, simple to manufacture and shows optimal thermal and mechanical properties. Silicon is the electronic material per excellence and is the most used semiconductor for solar applications. Nevertheless the increasing demand for innovative and more efficient devices has driven scientists to explore new functionalities in Si-based materials. This objective can be realized by exploring Si new properties, that is by "teaching silicon to do what silicon is currently not able to do". Our aim, here, is to provide a theoretical framework for the prediction and the study of novel behaviors in Si-based systems for practical applications in photonics and photovoltaics.

In these last years, Si photonics is looking at the nonlinear optics to generate new light sources, starting from one or more pump beams. Until now, nonlinear conversion of light into silicon devices has been based on third-order-effects. This is because Si itself, in its bulk crystalline form, has a second-order tensor equal to zero. In 2012 in a theoretical-experimental collaboration, we performed second-harmonic-generation (SGH) experiments and first-principle calculations proving, for the first time, that large values of the second-order nonlinear susceptibility $\chi^{(2)}$, up to 40 pmV⁻¹ at 2,300 nm, can be induced in strained silicon bulk. As a consequence nonlinear strained silicon could provide a competing platform for a new class of integrated light sources spanning the near- to mid-infrared spectrum from 1.2 to 10 μ m. Thus, thanks to the development of new first principles numerical tools, ab-initio techniques have been applied with success to predict new non-linear optical properties of a medium, with an accuracy that complements experimental observations.

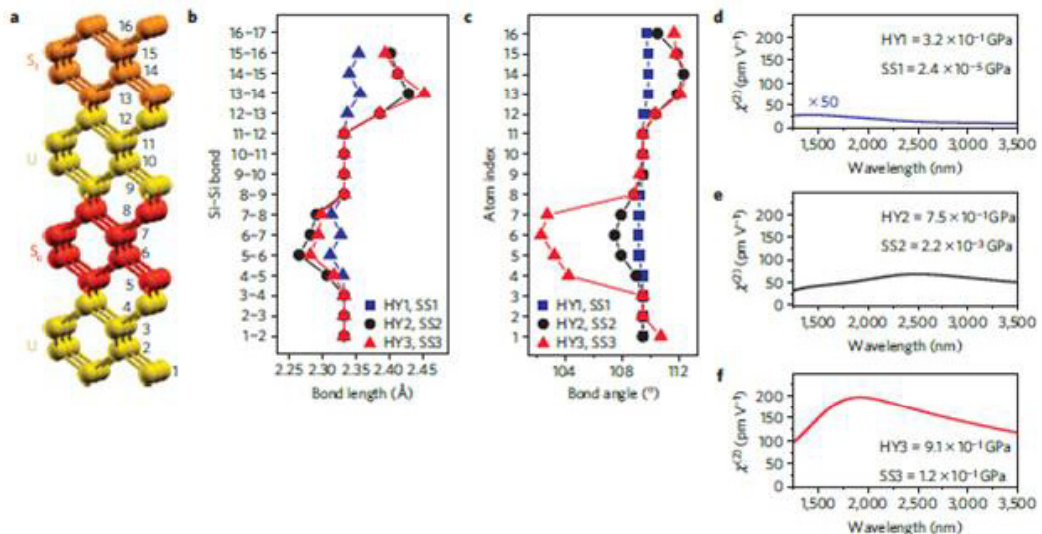


Figure 1.

First-principle calculations of strained Si second-order nonlinearity. a) Simulation unit cell: the different colours refer to the different bond deformations used. Orange: the bonds were elongated to represent a tensile stress, indicated by S_t . Yellow: no bond variation with respect to the relaxed Si lattice (unperturbed region). Red: the bonds were shortened to represent a compressive stress, indicated by S_c .

Contact Person

Stefano Ossicini (stefano.ossicini@unimore.it)

Collaborators

I. Marri, M. Govoni, E. Luppi, V. Vénier, F. Bianco, E. Borga, M. Cazzanelli, L. Pavesi, M. Ghulinyan, G. Pucker, D. Modotto, S. Wabnitz, R. Pierobon.

b) Maximum bond-length distortions for US_cUS_t structures. The unstrained bulk-Si bond length is 0.2332 nm. The colours (blue–black–red) refer to the calculations shown in d–f). c) Maximum bond-angle distortions for US_cUS_t structures. The unstrained bulk-Si angles are $109,5^\circ$. The colours (blue–black–red) refer to the calculations shown in d–f). The constant bond lengths and angles represent the unstrained region and coincide with Si-bulk values. The hierarchy of increasing strain in the three structures (blue–black–red), which is reflected also in the corresponding values of pressure (HY) and in the YZ component of the shear stress, is evident. d–f) The results of the simulations in terms of the $\chi(2)$ values. d) A weakly strained Si. e) A medium strained Si. f) A heavily strained Si.

The conversion of solar energy into electric current with high efficiency is one of the most important and promising topics in modern science and technology. Solar cell performances can be improved by promoting fast and non-dissipative recombination mechanisms that prevent loss in thermalization processes. In this context, carrier multiplication (CM) can be used to increase solar cell efficiency, limiting the heat generation that results from phonon scattering. CM is a Coulomb driven recombination mechanism that occurs when highly-excited carriers decay to a lower energy state and its excess energy is transferred non-radiatively to generate extra electron-hole (e-h) pairs. If favored by quantum confinement of the electronic density, CM can be as fast as or even faster than thermalization processes induced by phonons relaxation, extending therefore the portion of solar radiation that can be converted into photocurrent. Recently we have developed a new full ab-initio code in order to calculate, within first order perturbation theory, CM and Auger recombination in nanocrystals (NCs). Thus we have calculated CM effects in both isolated and interacting Si-NCs, demonstrating that one-site CM can benefit from size reduction and that efficiency of two-site processes is strongly affected by wave functions delocalization on different NCs that can boost CM dynamics when NC-NC interaction is not negligible.

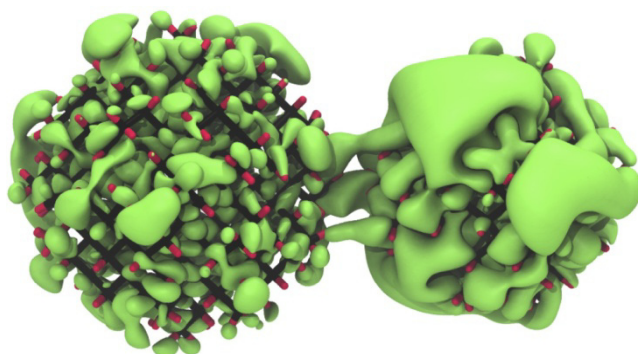


Figure 2.
Wave function localization for a couple of closely spaced and interacting Si NCs. The wave function sharing regime is evident. From Ref. 2.

Related publications *Second harmonic generation in silicon waveguides strained by silicon nitride.* M. Cazzanelli, F. Bianco, E. Borga, G. Pucker, M. Ghulinyan, E. Degoli, E. Luppi, V. Vénier, S. Ossicini, D. Modotto, S. Wabnitz, R. Pierobon, and L. Pavesi, *Nature Materials* **11**, 148–154 (2012).

Carrier multiplication between interacting nanocrystals for fostering silicon-based photovoltaics. M. Govoni, I. Marri, and S. Ossicini, *Nature Photonics* **6**, 672–679 (2012).

Non-equilibrium dynamics of hot carriers in graphene and carrier multiplication

Graphene is emerging as a viable alternative to conventional optoelectronic, plasmonic, and nanophotonic materials. The interaction of light with carriers in graphene creates an out-of-equilibrium carrier distribution, which relaxes on an ultrafast timescale to a hot Fermi-Dirac distribution, that subsequently cools via phonon emission. While the slower relaxation mechanisms have been extensively investigated, the initial stages, ruled by fundamental electron-electron (e-e) interactions, still pose a challenge. Experimentally, they defy the resolution of most pump-probe setups, due to the extremely fast sub-100 fs carrier dynamics spanning a broad range of energies. Theoretically, the linear dispersion of massless Dirac fermions poses a novel many-body problem, fundamentally different from that based on Schrödinger fermions, used for decades in ordinary metals and semiconductors. Here we combine pump-probe spectroscopy, with extreme temporal resolution and broad spectral coverage, with a microscopic theory, based on the semiclassical Boltzmann equation, to investigate e-e collisions during the very early stages of relaxation. We identify the mechanisms controlling the ultrafast dynamics, in particular the significant role of collinear scattering. This gives rise to Auger processes, including charge (or carrier) multiplication, which is key in photovoltage generation and photodetectors.

Photonics encompasses the generation, manipulation, transmission, detection, and conversion of photons. Applications of photonics are nowadays ubiquitous, affecting all areas of everyday life. Photonic devices, enabled by a continuous stream of novel materials and technologies, have evolved with a steady increase in functionalities and reduction of device dimensions and fabrication costs. Graphene has decisive advantages, such as wavelength-independent absorption, tunability via electrostatic doping, large charge-carrier concentrations, low dissipation rates, high mobility, and the ability to confine electromagnetic energy to unprecedented small volumes. These unique optoelectronic properties make it an ideal platform for a variety of photonic applications, including fast photodetectors, transparent electrodes in displays and photovoltaic modules, optical modulators, plasmonic devices, microcavities, ultrafast lasers, to cite a few.

Understanding the interaction of light with graphene is pivotal to all these applications. In the first instance, absorbed photons create optically excited ("hot") carriers. Their non-equilibrium dynamics can be very effectively studied by ultrafast pump-probe spectroscopy (see Fig. 1). In this technique, an ultrashort laser pulse creates a strongly out-of-equilibrium (non-thermal) distribution of electrons in conduction band and holes in valence band. The optically-excited carriers then relax, eventually reaching thermal equilibrium with the lattice. The relaxation dynamics, due to various processes, including e-e and electron-phonon (e-ph) scattering, as well as radiative electron-hole (e-h) recombination, is then accessed by a time-delayed probe pulse. The time-evolving hot electron distribution inhibits, due to Pauli blocking, the absorption of the probe pulse at lower photon energies with respect to the pump, thus yielding an increase in transmission (photobleaching).

Contact Persons

Marco Polini (marco.polini@nano.cnr.it)
Andrea Tomadin (andrea.tomadin@nano.cnr.it)

Collaborators

A. C. Ferrari, G. Cerullo, K. Novoselov.

Thus, monitoring this transient absorption enables the direct measurement of the distribution function in real time. In the sub-ps temporal domain, two main processes occur: firstly, the initial peak produced by the pump laser broadens, due to e-e collisions, converging towards a hot Fermi-Dirac (FD) shape on an ultrashort time scale. Subsequently, optical phonon emission drives a cooling in which the FD distribution shifts towards the Dirac point. In our work we investigated the role of e-e interactions on the initial stages of the non-equilibrium dynamics. We demonstrated that extremely fast e-e relaxation occurs via crucially important “collinear” scattering events (i.e., with the scattering particles' incoming and outgoing momenta on the same line). By combining extreme temporal resolution broadband pump-probe spectroscopy with a microscopic semi-analytical theory based on the semiclassical Boltzmann equation, we have been able to investigate e-e collisions in graphene during the very early stages of relaxation. We identified the fundamental processes controlling the ultrafast dynamics in graphene, in particular the significant role of Auger processes and carrier multiplication.

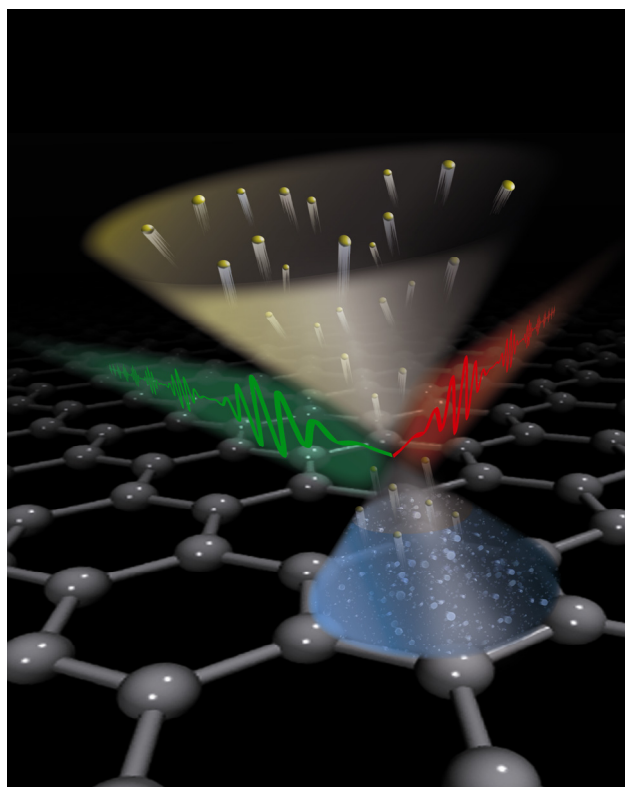


Figure 2.

A pictorial description of carrier multiplication as probed in a two-color pump-probe experiment. The pump and probe light beams are shown. Yellow spheres represent electrons, which, after the initial strong photo-excitation, are promoted from the valence band to the conduction band via collinear scattering processes. Although these two-body scattering processes are kinematically blocked when momentum and energy are simultaneously conserved, three-body collisions (electron-electron scattering assisted by impurities or electron-lifetime effects due to electron-electron interactions) effectively restore a finite phase space for these processes. Image courtesy of Andrea Freccioni (SNS).

Related publication *Ultrafast collinear scattering and carrier multiplication in graphene.* D. Brida, A. Tomadin, C. Manzoni, Y. J. Kim, A. Lombardo, S. Milana, R. R. Nair, K. S. Novoselov, A. C. Ferrari, G. Cerullo, and M. Polini, *Nat. Comm.* **4**, 1987 (2013).

Nonequilibrium dynamics of photoexcited electrons in graphene: Collinear scattering, Auger processes, and the impact of screening. A. Tomadin, D. Brida, G. Cerullo, A. C. Ferrari, and M. Polini, *Phys. Rev. B* **88**, 035430 (2013).

Electron and optical spectroscopies of graphene nanoribbons: insights from ab-initio calculations

Some of the most intriguing properties of graphene are predicted for specifically designed nanostructures such as nanoribbons. Here, we report on the fundamental band gap and dispersion of atomically precise graphene nanoribbons fabricated via on-surface synthesis. Angle-resolved photoelectron spectroscopy and scanning tunneling spectroscopy data are obtained for armchair graphene nanoribbons of width $N=7$ supported on Au(111). These results are in quantitative agreement with theoretical predictions that include image charge corrections accounting for screening by the metal substrate, and confirm the importance of electron-electron interactions in graphene nanoribbons.

Graphene nanoribbons (GNRs), defined as nanometer-wide strips of graphene, have recently triggered a wealth of studies as promising candidate for digital electronics, since their lateral confinement can open a band gap and induce semiconducting behavior, while retaining the unique electronic properties of graphene. Moreover, depending on the details of the atomic structure, a variety of peculiar width- and edge-related phenomena can arise. Key features connected to the tunability of electronic and optical properties as a function of structural parameters have been predicted theoretically. However, only recently atomic control of GNR geometry (orientation, width, and edge termination) was demonstrated by bottom-up approaches. These advancements in the fabrication procedure have thus allowed the first measurements (Fig. 1) of the band gap and the topology of the occupied bands of atomically precise armchair GNRs (A-GNRs) by scanning tunneling spectroscopy (STS) and angle-resolved photoelectron spectroscopy (ARPES) techniques.

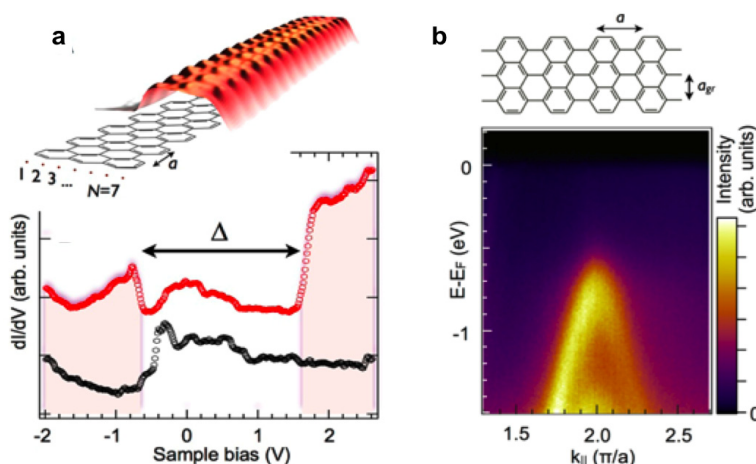


Figure 1.

(a) Scanning tunneling microscopy (STM) image ($U = 2.2$ V, $I = 0.15$ nA, 5 K) and chemical structure of an armchair graphene nanoribbon of width $N=7$ (7-AGNR) on Au(111). (b) ARPES intensity plot $I(E, E_F, k_{||})$ recorded along the ribbon axis revealing the two occupied frontier bands (raw data, $h\nu = 37$ eV, $T = 300$ K). The atomic structure of the H-terminated 7-AGNR is reported for clarity.

Contact Person

Deborah Prezzi (deborah.prezzi@nano.cnr.it)

Collaborators

A. Ferretti, S. Wang, A. Ruini, E. Molinari, P. Ruffieux, J. Cai, N. C. Plumb, L. Patthey, X. Feng, K. Müllen, C. A. Pignedoli, R. Fasel.

In this work we combine ARPES and STS data with density-functional theory (DFT) and many-body perturbation theory (MBPT) calculations to study the electronic structure of the N=7 AGNR (7-AGNR). In order to compare ARPES and STS experiments, we have computed the self-energy corrections to the DFT electronic structure of the free standing 7-AGNR by means of the so-called G0W0 approximation. The presence of the substrate is accounted for by means of a classical image charge model for the screened Coulomb interaction. As shown in Fig. 2, overall this results in a theoretical estimate of the energy band gap of 2.3 to 2.7 eV for the 7-AGNR on Au(111), in very good agreement with the experimental value of 2.3 ± 0.1 eV. The above results show that our ab-initio theoretical scheme can provide quantitative predictions for electron spectroscopies of nanoribbons on weakly coupled substrates, such as Au.

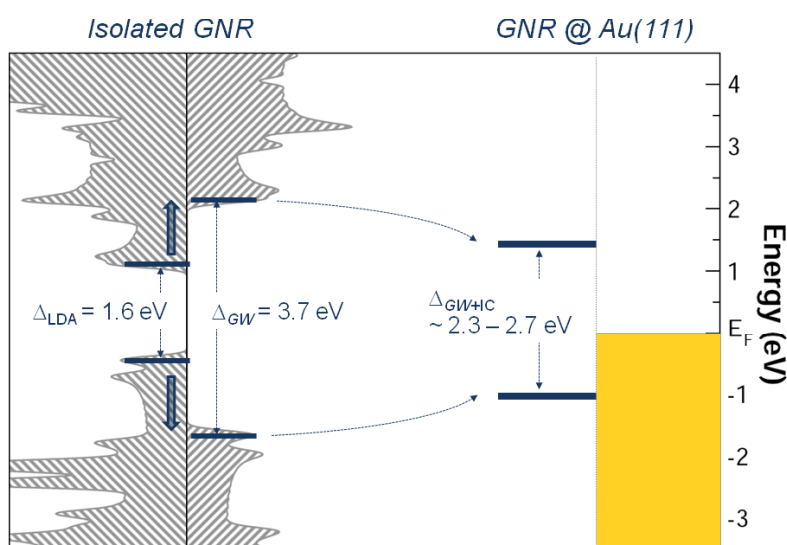


Figure 2.

LDA and GW-corrected DOS (energy gap highlighted) for the gas phase 7-AGNR are shown on the left side. By taking into account the surface screening, the gap is reduced to 2.3 - 2.7 eV, as shown on the right side. The molecule-Au(111) distance has been estimated to be 3.15 Å.

Related publication

Electron and Optical Spectroscopies of Graphene Nanoribbons: Insights from Ab-Initio Calculations. P. Ruffieux, J. Cai, N. C. Plumb, L. Patthey, D. Prezzi, A. Ferretti, E. Molinari, X. Feng, K. Mullen, C. A. Pignedoli, and R. Fasel, ACS Nano **6**, 6930 (2012).

Observation and spectroscopy of a two-electron Wigner molecule in an ultraclean carbon nanotube

We have observed a “Wigner molecule” in an ultraclean carbon nanotube. As well as confirming a theoretical prediction that dates back to the 1930s, this joint theoretical and experimental work also proves that extremely clean structures, like carbon nanotubes, can be used to manipulate delicate electronic states that do not otherwise exist in ordinary materials.

One of the simplest quantum mechanical systems is that of two electrons on a string. When the two electrons interact strongly, a Wigner molecule ground state is formed. Here, the two particles repulse each other to the opposite ends of the string. Named after Eugene Wigner, who predicted the existence of this quantum crystallization phenomenon back in 1934, this unique state of matter is very difficult to observe in experiments.

The Wigner molecule is a very fragile quantum state and is only due to the Coulomb forces between electrons. These electrostatic interactions can easily be disturbed by the millions of other nearby electrons and atoms existing in the host material. To observe the molecule, we used the cleanest conceivable condensed matter setup. We started with an electrically neutral nanotube suspended in vacuum that was touching nothing but two metal electrodes, and we charged it exactly with two electrons. By then passing electrical current through the nanotube, we could infer how the two electrons were interacting.

Combining a technique called “transport spectroscopy” with a sophisticated calculation known as “exact diagonalization”, we found that, as predicted by Wigner, the electrons pushed each other apart so that each electron sat on one side of the nanotube, forming a molecule. Then, when we deliberately squeezed the two electrons to one side of the nanotube, the electrons still kept themselves some distance apart. Pushing the electrons from side to side also proved that the molecule forms as a result of intrinsic electron interactions and not merely because it is being affected by its surrounding environment.

According to quantum mechanics, electrons always tend to spread out and fill any given volume. However when the repulsive interactions between electrons are strong enough, they can overcome this tendency to spread. In this situation, the electrons form an ordered Wigner crystal of equally distanced, well-spaced electrons.

Besides confirming Wigner’s old theoretical prediction, our work also demonstrates how an extremely clean system, like a carbon nanotube, can be used to manipulate delicate electronic states in a controlled way.

Contact Person Massimo Rontani (massimo.rontani@nano.cnr.it)

Collaborators A. Secchi, S. Pecker, S. Ilani, F. Kuemmeth, D. C. Ralph, P. L. McEuen.

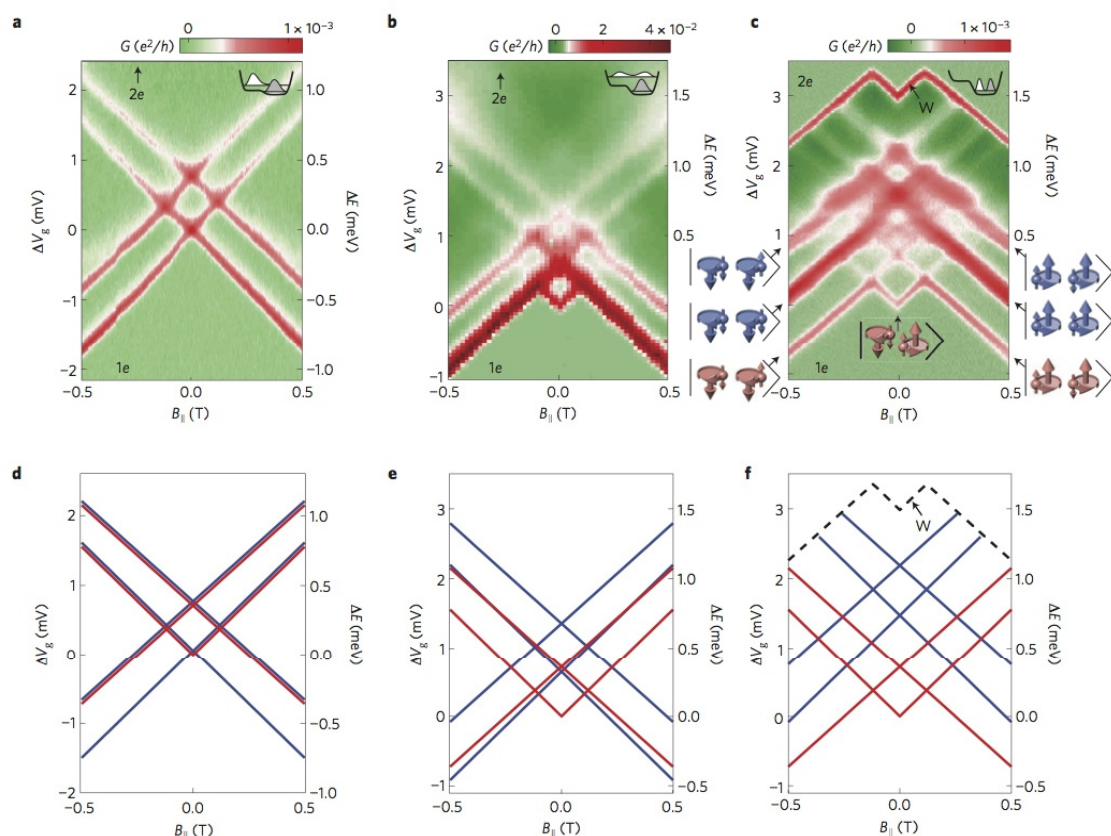


Figure 1.

Tunneling spectroscopy of a Wigner Molecule state showing its quantum excitations at three different molecular sizes.

Related publications *Observation and spectroscopy of a two-electron Wigner molecule in an ultraclean carbon nanotube.* S. Pecker, F. Kuemmeth, A. Secchi, M. Rontani, D. C. Ralph, P. L. McEuen, and S. Ilani, *Nature Physics* **9**, 576 (2013).

Intervalley scattering induced by Coulomb interaction and disorder in carbon-nanotube quantum dots. A. Secchi and M. Rontani, *Phys. Rev. B* **88**, 125403 (2013).

Quantum coherence controls the charge separation in a prototypical artificial light-harvesting system

In a joint theoretical and experimental collaboration we have studied the dynamics of a photoexcited supramolecular carotene-porphyrin-fullerene triad by means of high time-resolution femtosecond spectroscopy and first-principles quantum-dynamical simulations. The triad is a prototypical artificial reaction center, and upon photoexcitation of the porphyrin moiety, the primary event is the electron transfer to the fullerene. We provide evidence that the driving mechanism of this process is a correlated wavelike motion of electrons and nuclei on a timescale of few tens of femtoseconds, thus establishing the role of vibronic coherence in artificial light harvesting.

Photosynthesis consists of the following processes: light harvesting via a cascade of energy transfer steps, subsequent charge separation at the reaction center and multi-electron catalysis. One of the key challenges for the future will be to learn how to construct artificial molecular devices enabling the harvesting of sunlight and their use either for direct electric power generation or to drive fuel-producing photochemical reactions.

We have studied the microscopic mechanisms underlying the primary charge-transfer dynamics in a supramolecular carotene-porphyrin-fullerene triad by impulsively exciting the system using broadband visible pulses. The time-dependent spectra (Fig. 1) show a novel and striking feature, i.e., a red-shifting transient emission band in the region between 540 nm and 580 nm. Because of its pronounced spectral shift with time, we attribute this emission to a transient intermediate, and not to a final state.

In order to clarify the influence of coherent charge motion on the electron transfer dynamics we performed a detailed TDDFT quantum-dynamical description of the system.

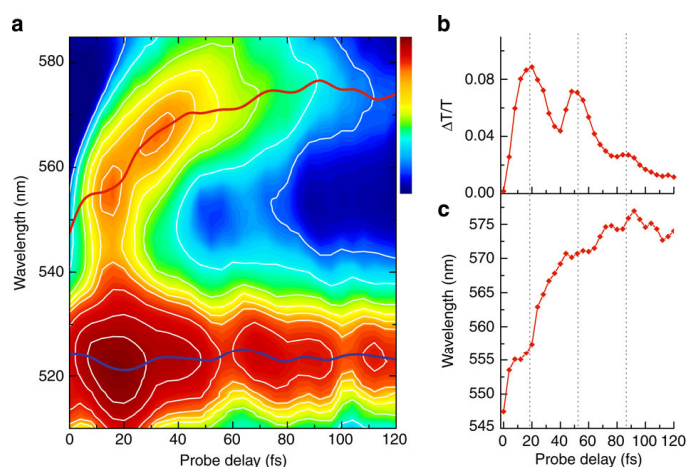


Figure 1.

Coherent charge transfer dynamics in a carotene-porphyrin-fullerene triad. (a) Experimental differential transmission map as a function of time delay and probe wavelength recorded following impulsive excitation of the triad at around 550 nm. The blue and red lines highlight the time evolution of the center wavelengths of the porphyrin and charge transfer bands, respectively.

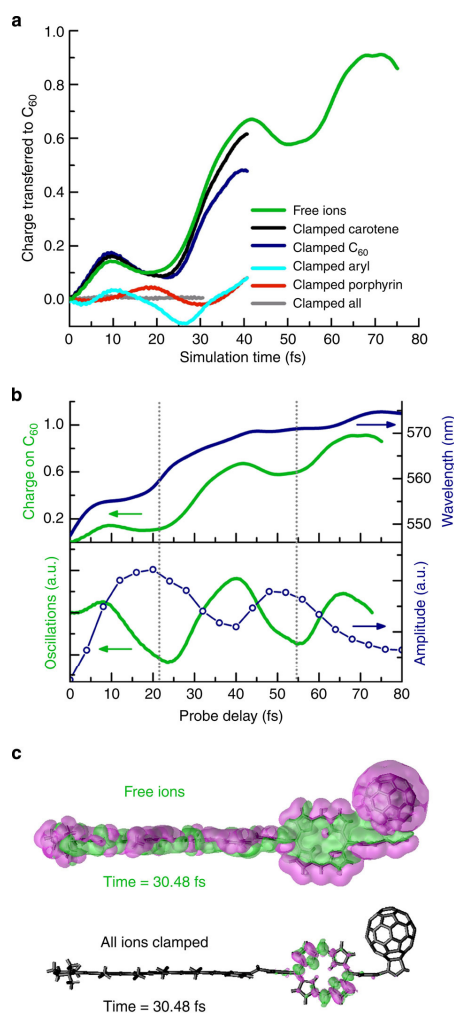
These center wavelengths have been extracted from the experimental data by fitting the spectra of both bands to Gaussian line-shape functions. (b,c) Temporal evolution of the amplitude (b) and spectral position (c) of the charge transfer band. The dashed lines are guides to the eye, emphasizing coherent oscillations of both amplitude and center wavelength of the charge transfer resonance.

Contact Person

Carlo Andrea Rozzi (carloandrea.rozzi@nano.cnr.it)

Collaborators

S. M. Falke, N. Spallanzani, A. Rubio, E. Molinari, D. Brida, M. Maiuri, G. Cerullo, H. Schramm, J. Christoffers, C. Lienau.



The time evolution of the fractional charge on the pyrrole–fullerene part of the triad is presented in Fig. 2 for different simulation scenarios.

The simulations suggest a rapid and almost complete charge flow to the fullerene moiety within ~70 fs when allowing all ions to freely move during the charge-transfer process. Within the accuracy of the presented results, the experimentally observed and simulated oscillation period is ~30 fs. This suggests that nuclear motion delocalized across the porphyrin/fullerene region drives the charge transfer. On the other hand the charge accumulation on the fullerene can be greatly affected by even minor changes of the nuclear vibrations in the porphyrin-linker-fullerene region of the molecule. Fixing the position of all ions suppresses both charge oscillation and accumulation.

Taken together, our experimental and theoretical data shine new light onto the microscopic origin of the experimentally observed charge-transfer dynamics, and provide compelling evidence that the correlated, quantum-coherent motion of ions and electrons not only governs the first steps of the photoinduced electron dynamics but also the yield of the charge separation in this prototypical artificial light-harvesting system, in stark contrast to prevailing statistical models for electron transfer reactions.

Figure 2.

Quantum dynamics simulations of the charge transfer process. (a) Simulated charge transfer in the triad occurs in about 70 fs (green line). Temporal oscillations with a period of about 30 fs suggest that coherent nuclear motion drives this charge transfer. The dynamics remain unaltered when locking the positions of either the carotene (yellow line) or the fullerene (blue). Clamping the porphyrin (red), or only 4 atoms (cyan) on the connector between porphyrin and fullerene fully suppresses the charge accumulation.

(b) Correlation between temporal oscillations in the simulated transferred charge (green lines, in lower panel the slow exponential rise was subtracted, and a time shift of 15 fs was applied) and in the resonance wavelength (blue, upper panel) and the amplitude (blue, lower panel) of the differential transmission spectrum of the charge transfer band.

This correlation is evidence for the coherent motion of electrons and nuclei during the charge transfer. (c) Snapshots of the photoinduced change in charge density at a time delay of 30.48 fs for the free triad (upper panel) and with all atoms clamped. Magenta indicates an increase in electronic charge density, whereas a decrease is shown in green.

Related publication

Quantum coherence controls the charge separation in a prototypical artificial light harvesting system. C. A. Rozzi, S. M. Falke, N. Spallanzani, A. Rubio, E. Molinari, D. Brida, M. Maiuri, G. Cerullo, H. Schramm, J. Christoffers, and C. Lienau, *Nat. Comm.* **4**, 1602 (2013).

Quantum Hall Interferometry

Two-dimensional electron systems in a strong magnetic field are used to investigate the physics of edge modes in the quantum Hall regime. On the experimental side, we have used scanning-gate microscopy to demonstrate that fractional features can be unambiguously observed in every integer quantum Hall constriction studied, namely corresponding to filling factors $1/3$, $2/5$, $3/5$, and $2/3$. On the theory side, we have found that Coulomb interactions give rise to unusual features in the finite bias response of Mach-Zehnder interferometers which exploit co-propagating edge states in the integer quantum Hall effect, such as the enhancement of the visibility of the current oscillations.

Topological edge states in the integer Quantum Hall (QH) effect realize ideal chiral one-dimensional electron beams which can be used both for the study of transport phenomena in one dimension and as building blocks for the construction of advanced electronic interferometers. In our investigation we address two important issues related to electron-electron (e-e) interactions in integer QH systems.

The first one concerns the emergence of an inner fractional structure of integer QH edges. To explore it, we combine transport measurements and the scanning gate microscopy (SGM) technique to directly manipulate edge channels. Our SGM maps provide the first images of the fractional features (corresponding to filling factors $1/3$, $2/5$, $3/5$, and $2/3$) that form the inner edge structure. SGM maps show that the edge consists of a series of alternating compressible and incompressible stripes (see Fig. 1). The high resolution of the SGM technique allows us to directly measure stripe widths and compare them with the predictions of the edge-reconstruction theory. The experimental demonstration of fractional structures within integer edge channels explains how edge channels behave at the interface between an integer and a fractional QH phase.

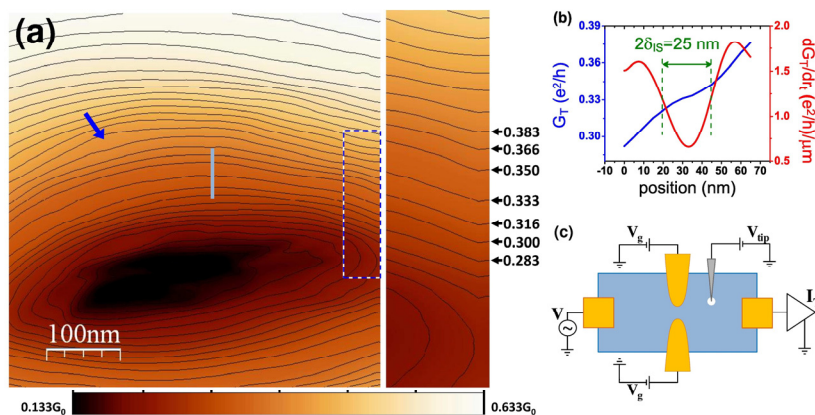


Figure 1.

(a) SGM scan at the center of a quantum point contact in a quantum Hall system at integer filling factor 1. The map shows the transmitted differential conductance as a function of the tip position, together with contour lines at constant differential conductance. On the right, a zoom of the 50×200 nm region corresponding to the dashed rectangle is displayed. (b) Profile of the differential conductance along the light blue line in (a), together with its derivative. (c) Scheme of the SGM experimental setup.

Contact Persons

Fabio Taddei (fabio.taddei@nano.cnr.it)
Stefan Heun (stefan.heun@nano.cnr.it)

Collaborators

G. Biasiol, F. Beltram, L. Chirulli, R. Fazio, V. Giovannetti, N. Paradiso, L. N. Pfeiffer, S. Roddaro, L. Sorba, D. Venturelli, K. W. West.

The second issue concerns the effect of e-e interactions on the performance of Mach-Zehnder interferometers (MZI) which exploit co-propagating edge states (see Fig. 2). In particular, we consider the case where the beam splitters are implemented through arrays of top gates of given periodicity which induce coherent mixing of edge-states. We show that the major impact of e-e interactions is the spoiling of such resonant coherent mixing, while the oscillating component of the interferometer current is only marginally affected because inter-edge interactions are negligible in the interference region. This leads to the unexpected result that strong interactions yield a reduction of the current visibility for small voltages, but an enhancement for larger voltages, with respect to the noninteracting case.

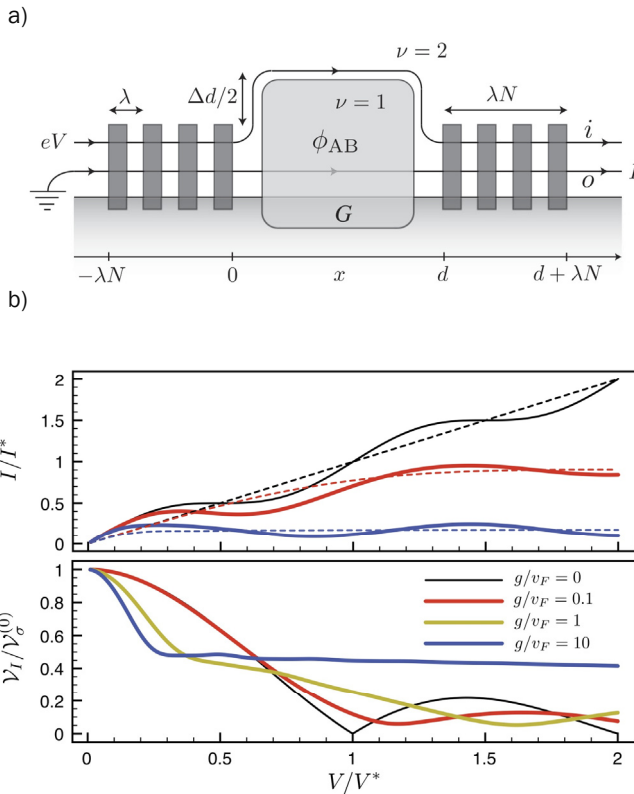


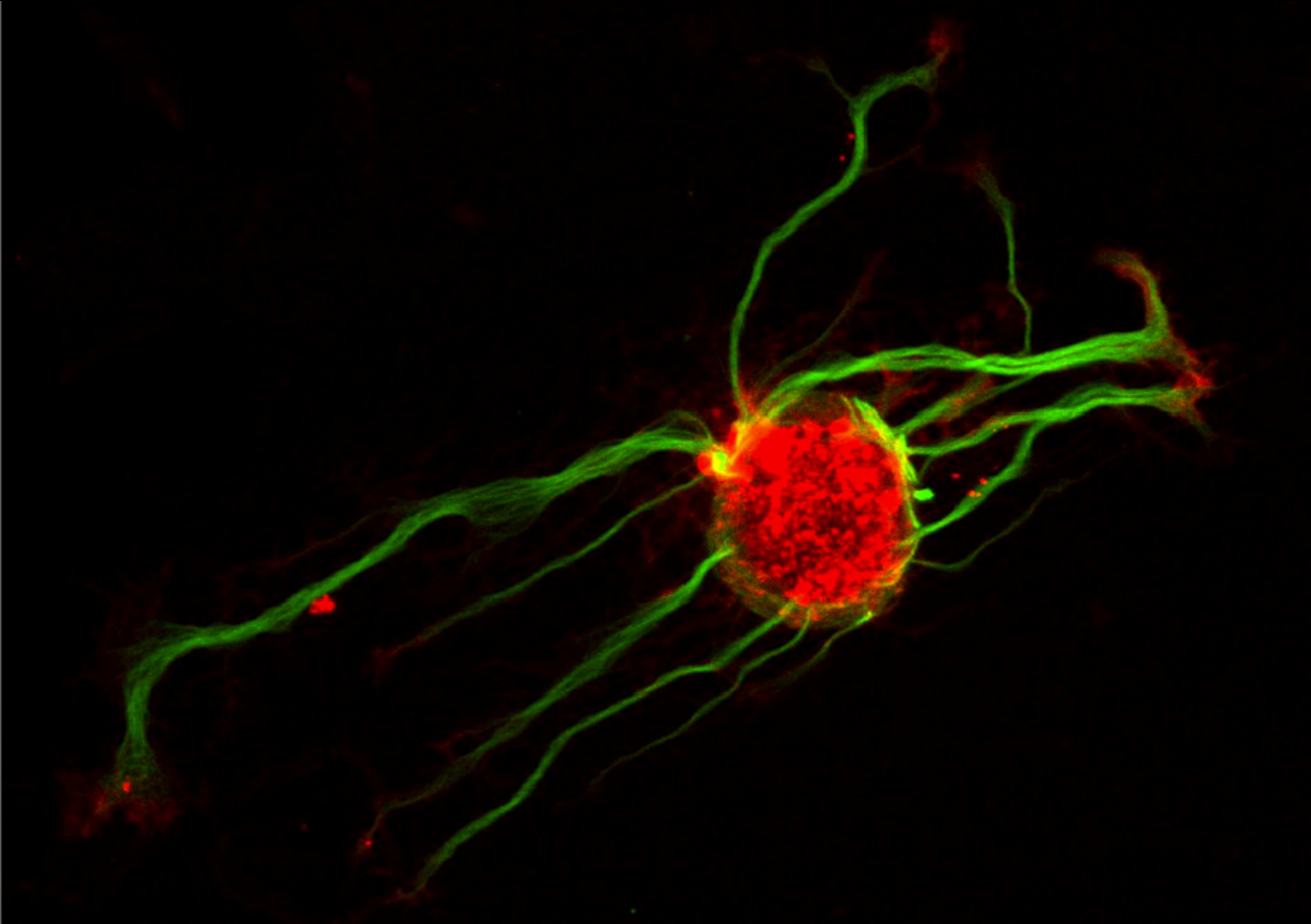
Figure 2.

(a) Sketch of the MZI. Two sets of N top gates arranged in arrays with periodicity λ and separated by the distance d represent the two beam splitters of the interferometer. A central top gate G locally lowers the filling factor to $\nu=1$ and separates inner and outer edge states (i and o), which experience a path length difference Δd and acquire an Aharonov-Bhm (AB) phase Φ_{AB} . (b) Response of the MZI versus bias voltage V [in units of $V^* = 2\pi v_F / (e\Delta d)$, where v_F is the Fermi velocity] for different values of the interaction parameter g/v_F . We have assumed $\Phi_{AB} = 0$, and that the resonant condition $\Delta k = 2\pi/\lambda$ is satisfied, where Δk is the momentum difference between the two edge channels. Top: total current I (full curves) and the non-oscillating component of the current (dashed curves). Bottom: visibility V_I of the AB oscillations in the current. We set $\lambda N/\Delta d = 3$ and $d/\Delta d = 1$.

Related publications *Imaging Fractional Incompressible Stripes in Integer Quantum Hall Systems.* N. Paradiso, S. Heun, S. Roddaro, L. Sorba, F. Beltram, G. Biasiol, L. N. Pfeiffer, and K. W. West, *Phys. Rev. Lett.* **108**, 246801 (2012).

Interactions in Electronic Mach-Zehnder Interferometers with Copropagating Edge Channels. L. Chirulli, F. Taddei, R. Fazio, and V. Giovannetti, *Phys. Rev. Lett.* **111**, 036801 (2013).

Imaging backscattering through impurity-induced antidots in quantum Hall constrictions. N. Paradiso, S. Heun, S. Roddaro, G. Biasiol, L. Sorba, D. Venturelli, F. Taddei, V. Giovannetti, and F. Beltram, *Phys. Rev. B* **86**, 085326 (2012).



Highlights Nanobioscience

Multipurpose Lab-on-chip devices for cancer diagnosis

Cancer diagnosis is currently based on Positron Emission Tomography (PET) imaging and specific biomarkers detection in serum of patients. In the perspective of achieving a fast and early stage diagnosis, innovative technologies are needed. In this respect, the Lab-On-Chip (LOC) approach offers the capability to improve the traditional methods in terms of speed, sensitivity, automation, and costs as well as the versatility to be adapted to several purposes. In the PET field, we demonstrated the potentiality of LOC and microfluidics to fasten and improve the production of radiopharmaceuticals, the drugs used in PET scans. On the other hand, using specific biomarkers we developed multipurpose LOCs for early-stage cancer diagnosis from patients' sera.

Application of LOC devices for cancer diagnosis is very promising with respect to conventional methods. It allows to achieve better performances in terms of speed, flexibility, automation and costs. In this respect, we recently optimized multipurpose platforms for the production of radiopharmaceuticals for PET and for early detection of the disease.

The integrated microfluidic "Radiochemistry on chip" (ROC) platform (see Fig. 1a) was designed for producing 2-[^{18}F]-fluoro-2-deoxy-D-glucose (^{18}F -FDG) in continuous flow from a single bolus of radioactive isotope solution to obtain radiopharmaceuticals in a dose-on-demand setting within a few minutes. Compared with traditional systems, the microfluidic approach to ^{18}F -FDG production is faster and the collection of a single dose is possible with significant product loss reduction. Reagent consumption, waste production, and operator interactions with radioactivity are minimized in microliter-scale reactors. The modular architecture of the platform guarantees the flexibility to apply standard synthesis protocols (e.g., ^{18}F -FDG) as well as to develop new synthetic routes (e.g., ^{18}F -fluorocholines).

Dedicated multipurpose impedimetric biochips (Fig. 1b) were also implemented to allow an early-stage detection of both aggressive and treatment-resistant cancers like the Pancreatic Ductal Adenocarcinoma (PDAC) or less aggressive but very common forms like prostate cancer (PC). Based on the evaluation of new biomarkers for PDAC or the free-to-total PSA ratio for PC, impedimetric biochips were tested with patients serum samples and demonstrated to have a potential diagnostic and prognostic value with better performance than traditional techniques, such as ELISA. A modified layout for on chip impedimetric-based migration assays was also optimized to evaluate the invasiveness of cell lines (e.g., hepatocellular carcinoma) as a function of the microenvironment.

The strong impact on the market and patient health of these multipurpose microfluidic platforms is confirmed by our interaction with companies as active partners or sponsors in several national and international projects.

Contact Persons

Valentina Arima (valentina.arima@nano.cnr.it),
Giuseppe Maruccio (giuseppe.maruccio@unisalento.it)

Collaborators

R. Rinaldi, M. Bianco, M. S. Chiriaco, F. De Feo, E. Perrone, E. Primiceri, A. Zacheo, A. Zizzari.

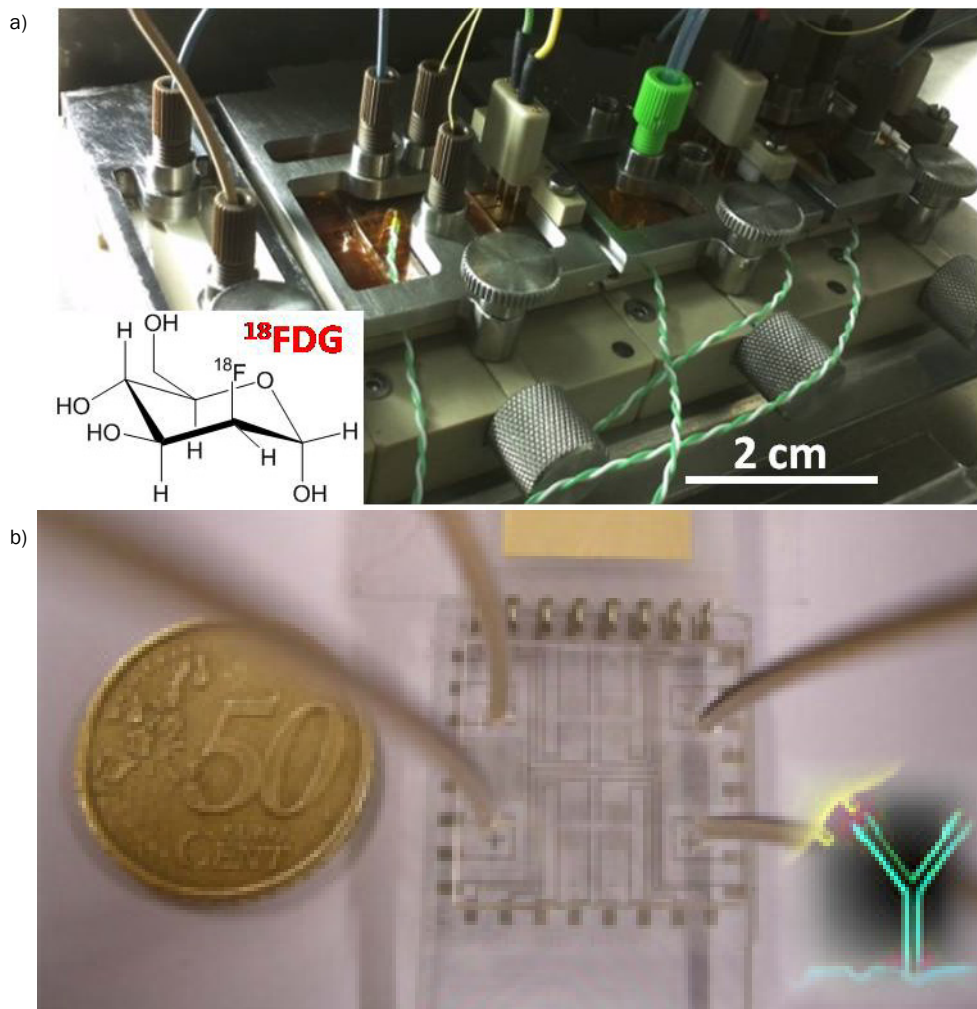


Figure 1.
Lab on chip devices for a) production of radiopharmaceuticals and b) for cancer diagnosis.

Related publications *Radiochemistry on chip: towards dose-on-demand synthesis of PET radiopharmaceuticals.* V. Arima et al., *Lab on a Chip* **13**, 2328 (2013).

Towards pancreatic cancer diagnosis using EIS biochips. M. S. Chiriaco et al., *Lab on a Chip* **13**, 730 (2013).

Cell chips as new tools for cell biology – results, perspectives and opportunities. E. Primiceri et al., *Lab on a Chip* **13**, 3789 (2013).

High-resolution Imaging of physicochemical parameters in living cells by novel bioconjugable fluorescent probes

High-resolution fluorescence imaging techniques make now accessible the detection of meso-nanoscale features in living cells by non-ionizing visible radiation. Accordingly, recent years witnessed a considerable effort towards the development of novel fluorescent probes targeted at real-time visualization of physicochemical parameters in living cells. In this field, we developed novel bioconjugable organic probes reporting on the dielectric constant and viscosity of their immediate nanoenvironment, as well as genetically-encoded protein reporters of local pH. The utility of these probes was demonstrated in several biological contexts.

The arsenal of fluorescent probes tailored to functional imaging of cells is rapidly growing and benefits from recent developments in imaging strategies. Fluorescent probes can be roughly classified into two major families: 1) systems whose excited state energy and lifetime are modulated by local properties, such as polarity and viscosity, 2) systems characterized by multiple ground/excited states owing to binding to target molecular species. Following our long-standing interest in this field, we successfully accomplished the rational development of effective and bioconjugable probes belonging to both families. As for the first family, we engineered a visible-absorbing/emitting fluorescent analog of GFP chromophore (Ge1), which efficiently reports on nanoscale dielectric constant ϵ with good accuracy. This probe is suitable for bioconjugation, and its derivatives were applied to report on local polarity of micelles, LUVs, and protein surfaces in vitro. By confocal microscopy we obtained spatially resolved ϵ maps for many subcellular compartments, such as endoplasmic reticulum, nuclear envelope, and plasma membrane in cultured CHO cells (Fig. 1).

Then, we developed the blue-absorbing/green-emitting “molecular rotor” (i.e., a fluorescent nanorheometer) S3 based on a hyperconjugated stilbene structure. S3 allows for efficient intracellular viscosity measurements by means of the phasor approach to fluorescence lifetime imaging, a fit-free method that overcomes the main drawbacks of conventional lifetime imaging. Viscosity-sensitive S3 was applied to monitor the local viscosity in live cell membrane, lysosomes, and mitochondria, both in physiological and non-physiological states.

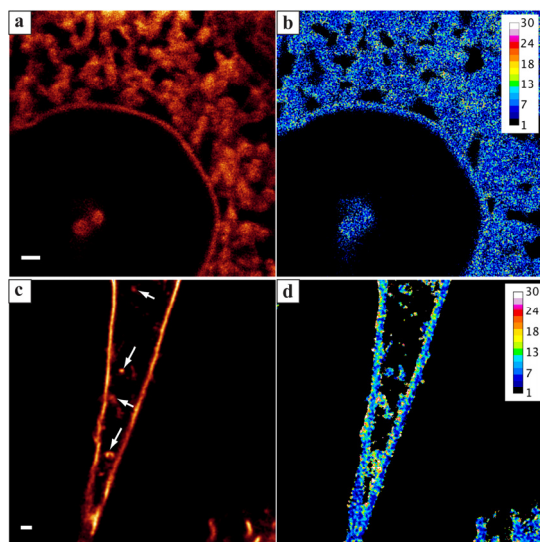


Figure 1.

Fluorescence images (a, c) and ϵ maps (b, d) of subcellular regions of CHO cells treated with the probe of dielectric constant (c) Ge1. Scale bar: 1 μ m. (a) Ge1 localizes mostly in the endoplasmic reticulum and nuclear envelope. (b) ϵ map referring to (a). (c) Lipid-bound Ge1 stains the plasma membrane and vesicles budding therefrom (arrows). (d) ϵ map referring to (c).

Contact Person

Ranieri Bizzarri (ranieri.bizzarri@nano.cnr.it)

Collaborators

G. Abbandonato, A. Battisti, M. Digman, E. Gratton, E. Jacchetti, G. Signore, M. Stoeckl, B. Storti, V. Subramaniam, F. Beltram.

As for the second family, we applied the phasor approach to a green fluorescent protein mutant (E2GFP) associated with two pH-dependent states with different optical properties. By this method we were able to obtain pH maps in living cell, both in physiological and non-physiological states (Fig. 2), by single-photon confocal or two-photon microscopy.

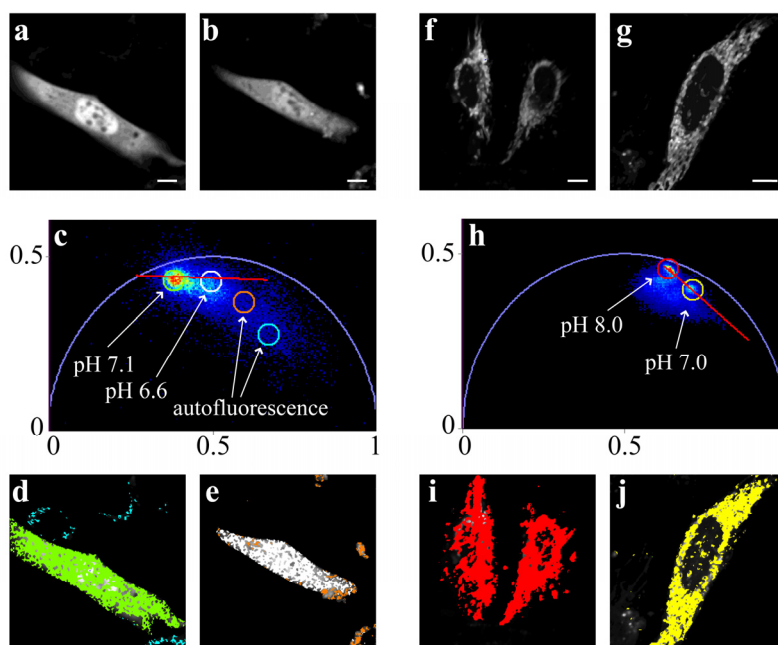


Figure 2.

pH analysis of cells expressing E²GFP in cytoplasm or mitochondria under resting conditions or pro-apoptotic oxidative stress (1.5 % H₂O₂ for 5 min). (a,b) Cytoplasmic E²GFP was imaged by two-photon excitation at 740 nm in a 3T3 fibroblast at rest (a) or under oxidative stress (b). (c) Phasor plots for images (a) and (b) together with pH calibration (red line); relevant pH and autofluorescence phasors are enclosed in colored circles. Two-photon excitation at 740 nm was carried out to increase the amount of collected autofluorescence compared to 800 nm, in order to demonstrate more clearly that autofluorescence can be discriminate from E²GFP signal in the phasor plot; note that measurements at 740 and 800 nm differed on average by 0.06 pH units at pH 6.8-7.2, a pH drift consistent with the accuracy of pH measurement. (d) Same as image (a), but the pixels corresponding to pH 7.1 and autofluorescence are highlighted by the corresponding circle colors of phasor plot. (e) Same as image (b), but the pixels corresponding to pH 6.6 and autofluorescence are highlighted by the corresponding circle colors of phasor plot. (f,g) Mitochondrion-targeted E²GFP was imaged by single-photon excitation at 405 nm in a HeLa cell at rest (f) or under pro-apoptotic oxidative stress (g). (h) Phasor plots for images (f) and (g) together with pH calibration (red line); relevant pH phasors are enclosed in colored circles. (i) Same as image (f), but the pixels corresponding to pH 8.0 are highlighted by the corresponding circle color of phasor plot. (j) Same as image (g), but the pixels corresponding to pH 7.0 are highlighted by the corresponding circle color of phasor plot. In all images, scale bar = 10 μm.

Related publications *Imaging the static dielectric constant in vitro and in living cells by a bioconjugable GFP chromophore analog.* G. Signore, G. Abbandonato, B. Storti, M. Stockl, V. Subramaniam, and R. Bizzarri, *Chem. Comm.* **49**, 1723-1725 (2013).

Intracellular pH measurements made simple by fluorescent protein probes and the phasor approach to fluorescence lifetime imaging. A. Battisti, M. A. Digman, E. Gratton, B. Storti, F. Beltram, and R. Bizzarri, *Chem. Comm.* **48**, 5127-5129 (2013).

Neuronal differentiation on anisotropic substrates and the influence of nanotopographical noise on neurite contact guidance

Cells are exposed to directional physical signals determined by the environment that in vivo coexist with some degree of topographical noise. Here we study neuronal response to directional stimuli by exploiting nanogratings (NGs) with controlled amount of random nanotopographical noise. We show that the loss of neurite guidance is not linear with noise, but is a threshold effect, correlating with changes in focal adhesion (FA) maturation and spatial organization. Finally nocodazole, a drug that increases cell contractility, can improve neurite alignment by promoting aligned FA maturation. These results show new possibilities for successful implant strategies for nerve-regeneration devices.

It is now well established that neurons respond to the morphology of extracellular environment at the nanoscale level. Topological and mechanical features of the extracellular matrix (ECM) are read by specific cellular systems, including integrin-based adhesion clusters [Focal Adhesions (FAs)]. FAs act as topographical sensors, capable of integrating multiple nanotopographical information sources into specific biomolecular instructions via cytoskeletal signaling that regulates cell sensing, shape, and contractility. Thanks to the recent developments in micro/nanoengineering techniques, the processes that control neuronal adhesion and differentiation can now be directly investigated by using nanotextured substrates.

Here, we study neuronal cell responses to hidden directional stimuli by exploiting NGs with a controlled degree of random nanotopographical noise and overall substrate directionality.

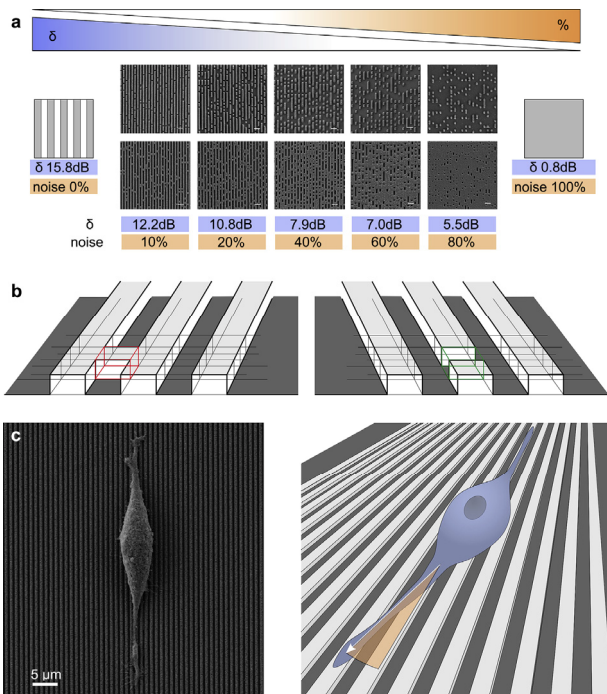


Figure 1.

Noisy nanogratings (NGs) and PC12 cells. (a) Scanning electron images of noisy NGs (500 nm ridge and 500 nm grooves). Each substrate is characterized by a percentage of noise and a cell-dependent directionality (δ). (b) Negative noise (left panel) consists in links between adjacent ridges; positive noise (right panel) consists in gaps along the ridges. (c) Typical SEM image of a PC12 cell differentiating on an unperturbed NG (left panel). Neurite alignment is defined by approximating the neurite as a straight line from the initial to the end point and taking the angle of this line versus the NG orientation (right panel).

Contact Person

Marco Cecchini (marco.cecchini@nano.cnr.it)

Collaborators

I. Tonazzini, S. Antonini, S. Meucci, F. Beltram.

Our data show that the loss of neurite guidance does not increase linearly with nanotopographical noise, but is a threshold process. Nanotopographical noise also impacts FA maturation and directionality, and exhibits a non-linear behavior correlating with neurite alignment. This demonstrates that neurite path finding, through FA sensing, is capable of retrieving information from partially ordered topographies, in agreement with the presence of physiological structural noise in the extracellular environment in vivo. Moreover, in differentiating PC12 neuronal cells, enhanced contractility can improve mechanotransduction. Nocodazole, a potent microtubule depolymerizing agent that is known to increase cell contractility via Rho-A pathway activation, emerges as an effective pharmacological tool to improve neurite alignment by promoting aligned FA maturation in the case of nanotopographical noise. Since topographical modification of the cell substrate interface is an important regulator of cellular adhesion and function, our results suggest that pharmacological treatments may significantly improve implant success in clinical use, particularly for nerve-regeneration devices.

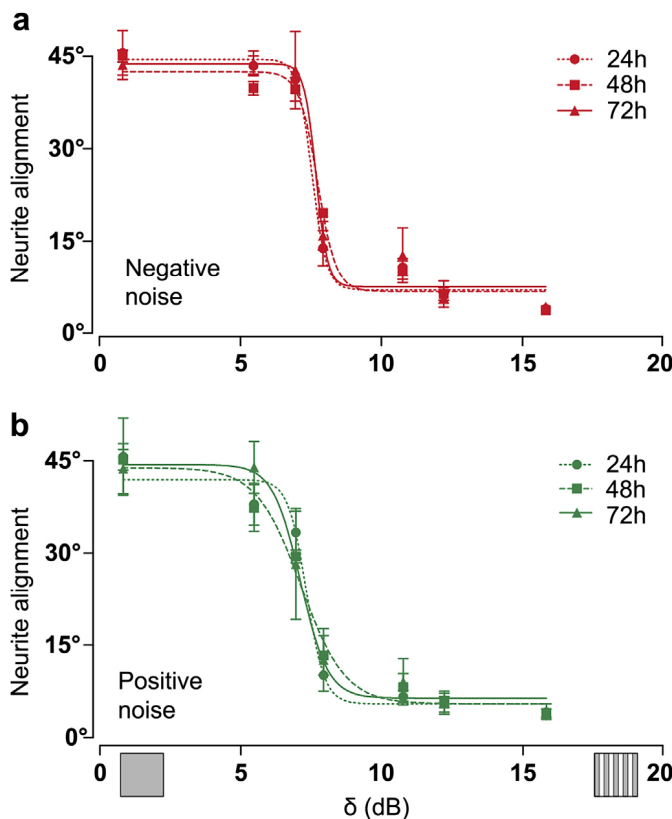


Figure 2. Neurite alignment vs. substrate directionality for (a) negative noise and (b) positive noise: tolerance to nanotopographical noise.

Related publications *Neuronal differentiation on anisotropic substrates and the influence of nanotopographical noise on neurite contact guidance.* I. Tonazzini, S. Meucci, P. Faraci, F. Beltram, and M. Cecchini, *Biomaterials* **34**, 6027 (2013).

Biocompatible noisy nanotopographies with specific directionality for controlled anisotropic cell cultures. S. Meucci, I. Tonazzini, F. Beltram, and M. Cecchini, *Soft Matter* **8**, 1109 (2012).

Studying folding pathways and energy landscapes of single protein molecules using optical tweezers and MD simulations

Protein folding remains a major unsolved challenge for modern biophysics. Despite the experimental and theoretical efforts of many laboratories in the last 40 years, our understanding of the mechanisms by which proteins lose or gain structure is still largely incomplete. This lack of information is partly due to the inadequacy of conventional ensemble methods to study a process that is highly heterogeneous. Using single-molecule optical tweezers, in combination with molecular dynamics simulations, Cnr researchers have described the behavior under tension of the acyl-CoA binding protein (ACBP) and the intricacies of the folding mechanism of the neuronal calcium sensor-1 protein (NCS-1).

1) Mechanical unraveling of ACBP.

Previous studies, performed in the high force regime of atomic force microscopy, had shown that natively folded proteins are brittle under tension, unfolding after small mechanical deformations, while molten globule intermediate states are pliable structures.

Moreover, under force proteins appeared to unfold more through a different sequence of events than during spontaneous unfolding. Cnr researchers have employed optical tweezers (Fig. 1), in combination with MD simulations, to show that in the low force regime explored by this technique the four- α -helix acyl-CoA binding protein (ACBP) displays an atypical compliance along two nearly orthogonal pulling axes, with a mechanically deformability greater than that observed for the highly pliant molten globule intermediate states. Furthermore, when manipulated from the N- and C-termini, ACBP unfolds by populating a transition state that resembles that observed during chemical denaturation. These data provide the first experimental evidence of a spontaneous-like mechanical unfolding pathway of a protein.

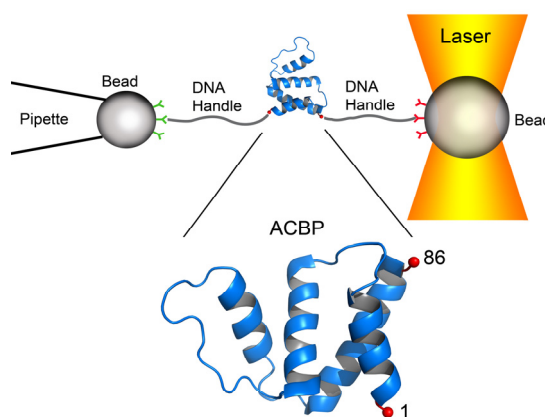


Figure 1.

Optical tweezers experimental setup. A single protein is manipulated between two polystyrene beads by means of DNA molecular handles.

Contact Person

Ciro Cecconi (ciro.cecconi@unimore.it)

Collaborators

P. O. Heidarsson, B. B. Kragelund, S. Corni, R. Di Felice, L. Bellucci I. Valpapuram, C. Camilloni, A. Imparato, G. Tiana, F. M. Poulsen, M. R. Otazo, A. Mossa, E. Paci.

2) Folding mechanism of single NCS-1 proteins.

The emerging family of EF-hand neuronal calcium sensor (NCS) proteins is responsible for sensing changes in neuronal Ca^{2+} concentration, and its members are linked to a number of disorders such as schizophrenia and autism. Despite impressive advances in decoding their structure-function relationship, the folding mechanism of these proteins remains widely unknown. Cnr researchers have used optical tweezers and MD simulations to intimately explore the folding trajectories of the human neuronal calcium sensor 1 (NCS1), the primordial member of the NCS family. The results of these studies revealed a remarkable folding network characterized by a precise sequence of events synchronized by Ca^{2+} binding. The equilibrium inter-conversion between different molecular states was monitored through constant-force experiments and analyzed with advanced statistical methods to reconstruct the free-energy landscape of the protein (Fig. 2). This study provides the first mechanistic and kinetic details on the folding process of a NCS protein.

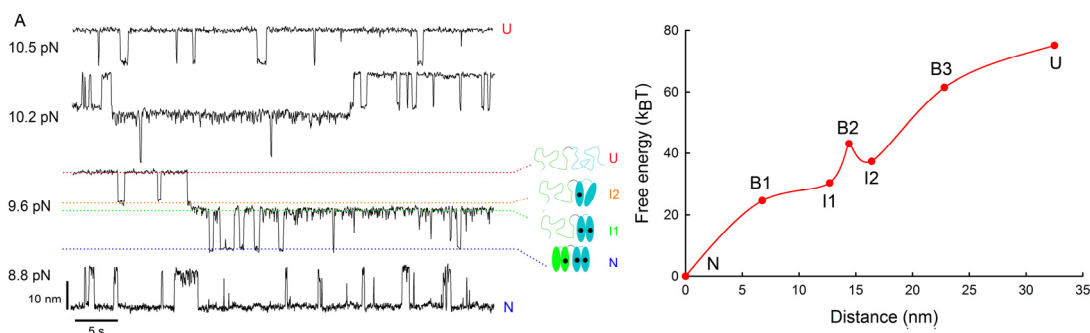


Figure 2.

A) Fluctuations of NCS-1 between different molecular conformations (U, I2, I1 and N) at indicated constant forces.
B) Energy landscape of NCS-1, where B1, B2, and B3 represent the energy barriers between the different states.

Related publications *A highly compliant protein native state with a spontaneous-like mechanical unfolding pathway.* P. O. Heidarsson, I. Valpapuram, C. Camilloni, M. Imparato, G. Tiana, F. M. Poulsen, B. B. Kragelund, and C. Cecconi, *J. Am. Chem. Soc.* **134**, 17068-17065 (2012).

Single-Molecule Folding Mechanism of an EF-Hand Neuronal Calcium Sensor. P. O. Heidarsson, M. R. Otazo, L. Bellucci, A. Mossa, A. Imparato, E. Paci, S. Corni, R. Di Felice, B. B. Kragelund, and C. Cecconi, *Structure* **21**, 1812-1821 (2013).

Lapatinib/Paclitaxel polyelectrolyte nanocapsules for overcoming multidrug resistance in ovarian cancer

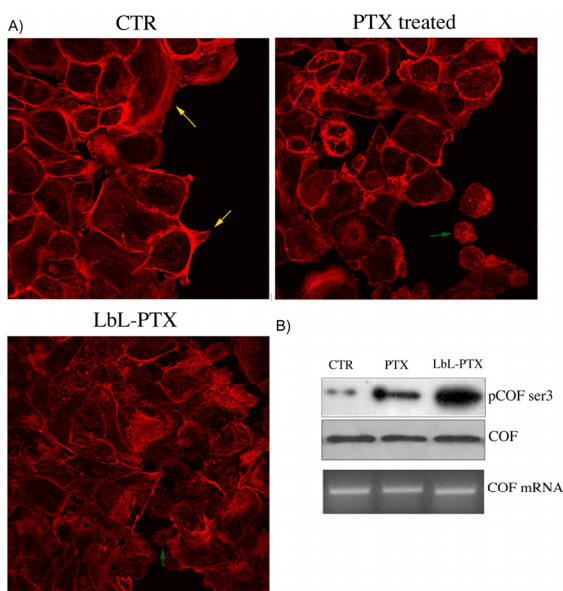
The sonication-assisted layer-by-layer (SLBL) technology was developed for producing an efficient drug-delivery system: (i) control of nanocolloid size within 100 – 300 nm, (ii) high drug content (70% wt), (iii) shell biocompatibility and biodegradability, (iv) sustained controlled release, and (v) multidrug-loaded system. Stable nanocolloids of Paclitaxel (PTX) and lapatinib were prepared by the SLBL method. In a multidrug-resistant (MDR) ovarian cancer cell line, OVCAR-3, lapatinib/PTX nanocolloids mediated an enhanced cell growth inhibition in comparison with the PTX-only treatment. The small size and functional versatility of these nanoparticles, combined with their ability to incorporate various drugs, indicates that lapatinib/PTX nanocolloids may have in vivo therapeutic applications.

Ovarian cancer still remains one of the most lethal malignancies among women. Despite enormous progress in understanding ovarian cancer biology to date, there are no examples of therapies leading to cures. Therefore, improving the efficacy of current therapeutics will have a great impact in the management of the disease. Paclitaxel (PTX) is widely used for the treatment of patients with ovarian cancer, but despite substantial clinical efficacy, the optimal administration regimen remains elusive. Many questions remain concerning the way to administer the drug and the molecular mechanisms at the basis of chemoresistance. Among the proteins related to the chemoresistance process, the overexpression of P-gp has profound implications in clinical practice.

In fact, the presence of drug-efflux pumps that mediate the active efflux of chemotherapeutics is one of the most extensively described mechanisms of drug resistance, and strategies to modulate or block this process have been investigated actively in oncology. In ovarian cancer, the expression of P-gp has been implicated in chemoresistance, correlated inversely with patient survival and associated with resistance to PTX.

Figure 1.

Confocal laser microscopic observation of OVCAR-3 cells. (A) Ovarian cancer cells plated on glass coverslips were treated with PTX or LBL-PTX nanocolloids at the concentration of 5 µg/mL for 24 h and then fixed. Cells were stained with TRITC-phalloidin. (B) The phosphorylation status of cofilin at ser3 was assessed with a phospho specific antibody, and then the blot was reprobed for total cofilin levels. The mRNA level of cofilin was assessed by using a specific set of primer (Reproduced with Permission from Ref. 1).



Contact Person

Stefano Leporatti (stefano.leporatti@nano.cnr.it)

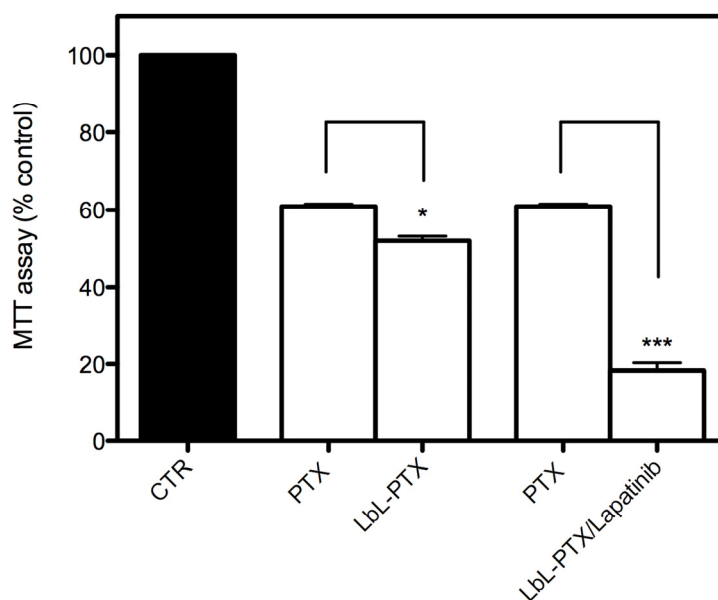
Collaborators

Y. M. Lvov, M. Maffia, D. Vergara, A. Tinelli, V. Lorusso.

These observations set the stage for the development of efficacious instruments to increase PTX efficacy by limiting adverse side effects and increasing its cytotoxic action. In this regard, nanotechnology has been recognized as a fundamental tool in cancer research, and the potential of nanocarriers to increase drug efficacy is well described. Here, we describe a SLBL method to efficiently convert PTX into drug NPs. It allows clinicians to combine many necessary factors for an efficient drug-delivery system: i) control of nanocolloid size within 100 – 300 nm, ii) high drug content of approximately 70% wt, iii) shell biocompatibility and biodegradability, and iv) sustained controlled release. Overall, these characteristics, including the small size and the net negative charge that can be advantageous for their penetration to and within tumors, make NPs attractive candidates for possible in vivo application. In addition, in this research we elaborated nano-formulation of two drugs in one nanocapsule locating PTX in the core and lapatinib on the shell periphery. The rationale for considering combination therapy is to overcome major problems associated with PTX administration, such as the counteraction of PTX resistance and, in combination with dose-escalation, the potential reduction of systemic toxicities. Moreover, with this strategy both drugs can be temporally co-localized in the tumor cells for optimal synergy, limiting possible differences in the pharmacokinetics and tumor accumulation of the two different agents. Given the molecular complexity of cancer, drug combinations are most likely to translate into a significant clinical benefits.

Figure 2.

LBL-lapatinib/PTX nanocolloids demonstrate significant cytotoxic activity in P-gp overexpressing ovarian cancer cells as determined by MTT test ($P < 0.05$; $P < 0.01$; $P < 0.001$).



Related publications

Lapatinib/Paclitaxel Polyelectrolyte Nanocapsules for Overcoming Multidrug Resistance in Ovarian Cancer. D. Vergara, C. Bellomo, X. Zhang, V. Vergaro, A. Tinelli, V. Lorusso, R. Rinaldi, Y. M. Lvov, S. Leporatti, and M. Maffia, *Nanomedicine: Nanotechnology, Biology and Medicine (NBM)* **8**, 891-899 (2012).

Polyelectrolyte Capsules as Carriers for Growth Factor Inhibitor Delivery to Hepatocellular Carcinoma. F. Baldassarre, V. Vergaro, F. Scarlino, F. De Santis, G. Lucarelli, A. della Torre, G. Ciccarella, R. Rinaldi, G. Giannelli, and S. Leporatti, *Macromol Biosci* **12**, 656-665 (2012).

Teaching new tricks to an old dog

Brain cells are immersed in a complex structure forming the extracellular matrix. The composition of the matrix gradually matures during postnatal development, as brain circuitry reaches its adult form. The fully developed extracellular environment stabilizes neuronal connectivity and decreases cortical plasticity. The mechanisms through which the matrix inhibits cortical plasticity are not fully clarified. Here we show that a prominent component of the matrix, chondroitin sulfate proteoglycans, restrains morphological changes of dendritic spines in the visual cortex of adult mice. By means of in vivo and in vitro two-photon imaging and electrophysiology, we find that after enzymatic digestion of CSPGs, cortical spines become more mobile and express a larger degree of structural and functional plasticity.

A large part of brain computation occurs in tiny structures, called dendritic spines, that decorate the surface of neurons: here inputs are received on the excitatory synapses. These structures are the first stage of the signal processing that leads to the generation of the neuron output (Fig. 1A-C). Size and shape of dendritic spines are tightly correlated with the underlying processes of memory formation and learning. Indeed, physiological or pathological processes that create and modify synaptic connections, are always reflected in changes in dendritic spines. A striking characteristic of learning processes is that they are much facilitated in young age but they are progressively restrained as the individual ages (Fig. 1D-E). This defines a “critical period” in which brain circuitry is strongly plastic and easily modeled by experience. Most brain regions become extremely stable after the closure of their critical period since the existing synapses are virtually unchangeable. Obviously, the possibility of controlling at will the opening or closing of critical periods is of great interest, given its potential importance for brain repair and for the correction of erroneous brain connectivity that might have occurred early in development because of a pathological condition. Unfortunately, the mechanisms responsible for the closure of critical periods are varied and only partially known.

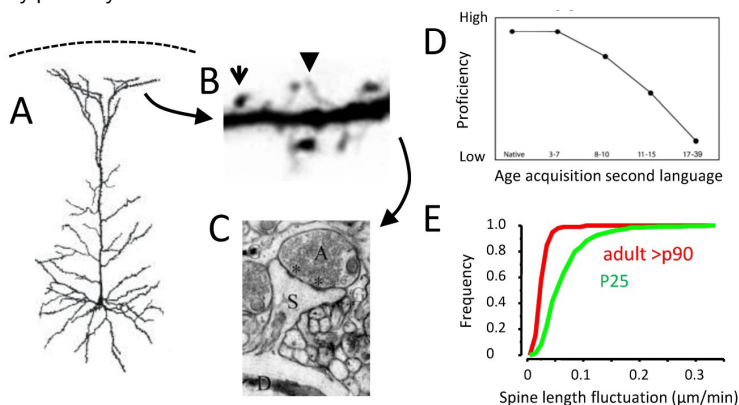


Figure 1.

Dendritic spine can be visualized in vivo by the expression of the Green Fluorescent Protein imaged by means of two-photon imaging. A) Drawing from Cajal showing a pyramidal neuron. The cell body is at the bottom of the drawing surrounded by a complex dendritic arborisation. The entire neuron is very large, its size depending on species: in the mouse a cell like this spans about 0.8 mm of cortical thickness.

B) High magnification shows that dendrites are covered with spines ranging in dimension between 0.5 to 2.5 μm . In the image, both mature, mushroom-like spines (arrow) and filopodia (arrowhead) are visible. C) Each mature spine carries a synapse (D: dendrite; S: dendritic spine; A: axon terminal; asterisks indicate presynaptic vesicles). D) Critical period for the learning of a second language. The critical period duration depends on the brain structure. The critical period in the sensory cortex of human ends at a few years of age, while it lasts about 4-5 weeks in mice. E) Dendritic spine mobility decreases after the closure of the critical period in the sensory cortex of mice, as measured by time lapse imaging in vivo by means of two-photon microscopy.

Contact Persons

Gian Michele Ratto (gianmichele.ratto@nano.cnr.it)
Silvia Landi (silvia.landi@nano.cnr.it)

Collaborators

P. Artoni, M. Brondi, R. Parra, F. Pederzoli, E. Pracucci, S. Sulis Sato, F. Trovato.

Here we studied one of the factors limiting plasticity in the adult: the extracellular matrix. The composition of the matrix gradually matures during postnatal development, as the brain circuitry reaches its adult form. The fully developed extracellular environment stabilizes neuronal connectivity and decreases cortical plasticity. However, the mechanisms through which the matrix inhibits cortical plasticity are not fully clarified. In this study we show that a prominent component of the matrix, chondroitin sulfate proteoglycans, restrains morphological changes of dendritic spines in the visual cortex of adult mice. By means of *in vivo* and *in vitro* two-photon imaging and electrophysiology, we find that after enzymatic digestion triggered by the proteolytic enzyme ChABC, cortical spines become more mobile and express a larger degree of structural and functional plasticity (Fig. 2).

Our results suggest that the degradation of the extracellular matrix removes an inhibitory constraint on dendritic spines and allows for the expression of their structural and functional plasticity, and that these processes might emerge as an important modulator of brain circuitry.

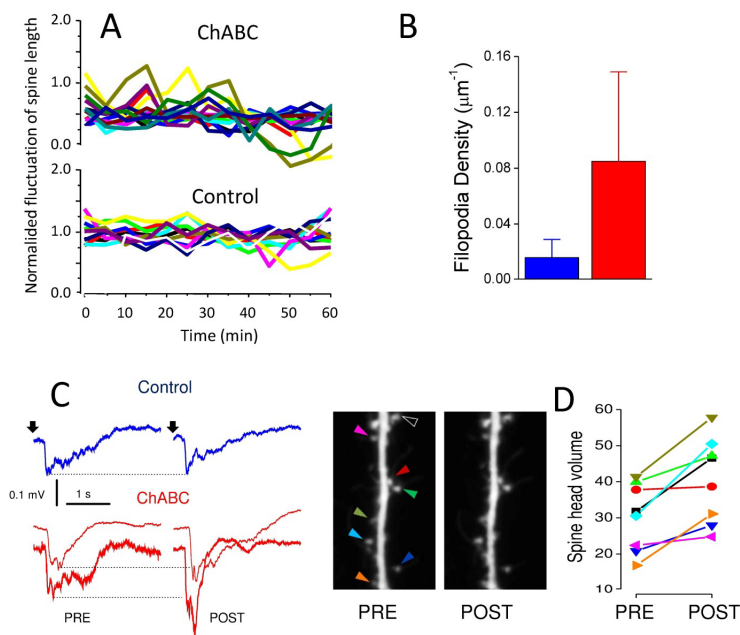


Figure 2.

Extracellular matrix and dendritic spine mobility and functional plasticity. A) Mobility of dendritic spines is measured by observing the variation of their length in the visual cortex of adult mice during a time lapse acquisition. In control conditions, dendritic spines are very stable and their length changes very little during imaging. In contrast, after matrix digestion, the variability of the spine length is much larger, indicating their destabilization. B) The density of immature filopodial protrusion is greatly increased after ChABC treatment indicating increased formation of new spines.

C) The transient electrical potentials evoked in the cortex by a visual stimulus are recorded before (PRE) and after (POST) an episode of high-frequency activity known to induce diffused synaptic potentiation. Physiological responses to visual stimuli are increased only after degradation of the extracellular matrix. D) Dendritic spines imaged at the two-photon microscope. The arrows indicate dendritic spines where head volume was measured before and after chemical potentiation. In control conditions we observed no changes in spine head volume (not shown here), while the increase was apparent when the cortex was pretreated with ChABC.

Related publication

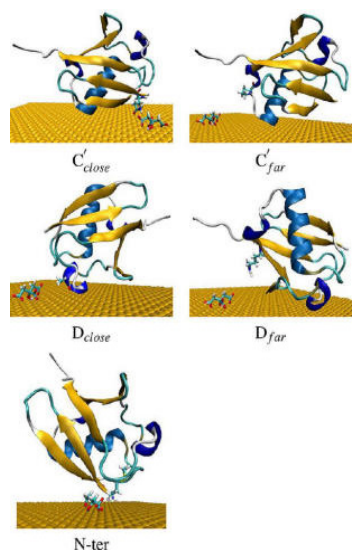
Extracellular matrix inhibits structural and functional plasticity of dendritic spines in the adult visual cortex. L. de Vivo, S. Landi, M. Panniello, L. Baroncelli, S. Chierzi, L. Mariotti, M. Spolidoro, T. Pizzorusso, L. Maffei, and G. M. Ratto, *Nat. Commun.* **4**, 1484 (2013).

Simulating protein-nanoparticle interactions at multiple scales

Protein-nanoparticle associations have important applications in nanoscience and nanotechnology such as targeted drug delivery and theranostics. However, the mechanisms by which proteins recognize nanoparticles and the determinants of specificity are still poorly understood at the microscopic level. Atomistic simulations have the potential to clarify such mechanisms. However, the multiple length and time scales of the phenomena involved require the coordinated use of different methods, from ab initio to rigid docking. We have developed and applied such methods, showing that they can indeed provide microscopic information not accessible to even the most accurate experiments available so far.

The interaction between proteins and nanoparticles (NPs) is central to many applications in nanoscience and nanotechnology. For example, the natural recognition capabilities of proteins have inspired novel bottom-up approaches to self-assembly complex nanostructures. Peptides have been used for the controlled and biocompatible synthesis of NPs. In the flourishing field of biological and biomedical applications of nanomaterials, much work is ongoing to characterize the physicochemical parameters for the interaction between NPs and proteins, and to determine their biological effects, including their potential toxicity. Despite its relevance, a detailed structural understanding of protein-nanoparticle interactions is still elusive.

Computer simulations at the atomistic level are a powerful tool that can effectively complement experimental studies of protein-NP and protein-surface systems. Based on the methods that we have developed in the last years, we have performed a comprehensive investigation of the interaction of a biologically relevant protein, Ubiquitin (Ubq), with citrate-stabilized gold nanoparticles. We have used atomistic simulations at multiple levels of theory, including Brownian dynamics, classical molecular dynamics, and Density Functional Theory (DFT) calculations.



The comparison of these simulations with experiments, provided molecular insights into the Ubq-gold NP interactions, is not directly accessible by experiments. In particular, we were able to reveal the nature of the interactions guiding the binding of Ubq to the gold nanoparticle. Docking results obtained in various conditions (bare surface, citrate-covered surface) suggested that some citrate molecules coexist with the adsorbed protein on the surface of the NP (Fig. 1) while others are displaced. Finally, DFT calculations explained the origin of the experimental NMR chemical shift perturbation upon binding. Our work demonstrated how experiments and simulations can be used together to reveal basic features of the protein-nanoparticle systems that cannot be inferred from either of them alone.

Figure 1.

Protein-Gold configurations obtained by Brownian dynamics rigid docking in the presence of a citrate molecule. The protein orientation in the structure dubbed N-ter is that in closer agreement with the experimental NMR data, and it is found only in the presence of citrates. Water is considered implicitly, and it is not shown for clarity.

Contact Person Stefano Corni (stefano.corni@nano.cnr.it)

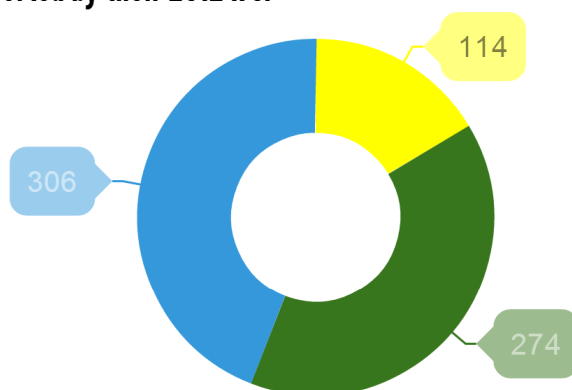
Collaborators G. Brancolini, D. B. Kokh, L. Calzolai, R. C. Wade.

Related publication *Docking of ubiquitin to gold nanoparticles.* G. Brancolini, D. B. Kokh, L. Calzolai, R. C. Wade, and S. Corni, ACS Nano **6**, 9863 (2012).



Publications

Total number of publications (694) in 2012-2013 sorted by their 2012 IFs.



EU Countries we collaborate with

Moreover, we have strong collaborations with Switzerland, Russia, Israel, USA, Canada, Australia, Japan, Singapore, South Africa



A list of publications from journals with $IF \geq 7.943$ (i.e., *Physical Review Letters*'s) ordered by their JCR 2012 IF is given. A full and updated list of publications is available on the Institute website: <http://www.nano.cnr.it/> at the page "Publications". Publications marked with © earned a cover in the relevant journal. Covers are all shown at the end of the section.

The Josephson heat interferometer.

F. Giazotto and M. J. Martínez-Pérez. *Nature* 492, 401-405 (2012).

Second-harmonic generation in silicon waveguides strained by silicon nitride.

M. Cazzanelli, F. Bianco, E. Borga, G. Pucker, M. Ghulinyan, E. Degoli, E. Luppi, V. Veniard, S. Ossicini, D. Modotto, S. Wabnitz, R. Pierobon, and L. Pavesi. *Nat Mater* 11, 148-154 (2012).

Graphene field-effect transistors as room-temperature terahertz detectors.

L. Vicarelli, M. S. Vitiello, D. Coquillat, A. Lombardo, A. C. Ferrari, W. Knap, M. Polini, V. Pellegrini, and A. Tredicucci. *Nat Mater* 11, 865-871 (2012).

Molecular electronics: Protein transistors strike gold.

G. Maruccio. *Nat Nanotechnol* 7, 147-148 (2012).

Carrier multiplication between interacting nanocrystals for fostering silicon-based photovoltaics.

M. Govoni, I. Marri, and S. Ossicini. *Nat Photonics* 6, 672 (2012).

Graphene plasmonics.

A. N. Grigorenko, M. Polini, and K. S. Novoselov. *Nat Photonics* 6, 749-758 (2012).

Quantum-limited frequency fluctuations in a terahertz laser.

M. S. Vitiello, L. Consolino, S. Bartalini, A. Taschin, A. Tredicucci, M. Inguscio, and P. De Natale. *Nat Photonics* 6, 525-528 (2012).

High-fidelity quantum driving.

M. G. Bason, M. Viteau, N. Malossi, P. Huillery, E. Arimondo, D. Ciampini, R. Fazio, V. Giovannetti, R. Mannela, and O. Morsch. *Nat Phys* 8, 147-152 (2012).

Charge down and heat up.

S. Heun. *Nat Phys* 8, 640-641 (2012).

Electrically tunable organic distributed feedback lasers embedding nonlinear optical molecules.

A. Camposeo, P. Del Carro, L. Persano, and D. Pisignano. *Adv Mater* 24, OP221 (2012).

© Two-photon continuous flow lithography.

S. C. Laza, M. Polo, A. A. R. Neves, R. Cingolani, A. Camposeo, and D. Pisignano. *Adv Mater* 24, 1304-1308 (2012).

© CdS-polymer nanocomposites and light-emitting fibers by in situ electron-beam synthesis and lithography.

L. Persano, A. Camposeo, F. Di Benedetto, R. Stabile, A. M. Laera, E. Piscopiello, L. Tapfer, and D. Pisignano. *Adv Mater* 24, 5320-2326 (2012).

Quantum channels and their entropic characteristics.

A. S. Holevo and V. Giovannetti. *Rep Prog Phys* 75, 046001 (2012).

Electron transport in SiGe alloy nanowires in the ballistic regime from first-principles.

M. Amato, S. Ossicini, and R. Rurali. *Nano Lett* 12, 2717-2721 (2012).

Electrostatic spin control in InAs/InP nanowire quantum dots.

L. Romeo, S. Roddaro, A. Pitanti, D. Ercolani, L. Sorba, and F. Beltram. *Nano Lett* 12, 4490-4494 (2012).

Connecting dopant bond type with electronic structure in N-doped graphene.

T. Schiros, D. Nordlund, L. Pálková, D. Prezzi, L. Zhao, K. Soo Kim, U. Wurstbauer, C. Gutiérrez, D. Delongchamp, C. Jaye, D. Fischer, H. Ogasawara, L. G. M. Pettersson, D. R. Reichman, P. Kim, M. S. Hybertsen, and A. N. Pasupathy. *Nano Lett* 12, 4025-4031 (2012).

Room-temperature terahertz detectors based on semiconductor nanowire field-effect transistors.

M. S. Vitiello, D. Coquillat, L. Viti, D. Ercolani, F. Teppe, A. Pitanti, F. Beltram, L. Sorba, W. Knap, and A. Tredicucci. *Nano Lett* 12, 96-101 (2012).

Direct determination of polarity, faceting, and core location in colloidal core/shell wurtzite semiconductor nanocrystals.

G. Bertoni, V. Grillo, R. Brescia, X. Ke, S. Bals, A. Catellani, H. Li, and L. Manna. *ACS Nano* 6, 6453 (2012).

Docking of ubiquitin to gold nanoparticles.

G. Brancolini, D. B. Kokh, L. Calzolari, R. C. Wade, and S. Corni. *ACS Nano* 6, 9863 (2012).

Magnetically driven floating foams for the removal of oil contaminants from water.
P. Calcagnile, D. Fragouli, I. S. Bayer, G. C. Anyfantis, L. Martiradonna, P. D. Cozzoli, R. Cingolani, and A. Athanassiou. *ACS Nano* 6, 5413–5419 (2012).

Water-soluble iron oxide nanocubes with high values of specific absorption rate for cancer cell hyperthermia treatment.
P. Guardia, R. Di Corato, L. Lartigue, C. Wilhelm, A. Espinosa, M. Garcia-Hernandez, F. Gazeau, L. Manna, and T. Pellegrino. *ACS Nano* 6, 3080–3091 (2012).

Blue-UV-emitting ZnSe(Dot)/ZnS(rod) core/shell nanocrystals prepared from CdSe/CdS nanocrystals by sequential cation exchange.
H. Li, R. Brescia, R. Krahne, G. Bertoni, M. J. P. Alcocer, C. D'Andrea, F. Scotognella, F. Tassone, M. Zanella, M. De Giorgi, and L. Manna. *ACS Nano* 6, 16347 (2012).

Controlled release of Doxorubicin loaded within magnetic thermo-responsive nanocarriers under magnetic and thermal actuation in a microfluidic channel.
M. L. Pernia, A. Torti, A. Riedinger, R. La Fleur, D. Petti, R. Cingolani, R. Bertacco, and T. Pellegrino. *ACS Nano* 6, 10535–10545 (2012).

Electronic structure of atomically precise graphene nanoribbons.
P. Ruffieux, J. Cai, N. C. Plumb, L. Patthey, D. Prezzi, A. Ferretti, E. Molinari, X. Feng, K. Müllen, C. A. Pignedoli, and R. Fasel. *ACS Nano* 6, 6930–6935 (2012).

A free-standing aligned-carbon-nanotube/nanocomposite foil as an efficient counter electrode for dye solar cells.
F. Malara, M. Manca, M. Lanza, C. Hubner, E. Piperopoulos, and G. Gigli. *Energ Environ Sci* 5, 8377–8383 (2012).

The reversible opening of water channels in cytochrome c modulates the heme iron reduction potential.
C. A. Bortolotti, A. Amadei, M. Aschi, M. Borsari, S. Corni, M. Sola, and I. Daidone. *J Am Chem Soc* 134, 13670 (2012).

A highly compliant protein native state with a spontaneous-like mechanical unfolding pathway.
P. O. Heidarsson, I. Valpapuram, C. Camilloni, A. Imparato, G. Tiana, F. M. Poulsen, B. B. Kragelund, and C. Cecconi. *J Am Chem Soc* 134, 17068–17075 (2012).

“Donor-Two-Acceptor” dye design: a distinct gateway to NIR fluorescence.
N. Karton-Lifshin, L. Albertazzi, M. Bendikov, P. S. Baran, and D. Shabat. *J Am Chem Soc* 134, 20412–20420 (2012).

Understanding the mechanism of short-range electron transfer using an immobilized cupredoxin.
S. Monari, G. Battistuzzi, C. A. Bortolotti, S. Yanagisawa, K. Sato, C. Li, J. Salard, D. Kostrz, M. Borsari, A. Ranieri, C. Dennison, and M. Sola. *J Am Chem Soc* 134, 11848–11851 (2012).

High-performance and site-directed in utero electroporation by a triple-electrode probe.
M. dal Maschio, D. Ghezzi, G. Bony, A. Alabastri, G. Deidda, M. Brondi, S. Sulis Sato, R. Proietti Zaccaria, E. Di Fabrizio, G. M. Ratto, and L. Cancedda. *Nat Commun* 3, 960 (2012).

Phase-locking to a free-space terahertz comb for metrological-grade terahertz lasers.
L. Consolino, A. Taschin, P. Bartolini, S. Bartalini, P. Cancio, A. Tredicucci, H. E. Beere, D. A. Ritchie, R. Torre, M. S. Vitiello, and P. De Natale. *Nat Commun* 3, 1040 (2012).

LY2109761-Loaded microcapsules as drug delivery system to inhibit TGF- β 1 pathway in hepatocellular carcinoma.
A. Mazzocca, F. Baldassarre, V. Vergaro, S. Leporatti, G. Ciccarella, S. Antonaci, and G. Giannelli. *J Hepatology* 56, S115 (2012).

Magnetic anisotropy of Cr₇Ni spin clusters on surfaces.
V. Corradini, A. Ghirri, E. Garlatti, R. Biagi, V. De Renzi, U. del Pennino, V. Bellini, S. Carretta, P. Santini, G. Timco, R. E. P. Winpenny, and M. Affronte. *Adv Funct Mater* 22, 3706 (2012).

Targeting of GSK3 β promotes imatinib-mediated apoptosis in quiescent CD34+ chronic myeloid leukemia progenitors preserving normal stem cells.
G. Reddiconto, C. Toto, I. Palamà, S. De Leo, E. de Luca, S. De Matteis, L. Dini, P. Gambacorti, C. Passerini, N. Di Renzo, M. Maffia, and A. M. Coluccia. *Blood* 119, 2335–2345 (2012).

Colloidal anisotropic ZnO-Fe@FexOy nanoarchitectures with interface-mediated exchange-bias and band-edge ultraviolet fluorescence.
A. Kostopoulou, F. Thetiot, I. Tsiaoussis, M. Androulidaki, P. D. Cozzoli, and A. Lappas. *Chem Mater* 24, 2722–2732 (2012).

Self-assembled CdSe/CdS nanorod micro-lasers fabricated from solution by capillary jet deposition.
M. Zavelani-Rossi, R. Krahne, G. Della Valle, S. Longhi, I. R. Franchini, S. Girardo, F. Scotognella, D. Pisignano, L. Manna, G. Lanzani, and F. Tassone. *Laser & Photonics Rev* 6, 678–683 (2012).

- Optimal correlations in many-body quantum systems.
L. Amico, D. Rossini, A. Hamma, and V. E. Korepin. *Phys Rev Lett* 108, 240503 (2012).
- Frictionless flow in a binary polariton superfluid.
E. Cancellieri, F. M. Marchetti, M. H. Szymanska, D. Sanvitto, and C. Tejedor. *Phys Rev Lett* 108, 065301 (2012).
- Nonuniform scaling applied to surface energies of transition metals.
L. Chiodo, L. A. Constantin, E. Fabiano, and F. Della Sala. *Phys Rev Lett* 108, 126402 (2012).
- Drude weight, cyclotron resonance, and the dicke model of graphene cavity QED.
L. Chiroli, M. Polini, V. Giovannetti, and A. H. MacDonald. *Phys Rev Lett* 109, 267404 (2012).
- Control and ultrafast dynamics of a two-fluid polariton switch.
M. De Giorgi, D. Ballarini, E. Cancellieri, F. M. Marchetti, M. H. Szymanska, C. Tejedor, R. Cingolani, E. Giacobino, A. Bramati, G. Gigli, and D. Sanvitto. *Phys Rev Lett* 109, 266407 (2012).
- Quantum measurement bounds beyond the uncertainty relations.
V. Giovannetti, S. Lloyd, and L. Maccone. *Phys Rev Lett* 108, 260405 (2012).
- Sub-Heisenberg estimation strategies are ineffective.
V. Giovannetti and L. Maccone. *Phys Rev Lett* 108, 210404 (2012).
- Master equations for correlated quantum channels.
V. Giovannetti and G. M. Palma. *Phys Rev Lett* 108, 040401 (2012).
- Spin-to-orbital angular momentum conversion and spin-polarization filtering in electron beams.
E. Karimi, L. Marrucci, V. Grillo, and E. Santamato. *Phys Rev Lett* 108, 044801 (2012).
- Positive Wigner functions render classical simulation of quantum computation efficient.
A. Mari and J. Eisert. *Phys Rev Lett* 109, 230503 (2012).
- Probing the topological exciton condensate via Coulomb drag.
M. P. Mink, R. A. Duine, H. T. C. Stoof, M. Polini, and G. Vignale. *Phys Rev Lett* 108, 186402 (2012).
- Imaging fractional incompressible stripes in integer quantum hall systems.
N. Paradiso, S. Heun, S. Roddaro, L. Sorba, F. Beltram, G. Biasiol, L. N. Pfeiffer, and K. W. West. *Phys Rev Lett* 108, 246801 (2012).
- Short-time spin dynamics in strongly correlated few-fermion systems.
S. Peotta, D. Rossini, P. Silvi, G. Vignale, R. Fazio, and M. Polini. *Phys Rev Lett* 108, 245302 (2012).
- Electron-electron interactions in artificial graphene.
E. Rasanen, C. A. Rozzi, S. Pittalis, and G. Vignale. *Phys Rev Lett* 108, 246803 (2012).
- Tunneling theory of two interacting atoms in a trap.
M. Rontani. *Phys Rev Lett* 108, 115302 (2012).
- Phase estimation via quantum interferometry for noisy detectors.
N. Spagnolo, C. Vitelli, V. G. Lucivero, V. Giovannetti, L. Maccone, and F. Sciarrino. *Phys Rev Lett* 108, 233602 (2012).
- Forbidden band gaps in the spin-wave spectrum of a two-dimensional bicomponent magnonic crystal.
S. Tacchi, G. Duerr, J. W. Klos, M. Madami, S. Neusser, G. Gubbiotti, G. Carlotti, M. Krawczyk, and D. Grundler. *Phys Rev Lett* 109, 137202 (2012).
- Propagation and amplification dynamics of 1D polariton condensates.
E. Wertz, A. Amo, D. D. Solnyshkov, L. Ferrier, T. C. H. Liew, D. Sanvitto, P. Senellart, I. Sagnes, A. Lemaitre, A. V. Kavokin, G. Malpuech, and J. Bloch. *Phys Rev Lett* 109, 216404 (2012).
- Photon production from the vacuum close to the superradiant transition: linking the dynamical Casimir effect to the Kibble-Zurek mechanism.
G. Vacanti, S. Pugnetti, N. Didier, M. Paternostro, G. M. Palma, R. Fazio, and V. Vedral. *Phys Rev Lett* 108, 093603 (2012).

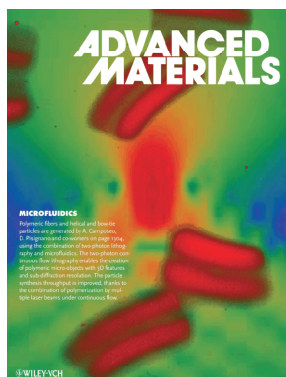
Selected Publications - 2013

- Dynamic control of magnetic nanowires by light-induced domain-wall kickoffs.
E. Heintze, F. Hallak, C. Clauss, A. Rettori, M. G. Pini, F. Totti, M. Dressel, and L. Bogani. *Nat Mater* 12, 202-206 (2013).
- Artificial honeycomb lattices for electrons, atoms and photons.
M. Polini, F. Guinea, M. Lewenstein, H. C. Manoharan, and V. Pellegrini. *Nat Nanotechnol* 8, 625-633 (2013).
- Anderson localization of entangled photons in an integrated quantum walk.
A. Crespi, R. Osellame, R. Ramponi, V. Giovannetti, R. Fazio, L. Sansoni, F. De Nicola, F. Sciarrino, and P. Mataloni. *Nat Photonics* 7, 322-328 (2013).
- Electromagnetic channel capacity for practical purposes.
V. Giovannetti, S. Lloyd, L. Maccone, and J. H. Shapiro. *Nat Photonics* 7, 834-838 (2013).
- Dye-containing polymers: methods for preparation of mechanochromic materials.
F. Ciardelli, G. Ruggeri, and A. Pucci. *Chem Soc Rev* 42, 857-870 (2013).
- Observation and spectroscopy of a two-electron wigner molecule in an ultra-clean carbon nanotube.
S. Pecker, F. Kuemmeth, A. Secchi, M. Rontani, D. C. Ralph, P. L. McEuen, and S. Ilani. *Nat Phys* 9, 576-581 (2013).
- Nanoscale poling of polymer films.
R. Castagna, A. Milner, J. Zyss, and Y. Prior. *Adv Mater* 25, 2234-2238 (2013).
- Magnetic cooling at a single molecule level: a spectroscopic investigation of isolated molecules on a surface.
V. Corradini, A. Ghirri, A. Candini, R. Biagi, U. del Pennino, G. Dotti, E. Otero, F. Choueikani, R. J. Blagg, E. McInnes, and M. Affronte. *Adv Mater* 25, 2816-20 (2013).
- Ultralow voltage, OTFT-based sensor for label-free DNA detection.
S. Lai, M. Demelas, G. Casula, P. Cosseddu, M. Barbaro, and A. Bonfiglio. *Adv Mater* 25, 103-107 (2013).
- Non-blinking single-photon generation with anisotropic colloidal nanocrystals: towards room-temperature, efficient, colloidal quantum sources.
F. Pisanello, G. Leménager, L. Martiradonna, L. Carbone, S. Vezzoli, P. Desfonds, P. D. Cozzoli, E. Giacobino, J.-P. Hermier, R. Cingolani, M. De Vittorio, and A. Bramati. *Adv Mater* 25, 1974-1980 (2013).
- Plasmon-controlled light-harvesting: design rules for biohybrid devices via multiscale modeling.
O. Andreussi, A. Biancardi, S. Corni, and B. Mennucci. *Nano Lett* 13, 4475-4484 (2013).
- Local mechanical properties of electrospun fibers correlate to their internal nanostructure.
A. Camposeo, I. Greenfeld, F. Tantussi, S. Pagliara, M. Moffa, F. Fuso, M. Allegrini, E. Zussman, and D. Pisignano. *Nano Lett* 13, 5056-5062 (2013).
- High mobility one- and two-dimensional electron systems in nanowire-based quantum heterostructures.
S. Funk, M. Royo, I. Zardo, D. Rudolph, S. Morkoetter, B. Mayer, J. Becker, A. Bechtold, S. Matich, M. Doeblinger, M. Bichler, G. Koblmüller, J. J. Finley, A. Bertoni, G. Goldoni, and G. Abstreiter. *Nano Lett* 13, 6189-6196 (2013).
- Modification of molecular spin crossover in ultrathin films.
A. Pronschinske, Y. Chen, G. F. Lewis, D. A. Shultz, A. Calzolari, M. Buongiorno Nardelli, and D. B. Dougherty. *Nano Lett* 13, 1429-1434 (2013).
- Subnanometer local temperature probing and remotely controlled drug release based on azo-functionalized iron oxide nanoparticles.
A. Riedinger, P. Guardia, A. Curcio, M. A. Garcia, R. Cingolani, L. Manna, and T. Pellegrino. *Nano Lett* 13, 2399-2406 (2013).
- Giant thermovoltage in single InAs nanowire field-effect transistors.
S. Roddaro, D. Ercolani, M. A. Safeen, S. Suomalainen, F. Rossella, F. Giazotto, L. Sorba, and F. Beltram. *Nano Lett* 13, 3638-3642 (2013).
- Antimicrobial peptides design by evolutionary multiobjective optimization.
G. Maccari, M. Di Luca, R. Nifosi, F. Cardarelli, G. Signore, C. Boccardi, and A. Bifone. *PLoS Biol* 9, e1003212 (2013).
- The unexpected role of arsenic in driving the selective growth of InAs quantum dots on GaAs.
F. Arciprete, E. Placidi, R. Magri, M. Fanfoni, A. Balzarotti, and F. Patella. *ACS Nano* 7, 3868-3875 (2013).
- Dynamical treatment of charge transfer through duplex nucleic acids containing modified adenines.
G. Brancolini, A. Migliore, S. Corni, M. Fuentes-Cabrera, F. J. Luque, and R. Di Felice. *ACS Nano* 7, 9396-9406 (2013).
- Crystal phase induced bandgap modifications in AlAs nanowires probed by resonant Raman spectroscopy.
S. Funk, A. Li, D. Ercolani, M. Gemmi, L. Sorba, and I. Zardo. *ACS Nano* 7, 1400-1407 (2013).

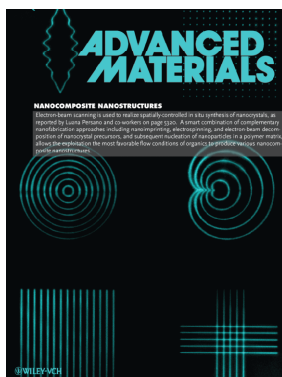
- Spin-polarization transfer in colloidal magnetic-plasmonic Au/iron oxide hetero-nanocrystals.
F. Pineider, C. de Julián Fernández, V. Videtta, E. Carlino, A. al Hourani, F. Wilhelm, A. Rogalev, P. D. Cozzoli, P. Ghigna, and C. Sangregorio. *ACS Nano* 7, 857–866 (2013).
- Metallic-like stoichiometric copper sulfide nanocrystals: phase- and shape-selective synthesis, near-infrared surface plasmon resonance properties, and their modeling.
Y. Xie, L. Carbone, C. Nobile, V. Grillo, S. D'Agostino, F. Della Sala, C. Giannini, D. Altamura, C. Oelsner, K. Krysch, and P. D. Cozzoli. *ACS Nano* 7, 7352–7369 (2013).
- Fabrication of flexible all-inorganic nanocrystal solar cells by room-temperature processing.
A. Louidice, A. Rizzo, G. Grancini, M. Biasiucci, M. R. Belviso, M. Corricelli, M. L. Curri, M. Striccoli, A. Agostiano, P. D. Cozzoli, A. Petrozza, G. Lanzani, and G. Gigli. *Energ Environ Sci* 6, 1565–1572 (2013).
- Shape-tailored TiO₂ nanocrystals with synergic peculiarities as building blocks for highly efficient multi-stack dye solar cells.
L. De Marco, M. Manca, R. Giannuzzi, M. R. Belviso, P. D. Cozzoli, and G. Gigli. *Energ Environ Sci* 6, 1791–1795 (2013).
- Donor-acceptor shape matching drives performance in photovoltaics.
T. Schiros, G. Kladnik, D. Prezzi, A. Ferretti, G. Olivieri, A. Cossaro, L. Floreano, A. Verdini, C. Schenck, M. Cox, A. A. Gorodetsky, K. Plunkett, D. Delongchamp, C. Nuckolls, and A. Morgante. *Adv Energy Mater* 3, 894–902 (2013).
- Extracellular matrix inhibits structural and functional plasticity of dendritic spines in the adult visual cortex.
L. De Vivo, S. Landi, M. Panniello, L. Baroncelli, S. Chierzi, L. Mariotti, M. Spolidoro, T. Pizzorusso, L. Maffei, and G. M. Ratto. *Nat Commun* 4, 1484 (2013).
- Quantum coherence controls the charge separation in a prototypical artificial light-harvesting system.
C. A. Rozzi, S. M. Falke, N. Spallanzani, A. Rubio, E. Molinari, D. Brida, M. Maiuri, G. Cerullo, H. Schramm, J. Christoffers, and C. Lienau. *Nat Commun* 4, 1602 (2013).
- All-optical polariton transistor.
D. Ballarini, M. De Giorgi, E. Cancelleri, R. Houdre, E. Giacobino, R. Cingolani, A. Bramati, G. Gigli, and D. Sanvitto. *Nat Commun* 4, 1778 (2013).
- Ultrafast collinear scattering and carrier multiplication in graphene.
D. Brida, A. Tomadin, C. Manzoni, Y. J. Kim, A. Lombardo, S. Milana, R. R. Nair, K. S. Novoselov, A. C. Ferrari, G. Cerullo, and M. Polini. *Nat Commun* 4, 1987 (2013).
- High performance piezoelectric devices based on aligned arrays of nanofibers of poly(vinylidene fluoride-co-trifluoroethylene).
L. Persano, C. Dagdeviren, Y. W. Su, Y. H. Zhang, S. Girardo, D. Pisignano, Y. G. Huang, and J. A. Rogers. *Nat Commun* 4, 1633 (2013).
- Steering the growth of metal ad-particles via interface interactions between a MgO thin film and a Mo support.
S. Benedetti, F. Stavale, S. Valeri, C. Noguera, H. J. Freund, J. Goniakowski, and N. Nilius. *Adv Funct Mater* 23, 75–80 (2013).
- Fast spatiotemporal correlation spectroscopy to determine protein lateral diffusion laws in live cell membranes.
C. Di Rienzo, E. Gratton, F. Beltram, and F. Cardarelli. *PNAS* 110, 12307–12312 (2013).
- Control of DNA minor groove width and fis protein binding by the Purine 2-amino group.
S. P. Hancock, T. Ghane, D. Cascio, R. Rohs, R. Di Felice, and R. C. Johnson. *Nucleic Acids Res* 41, 6750–6760 (2013).
- DNASHape: high-throughput prediction of DNA shape on a genomic scale.
T. Zhou, L. Yan, Y. Lu, I. Dror, A. C. Dantas Machado, T. Ghane, R. Di Felice, and R. Rohs. *Nucleic Acids Res* 41, W56–W62 (2013).
- Colloidal ordered assemblies in a polymer shell-A novel type of magnetic nanobeads for theranostic applications.
N. C. Bigall, C. Wilhelm, M. L. Beoutis, M. Garcia-Hernandez, A. A. Khan, C. Giannini, A. Sanchez-Ferrer, R. Mezzenga, M. E. Materia, M. A. Garcia, F. Gazeau, A. M. Bittner, L. Manna, and T. Pellegrino. *Chem Mater* 25, 1055–1062 (2013).
- MAPbI(3-x) Cl-x mixed halide perovskite for hybrid solar cells: the role of chloride as dopant on the transport and structural properties.
S. Colella, E. Mosconi, P. Fedeli, A. Listorti, F. Gazza, F. Orlandi, P. Ferro, T. Besagni, A. Rizzo, G. Calestani, G. Gigli, F. De Angelis, and R. Mosca. *Chem Mater* 25, 4613–4618 (2013).
- Random laser from engineered nanostructures obtained by surface tension driven lithography.
N. Ghofraniha, I. Viola, F. Di Maria, G. Barbarella, G. Gigli, and C. Conti. *Laser & Photonics Rev* 7, 432–438 (2013).

Selected Publications - 2013

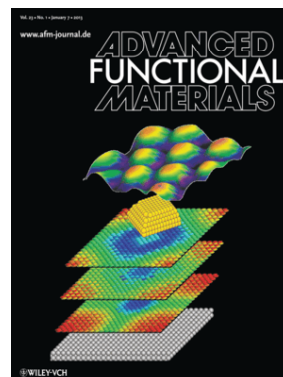
- Quantum information processing with hybrid spin-photon qubit encoding.
S. Carretta, A. Chiesa, F. Troiani, D. Gerace, G. Amoretti, and P. Santini. *Phys Rev Lett* **111**, 110501 (2013).
- Interactions in electronic mach-zehnder interferometers with copropagating edge channels.
L. Chirulli, F. Taddei, R. Fazio, and V. Giovannetti. *Phys Rev Lett* **111**, 036801 (2013).
- Extracting quantum work statistics and fluctuation theorems by single-qubit interferometry.
R. Dörner, S. R. Clark, L. Heaney, R. Fazio, J. Goold, and V. Vedral. *Phys Rev Lett* **110**, 230601 (2013).
- Environment-governed dynamics in driven quantum systems.
S. Gasparinetti, P. Solinas, S. Pugnetti, R. Fazio, and J. P. Pekola. *Phys Rev Lett* **110**, 150403 (2013).
- Oscillatory vertical coupling between a whispering-gallery resonator and a bus waveguide.
M. Ghulinyan, F. Ramiro-Manzano, N. Prtljaga, R. Guider, I. Carusotto, A. Pitanti, G. Pucker, and L. Pavesi. *Phys Rev Lett* **110**, 163901 (2013).
- Efficient universal blind quantum computation.
V. Giovannetti, L. Maccone, T. Morimae, and T. G. Rudolph. *Phys Rev Lett* **111**, 230501 (2013).
- Wick's theorem for matrix product states.
R. Huebener, A. Mari, and J. Eisert. *Phys Rev Lett* **110**, 040401 (2013).
- Photon solid phases in driven arrays of nonlinearly coupled cavities.
J. Jin, D. Rossini, R. Fazio, M. Leib, and M. J. Hartmann. *Phys Rev Lett* **110**, 163605 (2013).
- Measures of quantum synchronization in continuous variable systems.
A. Mari, A. Farace, N. Didier, and R. Fazio. *Phys Rev Lett* **111**, 103605 (2013).
- Quantum breathing of an impurity in a one-dimensional bath of interacting bosons.
S. Peotta, D. Rossini, M. Polini, F. Minardi, and R. Fazio. *Phys Rev Lett* **110**, 015302 (2013).
- Proposed alteration of images of molecular orbitals obtained using a scanning tunneling microscope as a probe of electron correlation.
D. Toroz, M. Rontani, and S. Corni. *Phys Rev Lett* **110**, 018305 (2013).
- Minimal self-contained quantum refrigeration machine based on four quantum dots.
D. Venturelli, R. Fazio, and V. Giovannetti. *Phys Rev Lett* **110**, 256801 (2013).
- Load-induced confinement activates diamond lubrication by water.
G. Zilibotti, S. Corni, and M. C. Righi. *Phys Rev Lett* **111**, 146101 (2013).



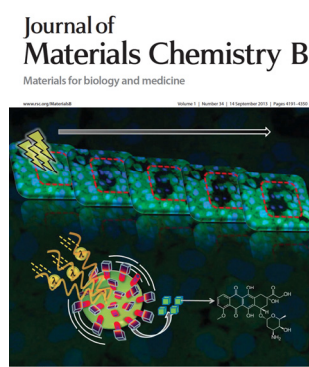
Adv Mater 24, 1304 (2012)



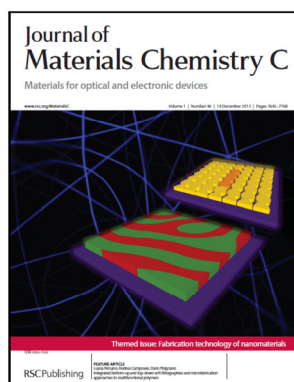
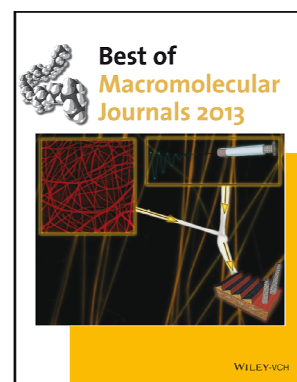
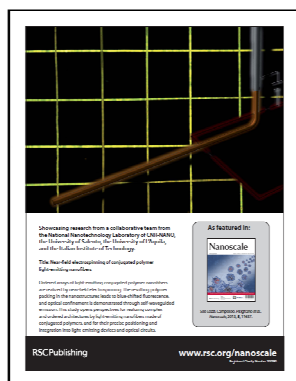
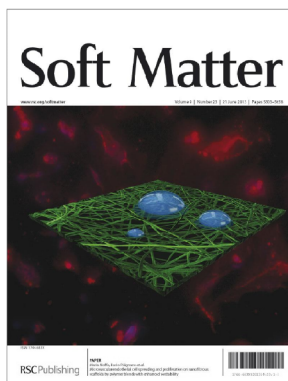
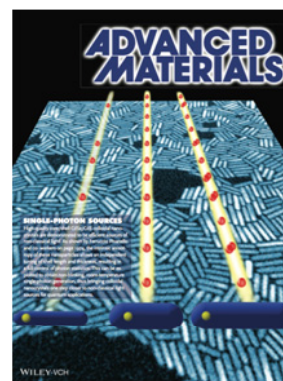
Adv Mater 24, 5320 (2012)



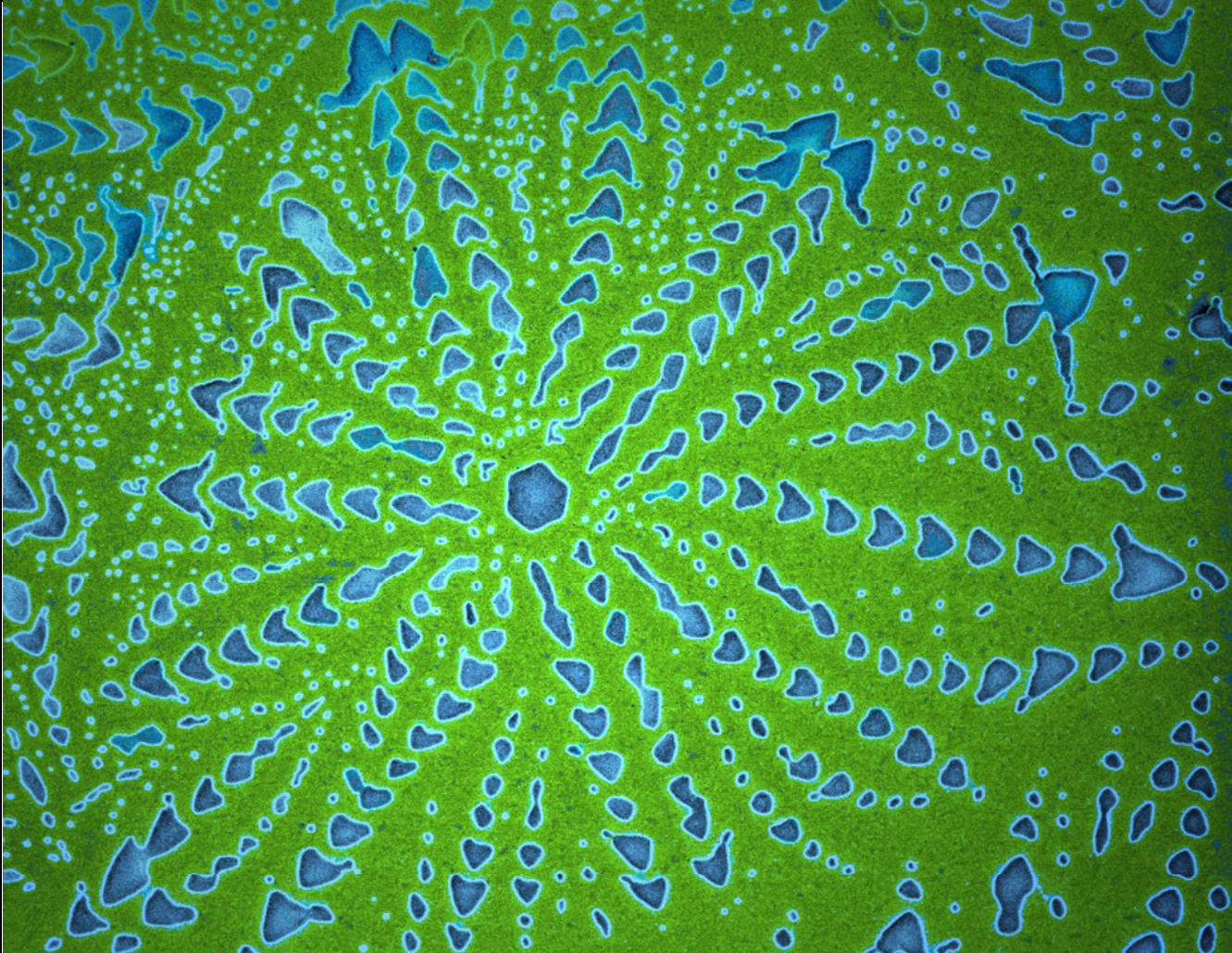
Adv. Funct. Mat 23, 75 (2013)



J. Mater. Chem. B 1, 4225 (2013)


Copyright, Royal Society of Chemistry, London
J Mater Chem C 1, 7645 (2013)

Copyright, Wiley-VCH, Weinheim
Macromol Mater Eng 504 (2013)

Copyright, Royal Society of Chemistry, London
Nanoscale 5, 11637 (2013)

Copyright, Royal Society of Chemistry, London
Soft Matter 9, 5529 (2013)


Adv Mat 25, 1974 (2013)



Projects and Grants

Projects & Grants

CnrNano research activity is mainly supported by funding obtained through competitive calls at different levels, from international to local.

Projects running in 2012-2013 are listed with following details: project name, type of call, coordinator, CnrNano principal investigator (if different), start and ending years, website (if available).

European Projects

AFM4NanoMed&Bio. European network on applications of Atomic Force Microscopy to NanoMedicine and Life Sciences. COST Action TD1002. CNRS Marcoule, FR (P. Parot); CnrNano S3 (P. Facci). 2010-2014. <http://www.afm4nanomedbio.eu/home.aspx>

CRONOS. Time dynamics and Control in nanostructures for magnetic recording and energy applications. UE FP7 NMP.2011.2.1-2. Trinity College Dublin, IE (S. Sanvito); CnrNano S3 (C. A. Rozzi). 2012-2015. http://www.cronostheory.eu/index.php?id=13&lang_id=eng

DEDOM. Development of Density Functional Methods for Organic-Metal Interaction. ERC Starting Grant 2007. CnrNano NNL (F. Della Sala). 2008-2013. <http://www.theory-nnl.it/dedom/>

FLAGSHIP GRAPHENE. Graphene-Based Revolutions in ICT And Beyond. FP7-ICT-2013.9.9. Chalmers Tekniska Hogskola AB, SE (J. Kinaert); CnrNano NEST (V. Pellegrini). 2013-2016. <http://graphene-flagship.eu/>

HY SUNLIGHT. Optical properties of Hybrid organic/inorganic nanoparticles for photovoltaic applications: toward a predictive computational approach. FP7-PEOPLE-2009-IIF. CnrNano S3 (G. Goldoni). 2010-2012.

INDEX. Indirect Excitons: Fundamental Physics and Applications. FP7-PEOPLE-2011-ITN. CNRS Montpellier, FR (M. Vladimirova); CnrNano S3 (M. Rontani). 2011-2014. <http://indexitn.ges.univ-montp2.fr/>

IT-LIVER. UE FP7-PEOPLE-2012-ITN. Fundacio Institut D'investigacio Biomedica De Bellvitge, ES (I. Fabregat); CnrNano NNL (S. Leporatti). 2013-2016.

MaECENAS. Nanoscale Optical-to-Mechanical Energy Conversion: Coupling Nano-Object with Light Powered Molecular Lifters. European NanoSci-Era. University of Ferrara, IT (M. A. Rampi); CnrNano S3 (S. Corni). 2009-2012.

MAGNIFYCO. Magnetic nanocontainers for combined hyperthermia and controlled drug release. FP7-NMP-2008-1.1-1. CnrNano NNL (T. Pellegrino). 2009-2012. <http://www.magnifyco.eu/>

MILES. Mid Infrared Laser System. EUROSTARS. CnrNano NEST (M. Tonelli). 2012-2015.

MOLARNET. Molecular Architectures for QCA-inspired Boolean Networks. UE FP7 ICT-2011.9.6. CnrNano NNL (R. Rinaldi). 2012-2016. <http://www.molarnet.eu/>

MOQUAS. Molecular Quantum Spintronics. FP7- ICT-2013.9.7. CnrNano S3 (M. Affronte). 2013-2016. <http://www.moquas.eu/>

NANO-JETS. Next-generation polymer nanofibers: from electrified jets to hybrid optoelectronics. UE FP7-IDEAS-ERC ERC-SG-PE8. Cnr Nano NNL (D. Pisignano). 2013-2018. <http://www.nanojets.eu/>

NANOSCI-EPLUS. Transnational call for collaborative proposals in basic nanoscience research. FP7-NMP. Centre National de la Recherche Scientifique, FR (J. L. Robert); CnrNano (E. Molinari). 2008-2012.

POLAFLOW. Polariton condensates: from fundamental physics to quantum based devices. UE FP7-IDEAS-ERC ERC-SG-PE2. CnrNano NNL (D. Sanvito). 2012-2017.

Q-NET. Quantum-Nano-Electronics Training. FP7-PEOPLE-2010-ITN. Institut Néel-UJF, FR (H. Courtois); CnrNano NEST (F. Giazotto). 2011-2015. <http://www.quantum-net.org/>

REDOX. Reducible oxide chemistry, structure and functions. COST ACTION CM1104. Universität Osnabrück, DE (M. Reichling); CnrNano S3 (P. Luches). 2012-2016. <http://www.cost-redox.nano.cnr.it/>

SOULMAN. Sound-Light Manipulation in the Terahertz. UE FP7-IDEAS-ERC ERC-AG-PE3. CnrNano NEST (A. Tredicucci). 2013-2018.

National Projects

Computer modeling and simulation of nucleic acids structure and dynamics. MAE Progetti Canaletto Italia-Polonia. CnrNano NEST (V. Tozzini). 2013-2015.

Controlling the structure and function of metal supported organometallic nanostructures. PRIN 2008. University of Rome La Sapienza (M. G. Betti); CnrNano S3 (R. Di Felice). 2009-2012.

Crescita e caratterizzazione microscopica di dispositivi ad effetto di campo basati su nanofili a semiconduttore. PRIN 2009. University of Naples (F. Tafuri); CnrNano NEST (L. Sorba). 2011-2013.

Crescita, nanofabbricazione e controllo ottico di punti quantici in cavità fotoniche. PRIN 2008. Politecnico di Torino (F. Rossi); CnrNano (V. Pellegrini). 2010-2012.

EC-SPECTRA. Sviluppo dell'ambiente elettrochimico nel calcolo delle spettroscopie di nano-sistemi ibridi. FIRB Futuro in Ricerca 2008. CnrNano S3 (A. Ferretti). 2010-2013.

Effetti della manipolazione della via di trasduzione ERK sulla plasticità strutturale della via cortico-striatale in vivo mediante microscopia a due fotoni. PRIN 2008. CnrNano NEST (G. M. Ratto). 2010-2014.

Energie da fonti rinnovabili. Progetto interdipartimentale Cnr. CnrNano NNL (G. Gigli). 2011-2014.

FLASHit RBFR12SWOJ. MIUR Firb Futuro in Ricerca 2012. University of Rome Tor Vergata (A. Marini); CnrNano S3 (D. Prezzi). 2013-2016.

Friction and adhesion of nano-particles on surfaces. PRIN 2008. University of Padova (G. Mistura); CnrNano S3 (S. Zapperi and G. Paolicelli). 2010-2012.

FRONTERA. Ricerca fondamentale sui dispositivi fotonici innovativi operanti nella regione spettrale Terahertz. Firb Futuro In Ricerca 2010. CnrNano NEST (M. S. Vitiello). 2012-2015.

GRAF. Frontiere della ricerca sul grafene: comprensione e controllo di funzionalità avanzate. PRIN 2010-2011. University of Trieste (A. Morgante); CnrNano NEST (V. Pellegrini). 2013-2016.

ITALNANONET. FIRB 2006. Cnr-Instm (R. Psaro); CnrNano NEST (R. Bizzarri), CnrNano NNL (G. Gigli), CnrNano S3 (P. Facci). 2009-2012.

Nanofibre biomedicali per ingegneria tissutale basata su cellule staminali renali. FIRB 2008 MERIT. CnrNano NNL (D. Pisignano). 2010-2013.

Nanofibre polimeriche attive multifunzionali per la fotonica e l'elettronica. FIRB Futuro in Ricerca 2008. CnrNano NNL (D. Pisignano). 2010-2014.

Nuove sfide nel nanomagnetismo molecolare (RBFR12RRPD1). MIUR Firb Futuro in Ricerca 2012. University of Parma (S. Carretta); CnrNano S3 (A. Ghirri). 2013-2016.

Ossidi nanostrutturati: multifunzionalità e applicazioni (RBAP115AYN). MIUR FIRB. University of Milano Bicocca (G. Pacchioni); CnrNano S3 (S. Valeri). 2012-2015.

PLASMOGRAPH. Plasmons and Terahertz devices in graphene. FIRB Futuro in Ricerca 2010. CnrNano NEST (M. Polini). 2011-2014. <http://www.plasmograph.it/>

Semiconduttori unidimensionali autoassemblati e loro applicazioni dispositivi. FIRB Italia/Canada 2007. CnrNano NEST (F. Beltram). 2007-2012.

Projects & Grants

Sviluppo di proteine fluorescenti per nanoscopia ottica orientata allo studio di dinamiche cellulari. PRIN 2008. University of Genoa (A. G. Diaspro); CnrNano NEST (V. Tozzini). 2010-2013.

Regional Projects

AEROCOMP. Studio Preliminare di Materiali Nanocompositi per Applicazioni Aeronautiche (Progetto DM 48391). DHITECH FAR. CnrNano NNL (A. Athanassiou). 2008-2012.

AMIDERHA. Sistemi avanzati mini-invasivi di diagnosi e radioterapia. MIUR MSE PON FSE. CnrNano NNL (R. Rinaldi). 2012-2015.

BEYOND-NANO. Materials and processes BEYOND the NANO scale. MIUR MSE PON FSE. CnrNano NNL (G. Gigli). 2012-2014. <http://www.ponrec.it/open-data/progetti/scheda-progetto?ProgettoID=5362>

Biosensor-based assay for high-throughput quantitative screening of chloride transport. Regione Toscana "Bando Salute 09". CnrNano NEST (D. Arosio). 2010-2012.

MAAT. Molecular Nanotechnology for Health and Environment. MIUR MSE PON FSE. Dhithec; CnrNano NNL (G. Gigli). 2012-2015.

NAMASTE. Nanomateriali per l'edilizia sostenibile. MIUR MSE POR FSE. Lorusso Vergara; CnrNano NNL (G. Ciccarella). 2012-2014.

OLED. Nuovi sorgenti OLED per l'illuminazione. DHITECH FAR. CnrNano NNL (G. Gigli). 2008-2012.

RINOVATIS. Activating RINOVATIS: Ingegneri Innovatori/Imprenditori specializzati in tecnologie e metodologie della Tissue Engineering. MIUR MSE PON FSE. Dhithec; CnrNano NNL (R. Rinaldi). 2012-2015. <http://www.ponrec.it/open-data/progetti/scheda-progetto?ProgettoID=5804>

SAFEMEAT. Innovazioni di processo e di prodotto per incrementare i profili di sicurezza e per diversificare la gamma dei prodotti (freschi e stagionati) a base di carne suina. Regione Puglia. Cnr Dipartimento Agroalimentare; CnrNano NNL (R. Rinaldi). 2011-2014.

Sviluppo e realizzazione di biochip per la diagnostica molecolare e la tipizzazione di virus patogeni umani (HPV, HCV, COXSACKLE B) PS 105. Strategico Regione Puglia. CnrNano NNL (R. Rinaldi). 2009-2012.

VINCENTE. Un ambiente virtuale di "Collective Intelligence" abilitante lo sviluppo di ecosistemi per l'imprenditorialità tecnologica sostenibile. MIUR MSE PON FSE PON02_00563_3470993. Dhithec; CnrNano NNL (G. Gigli). 2012-2015. <http://www.ponrec.it/open-data/progetti/scheda-progetto?ProgettoID=5805>

WAFITECH. Laboratorio regionale per le nuove nano e biotecnologie per la filtrazione dell'acqua: design e costruzione di membrane biomimetiche per applicazioni industriali, commerciali e ambientali. Regione Puglia. University of Bari (G. Calamita); CnrNano NNL (A. Camposeo). 2009-2012.

Other Funding Agencies

Development of cytochrome c assay marker of ischemia/reperfusion damage to the heart. Istituto Europeo di Oncologia - Bando Fondazione Umberto Veronesi. CnrNano NNL (R. Rinaldi). 2011-2012.

Few-body Physics of cold Fermi atoms. Fondazione Cassa di Risparmio di Modena "Internazionalizzazione". CnrNano S3 (M. Rontani). 2010-2012.

MARINE Materiali ad indice di rifrazione negativo nel visibile e criteri per l'invisibilità. Ministero Difesa. University of Rome La Sapienza; CnrNano NNL (A. Passaseo). 2010-2013.

MOPROSURF Modeling protein-surface interaction. IIT Istituto Italiano di Tecnologia Seed. CnrNano S3 (S. Corni; R. Di Felice). 2010-2013. <http://www.moprosurf.nano.cnr.it/>

Multi-scale modelling DNA. Fondazione Cassa di Risparmio di Modena "Internazionalizzazione". CnrNano S3 (R. Di Felice). 2010-2012.

Quantum Properties of Molecular Nanomagnetism. AOARD. CnrNano S3 (M. Affronte). 2013-2015.

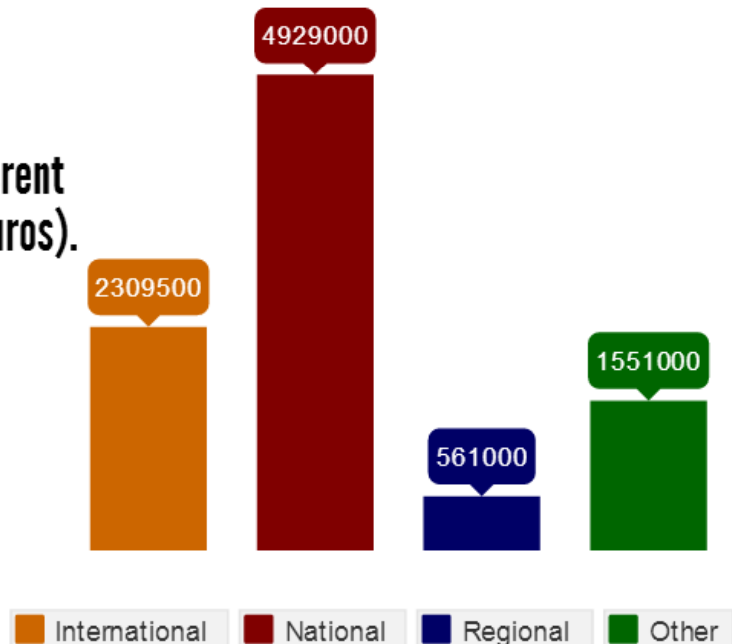
Role of dysregulated astrocyte-GABAergic interneuron interactions in the control of seizures in monogenic models of epilepsy. FONDAZIONE TELETHON. CnrNano NEST (G. M. Ratto). 2012-2015.

Theory of Switching and imaging molecular magnets on surfaces. Fondazione Cassa di Risparmio di Modena "Internazionalizzazione". CnrNano S3 (F. Manghi). 2010-2012.

Unravelling the Rett syndrome: effects of MeCP2 mutations on synaptic function. Fondazione Telethon. CnrNano NEST (G. M. Ratto). 2013-2016. <http://www.telethon.it/en/funding-research/funded-projects/details/unravelling-the-rett-syndrome-effects-of-mecp2-mutations-on-synaptic-function>

2012-2013 funding chart

Incoming funding
sorted as from different
kind of grants (in Euros).





CnrNano Life

2012

February

Imparare Sperimentando

CnrNano research went public during Imparare Sperimentando, an annual public science event in Pordenone. Citizens and school students had the chance to explore two stalls set by CnrNano showing research on microfluidic chips on and the extraordinary properties of graphene, and to watch a short video about the possible use of graphene to store hydrogen for energy applications.



CnrNano collaborates with the innovation's web tv

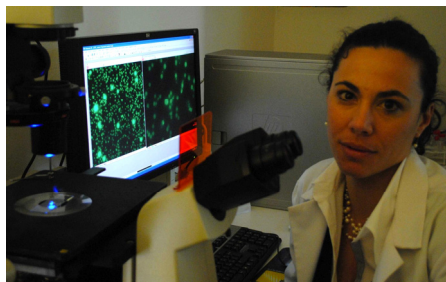


CnrNano goes into partnership with TRIWU, a new-born project launching a web portal and a web-tv channel dedicated to innovation, knowledge sharing, and technology transfer. In particular, CnrNano contributes to the section dedicated to nanotechnology that features a wide set of documents and news as well as interviews to experts on issues ranging from latest Italian nanotech innovations, to debates on nanoproducts regulation, to more research-oriented results.

March

TR35-Young Innovators award

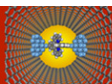
With a project dedicated to developing low-cost, smart nanomaterial based sensors for biomedical and diagnostic applications, Loretta del Mercato from CnrNano Lecce has been awarded the TR35-Young Innovators initiative, a competition aiming at collecting the best innovative ideas and applied research projects with a high business potential from under-35 researchers all over Italy.



June

A SINFOny of expertises

From June 20 to 22 in Parma, CnrNano scientists gathered with colleagues from other Cnr institutes to share the latest ideas on the fundamental properties of organic semiconductor and small molecule overlayers during the SINFO (Surfaces, INterfaces and Functionalization Processes in Organic Compounds and Applications) Workshop. The forum hosted more than 100 chemists, physicists, and material engineers who joined their expertise and addressed future applications for energy efficiency, environment control and health. The workshop also helped to develop a larger coordination capability and to single out the research directions to be implemented within the next European calls of the Horizon 2020 Program.



*Surfaces, Interfaces and Functionalization Processes
in Organic Compounds and Applications*

Fare Fisica

With the same enthusiasm of the previous years, CnrNano hosted for the third year Fare Fisica, a summer school organized by the University of Modena and Reggio Emilia and CnrNano aimed at introducing high-school juniors to a real research environment. About 30 students attended an intensive week of classes, hands-on laboratories, and workshops on nanoscience and material sciences taught by faculty members and CnrNano scientists.



Students could enjoy real academic and research life thanks to the in-campus accommodation, and familiarize with lab techniques developing a short research project. This annual event was successfully replied in 2013.

July

Graphene Day



On July 9 a workshop on graphene and its smart properties was held at CnrNano in Pisa. The workshop, organized by Stefan Heun, addressed current topics in graphene research and allowed for interesting discussions among the participants. It included a visit of the NEST laboratories and a meeting with researchers working in these labs.

September

Workshop on Nanomedicine and Nanobiosystems (WoMeN), Lecce

From September 6 to 8, international experts on nanomedicine and nanobiosystems participated to WOMEN, a workshop organized by CnrNano dedicated to the next wave of advancements in the healthcare field. They could discuss novel approaches to address major problems in modern medicine, like early detection and prevention, diagnosis improvement, diseases treatment and follow-up. The workshop closed a series of 3 jointly organized by CnrNano centers on their major topics.

A photonic prize

On September 17 the Italian Physics Society (SIF) awarded Miriam Serena Vitiello, a young CnrNano researcher, a prize dedicated to excellence in the field of Photonic and Optoelectronics. The jury considered Miriam's research on semiconductor laser sources and high frequency nanodetectors an activity "paving the way to new frontiers and innovation in Terahertz Photonics".



October

Science and society talks



On October 10 in Lecce opened a science-café series, La Scienza Spiegata (followed in 2013 by Scienza in Centro), organized by CnrNano Lecce, meant to give general public a chance to meet experts talking about main scientific themes in a non-academic way. The opening lecture was on the big steps of nano research and was hosted by Ross Rinaldi and Giuseppe Gigli. A wide variety of topics were addressed in following meetings: from science used in crime investigation or for sport performances, to exotic phenomena happening at the absolute zero temperature, to a narrated journey throughout the universe. The informal atmosphere and the copious time for debate made these events a successful opportunity to share knowledge, curiosity and experiences.

Two years in the life of CnrNano

November

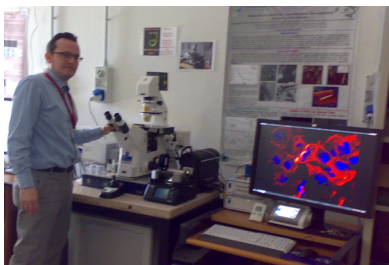
Focus on careers

In order to give college students an opportunity to be in close contact with science jobs and careers, CnrNano and the University of Modena and Reggio Emilia hosted Professione Fisica, a two-day workshop dedicated to meet physicists who developed a successful career in different fields, such as public and private research, or electronics, biomedical, mechanical companies. On November 12 and 13, students could see what these professionals actually do in their job activities, while school teachers attended refresher courses on new topics in the physical science of the matter and related technologies.



2013
February

With a CAT's eye



Three microscopes in one make the CAT. The new powerful instrument, supervised by Stefano Leporatti, got assembled and put to work on February 28 at the CnrNano labs in Lecce. Integrating a state-of-the art Confocal laser microscope, an Atomic force microscope and a Total internal reflection microscope, the innovative CAT facility permits high-resolution three-dimensional visualization of cells, enabling to perform research on engineered nanocapsules for anti-cancer drug delivery.

March

Greeting RedOx, Modena



On March 20-22 30 scientists active in REDOX, a COST project dedicated to explore and develop reducible oxides for chemical catalysis, sustainable energy conversion and novel electronic devices, met in Modena. Members of the Working Group led by Sergio Valeri, discussed ongoing research concerning the preparation and modelling of reducible oxide systems with designed functionality.

April

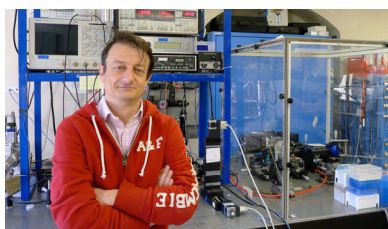
Hands on the code

35 highly-motivated young researchers attended the Yambo hands-on tutorial on electronic and optical excitations, a Cecam School event organized and tutored by CnrNano and other European research institutes, in Lausanne from April 8 to 12. Besides an overview of DFT based theoretical approaches to electronic and optical excitations, the most significant and successful part of the school consisted in hands-on sessions on the Yambo code under the guide of the code developers, who encouraged the students to adapt the code to their own projects.



May

Optical American Society award



Congratulations to Alessandro Tredicucci from CnrNano, who received the Nick Holonyak Jr. Award from the Optical Society of America. Dr. Tredicucci was recognized for demonstrating a Terahertz quantum cascade device, the first compact injection laser in the far-infrared. The Nick Holonyak Jr. Award, established in 1997 by OSA, is awarded for significant contributions to optics based on semiconductor-based optical devices and materials, including basic science and technological applications.

A universe of stories

"Universe is made of stories, not only atoms" the book written by CnrNano scientist Stefano Ossicini earned the Premio Divulgazione Scientifica Enrico Fermi, a prize assigned by a jury of teachers and students. The book narrates a century of scientific mistakes, frauds and controversies. A collection of stories full of passion and dramatic turns of events, the book reveals the dangerous temptations existing in modern science practice and stresses the importance of handling its mechanisms well in order to avoid being mistaken.



School of Photonics 2013

Where photonic meet electronics was the 4-day school organized by CnrNano that offered a wide perspective on areas of photonic research closely related to electronic technologies, linking with fundamental physics level, as well as materials or the device implementations. Almost 70 PhDs, graduating students, and junior post-docs gathered in Cortona to attend lessons from leading international scientists in fields such as plasmonics, terahertz technologies, graphene photonics, silicon photonics, metamaterials.

June

2nd CnrNano Institute Workshop, Modena

On June 10-11 more than one hundred researchers and technologists from all CnrNano sites convened in Modena for the 2nd CnrNano Institute Workshop, to discuss the most up-to-date scientific topics of the Institute, connect with colleagues, and establish new collaborations. Sessions were held on the main Institute topics, such as Light & matter, Frontier nanodevices and spectroscopies, Bio & Nano, Photovoltaics, nanocrystals, and Graphene & Co. The two-day 'retreat' was organized with oral and poster sessions and discussion groups, and a great attention was paid to social events, in order to offer the scientists a great



amount of time for informal exchange of ideas and experiences. The meeting was also attended by the international Scientific Advisory Committee of the Institute that praised the exceptional level and the broad spectrum of the CnrNano research activities.

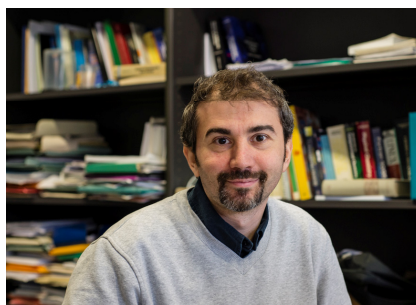
CnrNano leads the ranking of Cnr institutes publications in Nature journals



CnrNano was the Cnr institute with the highest number of publications in the Nature Group journals according to the recently published Nature Publishing Index 2012. In the chart, that shows the 2012 list of the top 100 global institutions that have published in Nature or Nature monthly research journals, Cnr is the only Italian institution and, within it, CnrNano had the highest number of articles published in the prestigious journals in 2012.

A surfacing prize

Stefano Corni from CnrNano has been named by the Italian Chemistry Society the recipient of the "Carla Roetti" Prize, dedicated to young researchers active in theoretical and computational chemistry. Stefano Corni's research focus on developing multiple-level computational methods for the investigation of organic and biological molecules at the interface with solids and inorganic nanostructures. These powerful computational methods allow to map the mysterious world of biomolecules and to study a wide range of crucial phenomena from plant photosynthesis to the functioning of digestive enzymes.



2013 Psi-K School

In between June 9-14, in a beautiful village close to L'Aquila, 36 students from all over Europe attended the summer school on Ab-initio Molecular Dynamics for Biomolecules, organized by CnrNano, University of L'Aquila, and King's College London. Conceived to train early stage researchers in the multi-disciplinary area of biological ab-initio simulations, highlights of the school included computer tutorials to put theory into practice and experimental lectures to illustrate open questions and areas of potential applications.

August

Gordon Research Seminar

Stefano Pittalis from CnrNano together with Florian Eich, University of Missouri, organized the Gordon Research Seminar on Time-Dependent Density-Functional Theory. During the forum, held at University of New England (ME) on August 10-11, grad students and post-docs discussed their cutting edge research among peers and mentors. The small size of the forum and the focus on young investigators provided an ideal interactive and unintimidating atmosphere.

September

Nanoscience goes to school-lab



NANOLAB, the first national continuing education course on nanoscience for school teachers, was launched on September 9 and was a great success. This innovative project, developed by physicist from University of Modena and CnrNano, aims at helping high-school science teachers to integrate nanoscience in their curricula by way of an inquiry-based approach. Nanoscience is in fact an ideal context to engage students in cutting edge research and to introduce the basics of modern physics in an operative and interdisciplinary way, linking fundamental science and technology. In the 4-day program of seminars and tutored lab sessions, teachers were taught how to set up a number of laboratory protocols, apt for school context and for transmitting the nanoscience key topics to students in the most practical way.

CnrNano shines at the 2013 Researchers' Night



The most widespread European general science event, that runs every year simultaneously in more than 300 EU cities, hosted CnrNano researchers in Pisa this year. On September 27 from late afternoon to night a great number of science demos, short talks, and science cafés let people explore science through fun learning. Researchers and postdocs from CnrNano and Scuola Normale Superiore introduced the public to graphene's incredible features: by way of a real research lab equipment, a Scanning Electron Microscope, they zoomed into details of grass leaves, bee's eyes, and pencil leads. By means of a big ball-and-stick model, they also explained to the public the origin of the unique structure of graphene and its innovative potential.

October

CnrNano on stage explains Graphene Superstar

CnrNano researcher Valentina Tozzini shared the stage of the conference-debate Graphene Superstar, during the Internet Festival in Pisa on October 10. Together with Pasqualantonio Pingue from NEST Lab, and Emanuele Treossi from Cnr-Isof, Valentina met the public and talked about the special features of the 'superstar' material.



November

Nanoscience Prize

CnrNano researcher Francesco Rossella was awarded the NEST Nanoscience prize, an annual prize for young scientists who led their activity entirely in Italy sponsored by Scuola Normale Superiore. Rossella earned the prize thanks to his studies that demonstrate how single nanotubes filled with cobalt when illuminated exhibit a strong enhancement of the temperature at the metal sites, a feature that has potential applications in nanomedicine. The research was published on Advanced Materials.



Outreach & Communication

CnrNano outreach activities aim at promoting public awareness and knowledge of sciences at the nanoscale, as well as the institute's ongoing research results. Thanks to the help of many scientists and of the staff, a great number of activities targeting a range of audiences, from high-school students to journalists, to policymakers, have been developed by the CnrNano Communication Office, in close agreement with the Cnr Press Office.

In 2012-2013 regular activities included the issuing of 17 press releases, and the organization of interviews with scientists, that gained a quite widespread presence of CnrNano in both general and scientific press. Media coverage reached a peak with the announcement of the selection of the Graphene Flagship as one of Europe's first FET flagships in January 2013. The Institute, that entered the consortium since the beginning playing an active role in drafting the pilot project, was a key player in launching the news at national level, and obtained a wide coverage by a variety of media, TV channels included.


CnrNano also supported a number of outreach activities for a wider scientific community, as well as for journalists, students, teachers, and general public, with the purpose of improving the collectivity's knowledge of nanosciences and more generally of raising their awareness on the impact of science on society. Among these activities, we mention: Fare Fisica, a summer school for high-school students on physics and physics of matter (June 2012, June 2013); Professione Fisica, a workshop on physics careers for students (November 2012); Nanolab, the first national educational program for secondary school science teachers aimed at integrating nanoscience in high-school curricula (September 2013); the participation at scientific festivals, science popularization events, and the European Researcher's night. (See the CnrNano Life section for details).


Playing with carbon at 2013 Researchers Night, Pisa



PISA NEST

NEST
Piazza San Silvestro 12
56127 Pisa, Italy


 +39 050 509418


 segreteria.nest@nano.cnr.it



LECCE NNL

NNL
Via Arnesano
73100 Lecce, Italy


 +39 0832 298239


 segreteria.nnl@nano.cnr.it



MODENA S3

S3
Via Campi 213/A
41125 Modena, Italy

 +39 059 2055629

 segreteria.s3@nano.cnr.it





 **CNRNANO**
ISTITUTO NANSCIENZE CONSIGLIO NAZIONALE DELLE RICERCHE

Pisa NEST, Lecce NNL, Modena S3
www.nano.cnr.it